Ph. D. Thesis

Effects of metal ions, pressure, temperature, and basalt on the polymerization reactions of amino acids in hydrothermal systems and Organic geochemical investigation for subseafloor biosphere

海底熱水中の溶存イオン，圧力，温度，玄武岩が アミノ酸重合反応に及ぼす影響 及び海底下地下生命圏に対する有機地球化学的考察

Kasumi Sakata　　坂田　霞

Department of Earth and Space Science,
Graduate School of Science, Osaka University

February, 2014

Abstract

Since the first discovery of hydrothermal systems in 1979, it has been suggested that hydrothermal systems are one of the suitable environments for the chemical evolution of life in the primitive earth. The most notable advantage of hydrothermal systems is that both of synthesis of organics and ecosystems can be supported in the hydrothermal systems. In the past, synthesis and polymerization of organics under the conditions simulating hydrothermal systems were actively studied. Typically, hydrothermal fluids are hot (< 400 °C), acidic (pH 2-4) and rich in metal ions. Experimental conditions of previous studies of chemical evolution of organics were only acidic or neutral condition. Recently, a new type of hydrothermal systems, Lost City hydrothermal system and south Chamorro sea mount, were discovered. This new type of hydrothermal systems eructs relatively cold (< 90°C) and basic (pH <12) fluids and attracts attention as a new environmental model for chemical evolution of organics. It is necessary to study about chemical evolution of organics under various physical and chemical conditions of hydrothermal fluids.

As well as hydrothermal systems, oceanic crust has been noticed as one of the possible environments supporting the earliest ecosystems in the earth. The uppermost about 500 m of basaltic ocean crust is permeable. In these areas, sea water oxidizes young basaltic crust (< 10 Ma) and the chemical reaction between basalt and sea water release energy for supporting chemosynthetic microbes. These water-rock reactions widely occur in the oceanic crust, as well as hydrothermal systems, and support a significant fraction of total biomass. Understanding about ecosystems in the basaltic oceanic crust, such as metabolic systems, activity, abundance, derivation of microbes living there, leads to revealing habitability in the primitive terrestrial deep biosphere.

In this Ph.D. thesis research, the authour noted the hydrothermal conditions such as pH, temperature, dissolved metal ions, basalt, and pressure to evaluate the effects of these parameters on the reaction rate constants of amino acids. The author also detected of organic carbon and analyzed carbon isotopes of basalt and sediments collected from North Pond located in the western flank of the Mid-Atlantic Ridge for understanding the origin of carbon compounds in relation to possible microbial activity in the basaltic crust.

In Chapter 2, the author analyzed the effects of pH and temperature on the

dimerization rate of glycine (Gly: NH_2-CH_2-COOH), one of the simplest amino acids. Gly dimerizes to form glycylglycine (GlyGly), and GlyGly further reacts to form diketopiperazine (DKP). Gly solutions with pH ranging from 3.1 to 10.9 were heated for 1–14 days at 140 °C, and changes in concentrations of Gly, GlyGly, and DKP were evaluated. At pH 9.8, the experiments were conducted at 120, 140, 160, and 180 °C. The dimerization rate of Gly was nearly constant at pH 3−7 and increased with increasing pH from 7 to 9.8 and then decreased with further increases in pH. To elucidate the reason for this pH dependency, we evaluated the role of the three dissociation states of Gly (cationic state: Gly^+, zwitterionic state: $Gly^{\pm}$, and anionic state: Gly^-). For pH > 6, the dominant forms are $Gly^{\pm}$ and Gly^-, and the molar fraction of $Gly^{\pm}$ decreases and that of Gly^- increases with increasing pH. The dimerization rate was determined for each dissociation state. The reaction between $Gly^{\pm}$ and Gly^- was found to be the fastest; the rate constant of the reaction between $Gly^{\pm}$ and Gly^- was 10 times the size of that between Gly^- and Gly^- and 98 times that between $Gly^{\pm}$ and $Gly^{\pm}$. The dimerization rate became greatest at pH 9.8 because the molar fractions of $Gly^{\pm}$ and Gly^- are approximately equal at this pH. The dimerization rate increased with temperature, and an activation energy of 88 kJ mol^{-1} was obtained. Based on these results and previous reports on the stability of amino acids under hydrothermal conditions, we determined that Gly dimerizes most efficiently under alkaline pH (~9.8) at about 150 °C.

In Chapter 3, the authour analyzed the effects of metal ions (Ca^{2+}, Mg^{2+}, Fe^{2+}, Mn^{2+}, Zn^{2+} and Cu^{2+}) on the reaction rates of amino aicds at pH 2.2-9.9 and 140°C. the effect of metal ions (Ca^{2+}, Mg^{2+}, Zn^{2+}, Fe^{2+}, Mn^{2+}, and Cu^{2+}) and pH on the formation and decomposition rates of glycylglycine (GlyGly), glycylglycylglycine (GlyGlyGly), and diketopiperazine (DKP) in aqueous solutions was investigated. Glycine (Gly) solutions with metal ions were heated for 1–74 days at 140°C at different pH conditions. GlyGly and DKP were produced from all the sample solutions, and were not affected by the presence or absence of metal ions. The GlyGly yields were higher under basic conditions (pH 9.8–9.9) than those under acidic and neutral conditions. Moreover, the GlyGly yields in the presence of Cu^{2+} and Zn^{2+} were higher compared to those in the absence of Cu^{2+} and Zn^{2+}, and in the presence of metal ions other than Cu^{2+} and Zn^{2+} the GlyGly yields were lower. The dimerization rate constant of Gly (k_1) increased in the presence of Cu^{2+}. GlyGlyGly was only produced in samples with Cu^{2+}, and the

yield was five times higher under basic condition (pH 9.8) than that under acidic (pH 3.4) and neutral (pH 7.1) condition. On the other hand, the other metal ions inhibited prebiotic peptide synthesis by catalyzing the hydrolysis or chelation with amino acids. Thus, the results reflect the high stability of Cu^{2+} complexes with amino acids or peptides in the salt-induced peptide formation reaction, particularly at high pH. Although the elongation of oligopeptides was not favored, the formation of metal–amino acid or metal–short peptide chelates might have facilitated primitive biological functions and expanded prebiotic reaction fields because of their mobility in the Earth's early oceans.

In Chapter 4, the authour analyzed the effects of basalt, pressure, and temperature on the reaction of glycine at pH 6.0. Gly solutions having pH 6.0 were heated within 12 hours at 100-200°C and 10-35 MPa with basalt. Gly solutions without basalt were also heated for 6 hours at 200 °C and 35 MPa. GlyGly and DKP were produced from all the sample solutions, and the yields of GlyGly and DKP were almost constant for 10-35 MPa. While, the both yields of GlyGly and DKP increased as temperature increased. Basalt promoted formation of GlyGly. The yields of GlyGly from the solutions containing basalt were 2.6 times higher than those without basalt. The yields of DKP from the solutions containing basalt were 0.86 times lower than those without basalt. The dimerization rate constant of Gly (k_1) was 13 times higher with basalt than that without basalt. These catalytic effects of basalt result from the removal of intramolecular interaction between $–COO^-$ and $–NH_3^+$ groups within amino acid molecules and increasing of the electrophilicity of carbonyl carbon in the amino acids.

In Appendix, the authour detected organic carbon and examined carbon isotopic ratio of sediments and basaltic samples obtained from North Pond, the western flank of the mid-Atlantic Ridge. Total carbon (TC) value ranged 6 ~ 11 % for whole sediment samples. Depth profiles of $\delta^{13}C$ (bulk) of sediments (−0.04 ~ +1.93 ‰) were similar to those of TC. These depth profiles of TC and $\delta^{13}C$ (bulk) of sediements appear to have inverse relation with the distributions of O_2 concentration. Organic carbon (TOC) of the sediments had the same depth profiles to those of NO_3^- and had the opposite depth profiles to those of oxygen. Organic carbon was detected from basaltic samples above 310 meter below sea floor (mbsf) and its carbon isotopic ratio may be reflected coexistence of methane- and sulfur-cycling microbes. TC (0.01 ~ 0.37 %) and TOC (0.01 ~ 0.03%) values of basalts were almost constant over the depth, while sediment

breccias and carbonates contained more carbon than basalts (3.56 ~ 11.9 %). $\delta^{13}C$ (bulk) of basalts ranged −21.8 ~ +2.69 ‰. Sediment breccias and carbonates had larger $\delta^{13}C$ (bulk), ranging −18.6 ~ +2.82 ‰. $\delta^{13}C$ (org) of hard rocks were lower as depth is deeper. $\delta^{13}C$ (kerogen) were slighty smaller than those of $\delta^{13}C$ (org).

Based on these results, the authour proposed that one of the most suitable hydrothermal environments for polymerization of amino acids is flow paths or voids of chimneys flowing basic and relatively cold hydrothermal fluids (~ pH 9.8 and 150-200 °C) containing Cu^{2+}. In recent earth, flow paths of south Chammoto sea mount are the best hydrothermal environments to fulfiil all the conditions.

Acknowledgements

I would like to appreciate Prof. Tadashi Kondo at Osaka University for a lot of discussions, supports, and provisions for progression of my study. Prof. Tadashi Kondo gave me research environments that I could study with free ideas. I greatly thank Assistant Prof. Hikaru Yabuta at Osaka University as much as Prof. Tadashi Kondo. She has provided me daily discussions, and a number of experimental supports. I greatly thank Associate Prof. Minoru Ikehara at Kochi University for his help in EA/IRMS analysis. I greatly thank Assistant Prof. Tadashi Yokoyama for the help in HPLC and BET analysis and his useful comments. I greatly thank Assistant Prof. Takeshi Sugahara and Ms. Hiroko Suzuki at Osaka University for their help in hydrothermal experiments under high-pressure condition. I also thank Associate Prof. Tetsuro Hirono at Osaka University and Dr. Norio Kitadai at Tokyo Institute of Technology for their useful comments. I also greatly thank the entire shipboard party of IODP Expedition 336. I would like to thank all members of Kondo laboratory, Matsuda Laboratory, and Terada laboratory, particularly Prof. Jun-ichi Matsuda, Prof. Kentaro Terada, Associate Prof. Chihiro Yamanaka, Associate Prof. Chiaki Uyeda, Associate Prof. Hidenori Terasaki, Assistant Prof. Koh Hashizume, and Assistant Prof. Tatsuhiro Sakaiya for their important comments and advices in laboratories seminars and their experimental helps. I also would like to thank Mr. Michio Sakamoto for giving me an environment to prepare the samples. I do not know how to appreciate Dr. Ken Takai and Dr. Takazo Shibuya at JAMSTEC. I would like to greatly appreciate them for their valuable discussions and great encouragements. I was helped them during I was in hard time. I could write this thesis thanks to their kind words. Finally, I would like to thank my families and friends for their understandings and great encouragements. This research was financially supported by JSPS Research Fellowship for Young Scientists to Kasumi Sakata.

Table of contents

Chapter 1

General introduction

The earth was formed about 4.6 billion years ago through the collision and coalescence of planetestimals in the early solar system and subsequently the ocean was formed about 4.3 billion years ago (Mojzsis et al., 2001). After that, the first life probably had appeared about 3.8 billion years ago (Mojzsis et al., 1996). Since then, the lives in the earth have survived as adapting many changes of environments and climates in the earth. And now, various lives flourish at wide variety of environments, even at the extreme environmental conditions, such as deep ocean floor, hydrothermal system, salty lake, ice and so on (Barros et al., 2007). However, it has not been resolved about when, where and how the first life which had metabolic, multiplication or self-replicating systems was born. To make clear these questions, it is essential to understand the chemical evolution of precursor materials for life. Chemical evolution of organics is processes by which complex organic molecules were formed from simpler organic and inorganic molecules through abiotic chemical reactions and finally these complex organic molecules have some biological functions as life. At 1953, Miller formed amino acids, acetic acids, urea from a mixture gas of methan, ammonia, hydrogen and water by spark discharge (Miller, 1953). Miller's study firstly showed that it is possible to form biological relevant molecules though abiotic chemical reaction. After this study, so many experiments were conducted to form biological relevant molecules such as amino acids, sugars and nucleotides under the conditions simulating prebiotic environments (e.g, Fox and Harada, 1958; Oró and Guidry, 1960; Oró, 1960; Oró and Kimball, 1961; Oró and Kimball, 1962; Sanchez et al., 1967; Lahav et al., 1978; Marshall, 1994; Shapiro, 1995, Ferris et al., 1996; Imai et al., 1999, Cody et al., 2000; Lemke et al., 2009; Furukawa et al., 2009).

In addition to the possibility that the primary materials were formed in the early earth, it has been proposed that meteorites are a potential source of organic matters (Chyba and Sagan, 1992; Pizzarello, 2004). These organic molecules probably built up in the early earth after simple organic molecules formed in the space and the earth. Both of terrestrial and universal environments are important as resources of organic molecules for chemical evolutions. These organic molecules must have participated in chemical evolutions of organics, for example, low moleculae-weight compounds might have polymerized to macro molecules or macro molecules might have hydrolyzed to smaller molecules to have biological functions.

Hydrothermal systems have been suggested as one of the suitable environment

where chemical evolutions presumably have occurred in the early Earth (e.g., Corliss, 1990; Holm, 1992; Yanagawa and Kobayashi, 1992; Macleod et al., 1994; Russell and Hall, 1997; Russell, 2003; Holm and Andersson, 2005; Martin et al., 2008). In primitive earth, several environmental conditions has been proposed for the chemical evolution of organics, such as meteorite impacts (Furukawa et al., 2009), diagenesis in deep sediments (Ohara et al., 2007), or lagoon and tidal pool (Rode, 1999). The most notable advantage of hydrothermal systems is that both of synthesis of organics and ecosystems can be supported in the hydrothermal systems. Obtainments of materials for synthesis organics, chemical evolutions of organics, and primitive microbial ecosystems can be supported in the hydrothermal systems. Hydrothermal activity has also been discussed in the concept of abiotic chemistry on Europa (McCollom 1999; Chyba and Hand, 2001; Chyba and Phillips, 2007; Irwin and Schulze-Makuch, 2011). Chemical evolution of organics also may occur in extraterrestrial planets.

In the terrestrial hydrothermal systems, seawater percolates into oceanic crusts and is heated, reacts with surrounding rocks and the resultant hot reductive fluids issues from the seafloor (Tivey, 2007). The temperatures of the hydrothermal fluids can reach about 400 °C, in contrast to a typical temperature of 2 °C for deep seawater (Tivey et al., 1995). The pH of the hydrothermal fluids have wide range and heavy metal ions, for example Fe, Mn, Zn, Cu, are rich and Mg is poor in these fluids. The pH values of 2−4 are most common (Fisher et al., 2007; Tivey, 2007), but values as high as 10−11 have been reported at the Lost City site (Kelley et al., 2001, 2005). South Chamorro seamount erupt the fluids having highest pH value (pH <12.5) and cold water (~2°C) (Mottl et al., 2003). Based on the petrological analysis of Archean basalt (Shibuya et al., 2010), it was proposed that the Archean subseafloor hydrothermal systems were characterized by high-pH fluids. The basic hydrothermal systems are new environmental models for chemical evolutions of organics (Russell, 2003).

In the hydrothermal systems, ecosystem in which chemoautotrophic microorganisms are as primary producers is prevailed. This ecosystem is totally different from an ecosystem based on photosynthesis. Chemoautotrophic microorganisms product chemical energy using reductive molecules in the fluids eructed from hydrothermal systems. At present, all the known reductive molecules used for redox reactions of metabolitic reaction of microbes in the hydrothermal conditions are hydrogen, sulfur, methane and iron (Fisher et al., 2007). It is the most primitive

microorganism that can be able to use hydrogen among these four reductive molecules (Takai et al., 2008). Therefore, the first life in the early earth might be able to use hydrogen for metabolism. Both of Lost City and south Chamorro seamount have sea floor bases that contain ultramafic rocks and produce hydrogen through serpentinization of olivine (Kelley et al., 2001; Kelley et al., 2005; Hulme et al., 2010; Wheat et al., 2010). Serpnetinization products hydrogen, methane and hydrogen sulfide that are energy source for lives under subsurface. Serpentinization also products highly basic (pH ~ 10) fluids at low temperature (~ 100°C) (McCollomn and Bach, 2009). These systems that eruct the fluids containing highly concentration of hydrogen and having relatively low temperature and high pH value are desirable for the birth of first life from the view of microbiological study.

At hydrothermal vents, organics such as aliphatic hydrocarbon, aromatic carbon, carboxylic acids (Konn et al., 2009), formate, and acetate (Lang et al., 2010), which might act as primary materials of life, have been found. Experimental studies that address the syntheses of amino acids, carboxylic acids and hydrocarbons and the polymerization of amino acids under hydrothermal conditions have also been conducted (e.g., Oró and Guidry, 1960; Ferris 1992; Marshall, 1994; Huber and Wächtershäuser, 1998; Imai et al., 1999; Cody et al., 2000; Kawamura et al., 2004; Lemke et al., 2009). A lot of experiments for abiotic synthesis of various organic molecules under the simulating hydrothermal conditions have been conducted (e.g., Ferris et al., 1978; Yanagawa et al., 1984; Harada and Fox, 1964; Imai et al., 1999; Rode, 1999; Huber and Wächetershäuser, 2003; Lambert, 2008; Lemke et al., 2009). Most of previous studies about polymerization of amino acids have been focused on elongation of peptide bonds (e.g., Lahav et al., 1978; Lawless and Lavi, 1979; Bujdák and Rode, 1997; Rode et al., 1999; Bujdák and Rode, 2003). However, it is still unclear that oligomers are main products and directly support the chemical evolutions of organics because degrees of polymerization of polymers abiotically formed are much lower than those of proteins. In primitive earth, many organics other than amino acids coexisted (Konn et al., 2009; Lang et al., 2010). The possibility of formation of oligomers under such primitive encironments has not been evaluated. Previous experiments have not attempted to control or measure such as oxidation state, pH, fugacities of dissolved gas species or major and trace element compositions of experimental systems (Holm and Andersson, 2005). To find the suitable environments for chemical evolution of organics, evaluation

of these parameters on formation of simple organics and revealing reaction mechanisms are more important. In hydrothermal systems, equilibrium conditions are not kept because mixing of hydrothermal fluids and sea water occur. Reaction rates for synthesis organics are also important as well as yields of orgnics. We think it is a sure and steady method to conduct kinetic studies about simple synthesis or polymerization of organics in order to reveal the reaction mechanisms and refine quantitatively effects of physical and chemical conditions of hydrothermal fluids.

It has been proposed that the effects of catalysis of minerals to synthesis and polymerization of amino acids (e.g., Lahav et al., 1978; Ponnamperuma et al., 1982; Bujdák and Rode, 2003; Lambert, 2008). Surfaces of minerals are elementally charged in aqueous solution. As a result, amino acids are adsorbed on the surface of minerals and polymerization reactions are promoted. The adsorption effects of minerals are also studied actively (Meng et al., 2004; Parbhakar et al., 2007; Stievano et al., 2007; Gao et al., 2008; Kitadai et al., 2009). Akabori et al. (1956) proposed the polyglycine hypothesis. In this paper, he confirmed that polymers of glycine are formed after heating experiments of amino acetonitrile and kaolinite. The polyglycine hypothesis suggests the possibility that prebiotic proteins are formed in the primitive hydrothermal systems. Reactions of organics with clay minerals are one of the attractive envirnemental models to form prebiotic organics having biofunctions. Although the effects of minerals on the polymerization of amino acids have been actively studied, the effects of basalt have not been studied yet. Basalt composes the oceanic crust and is widely prevailed in the subseafloor. It is more realistic environmental conditions to use basalt for the hydrothermal reactions of amino acids.

Typical acidic hydrothermal systems erupt fluids that are rich in heavy metal ions, (Tivey, 2007). On the other hand, Lost City hydrothermal field has characteristic conditions that differ from the typical hydrothermal vents, such as basic pH, low temperature (> ~90°C) and low metal ion compositions (Kelley et al., 2001, 2005). South Chamorro seamount eructs high basic (pH < 12), metal ions enrichment (Ca^{2+}, K^{+}, Mn^{2+}, Fe^{2+}, Cu^{2+} and Zn^{2+}) and low temperature (~4°C) fluids (Mottl et al., 2003; Hulme et al., 2010). Such divalent metal ions have known as effective catalysts for polymerization reaction of amino acids (e.g., Rode and Schwendinger, 1990; Saetia et al., 1993; Eder and Rode, 1994; Rode, 1999; Remko and Rode, 2000; Plankensteiner et al., 2002). Especially, Cu^{2+} has been studied the most actively under aqueous condition

(Schwendinger and Rode, 1991; Schwendinger and Rode, 1992; Suwannachot and Rode, 1999) and evaporation cycle experiments (Saetia et al., 1993; Son et al., 1998). Cu^{2+} is the most effective on the polymerization of amino acids under the acidic aqueous condition because copper ions and amino acids make complexes (Eder and Rode, 1994; Schwendinger and Rode, 1989; Tauler and Rode, 1990; Schwendinger and Rode, 1992; Suwannachot and Rode, 1999; Rode and Schwendinger, 1990). However, previous studies were conducted under acidic or neutral conditions simulating typical hydrothermal systems and no study has shown the effects of metal ions on polymerization reaction of amino acids under basic conditions. It is important to make clear the effects of metal ions on the polymerization of amino acids in basic conditions.

There are also fewer reports about polymerization rate constants of amino acids (Mitsuzawa and Yukawa, 2004; Cox and Seward, 2007; Sakata et al., 2010; Sakata et al., in press) than that about decomposition reaction (e.g., Lawrence and Moore, 1951; Qian et al., 1993; Radzicka and Wolfenden, 1996; Li and Brill, 2003). It is because numbers of products and reaction rate constants increase and numerical analysis becomes more difficult. The physical and chemical conditions in hydrothermal systems have various variations depending on geological setting. Therefore it is necessary to examine reaction rate constants including polymerization reactions under the various conditions such as pH, temperature, dissolved matter, oxygen fugacity, pressure and so on, in order to identify suitable conditions for chemical evolution of life. Most of experiments of synthesis and polymerization of amino acids have been conducted under acidic conditions because typical hydrothermal systems erupt acidic and high temperature solutions. Now basic hydrothermal systems are focused as one of a plausible condition for chemical evolution of life. Therefore, it is important to make clear the reaction rate constants of amino acids under the basic solutions containing metal ions.

It is also important pathway for revealing “origin of life” to investigate ecosystems of microbes in hydrothermal systems and subsurface biosphere. The majority of habitable environments in the earth are dark biosphere separated from sunlight. It is estimated that about one third of all biomass, and about three forth of all prokaryotic cells on the earth are in the sediments buried in oceanic subsurface (Whitman et al., 1998). In 1994, it was first proposed that microorganisms exist in deep sea sediment cores from several hundreds of meters obtained during the Ocean Drilling Program (Parkes et al., 1994).

Basaltic oceanic crust has been focused as a new deep submarine biosphere (Bach and Edwards, 2003). The uppermost about 500 m of basaltic oceanic crust is permeable and fluid flow is focused in specific areas at the contacts of lava flows or in brecciated zones (Fisher 2005). In these areas, chemical reaction between basalts and sea water release energy for supporting chemosynthetic microbes. Oceanic crust has been widely spread from the formation of the earth and has been noticed as one of the possible environments including the earliest ecosystems in the earth (Edwards et al., 2012). However the biosphere of basaltic oceanic crust has been poorly understood because of difficulty to access and return the samples. Understanding about ecosystems in the basaltic oceanic crust, such as metabolic systems, activity, abundance, derivation of microbes living there, leads to revealing habitability in the primitive terrestrial and extraterrestrial deep biosphere. In the past, Juan de Fuca Ridge in the eastern Pacific has been mainly studied because Juan de Fuca Ridge was an only site to observe clearly the water-rock reactions in basaltic crusts (e.g., Wheat et al., 2000; Fisher et al., 2003). In these basaltic oceanic crust, iron cycling, both oxidation and reduction of iron, supports metabolic activity in basalt, however, the microorganisms responsible for Fe oxidation on basalt are not clear (Orcutt et al., 2011). The colonization of basalt collected from subseafloor pillow basalt achieved detection of iron oxidation bacteria (Edwards et al., 2003; Mason et al., 2007; Singer et al., 2011). Fisk et al (1998) proposed that microbes promote the weathering of basaltic glass by morphologic observation and chemical analysis in the microscopic region of basaltic glass collected from Atlantic, Pacific and Indian Oceans. Lever et al. (2013) first measured carbon isotope of organic carbon of basalt collected from the eastern flank of the Juan de Fuca Ridge and confirmed the coexistence of methane- and sulfur-cycling microbes in the basalt. These studies have shown that microbes probably prevail in the oceanic crust and promote weathering of basaltic crust. However, it is unclear where deep-seated microbial communities come from, what the nature of the microbial communities harbored in young ridge flanks is, and what their role in the ocean crust weathering is (Edwards et al., 2012). Therefore, it is attractive studies to examine microbial activity in the hydrologically active, young ridge-flank crust being undergoing progressive oxidative alteration.

Scope of this study is to evaluate the possibility of a new type of hydrothermal systems eructing basic fluids, catalytic effects of natural basalt on the polymeriztion of organics. In this Ph.D. thesis research, the autour have examined (1) the effects of pH

and temperature on the products and reaction rates of Gly, (2) the effects of metal ions on the products and reaction rates of Gly under various pH conditions, (3) the effects of basalt and pressure. In Appendix, the author studied subsurface biosphere through carbon isotopic analysis of basaltic and sediment samples collected from North Pond on the western flank of the Mid-Atlantic Ridge

References

Akabori S., Okawa K. and Sato M. (1956) Intoduction of side chains into polyglycine dispersed on solid surface. I. *Bull. Chem. Soc. Jpn.* 29, 608-611.

Bach W. and Edwards K. J. (2003) Iron and sulfide oxidation within the basaltic ocean crust: Implications for chemolithoautotrophic microbial biomass production. *Geochim. Cosmochim. Acta* 67, 3871-3887.

Barros J. A., Huber J. A. and Schrenk M. O. (2007) Limits of carbon life on Earth and elsewhere. *Planets and Life* (Sullivan III W. T. and Baross J. A. eds.) Cambridge University Press 275-291.

Bujdák J. and Rode B. M. (1997) Glycine oligomerization on silica and alumina. *Reaction kinetics and catalysis letters* **62**, 281-286.

Bujdák J. and Rode B. M. (2003) Peptide bond formation on the surface of activated alumina: peptide chain elongation. *Catalysis Letters* **91**, 149-154.

Chyba C. and Sagan C. (1992) Endogenous production, exogenous delivery and impact-shock synthesis of organic molecules: an inventory for the origins of life. *Nature* **355**, 125-132.

Chyba C. F. and Hand K. P. (2001) Life without photosynthesis. *Science* 292, 2026-2027.

Chyba C. F. and Phillips C. B. (2007) Europa. *Planets and Life* (Sullivan III W. T. and Baross J. A. eds.) Cambridge University Press 388-423.

Cody G. D., Boctor N. Z., Filley T. R., Hazen R. M., Scott J. H., Sharma A. and Yoder Jr. H. S. (2000) Primordial carbonylated iron-sulfur compounds and the synthesis of pyruvate. *Science* **289**, 1337-1339.

Corliss J. B. (1990) Hot springs and the origin of life. *Nature* **347**, 624.

Cox J. S. and Seward T. M. (2007) The reaction kinetics of alanine and glycine under hydrothermal conditions. *Geochim Cosmochim. Acta* **71**, 2264-2284.

Eder A. and Rode B. M. (1994) Influence of alkali- and alkaline-earth-metal cations on

the 'salt-induced peptide formation' reaction. *J. Chem. Soc. Dalton Trans.* 1125-1130.

Edwards K. J., Rogers D. R., Wirsen C. O. and McCollom T. M. (2003) Proteobacteria from the deep sea chemolithoautotrophic α- and γ- psychrophilic, neutrophilic, Fe-oxidizing. *Appl. Environ. Microbiol.* 69, 2906-2913.

Edwards K. J., Bach W. and McCollom T. M. (2005) Geomicrobiology in oceanography: microbe-mineral interactions at and below the seafloor. *TRENDS in Microbiology* 13, 449-456.

Edwards K. J., Becker K. and Colwell F. (2012) The deep dark energy biosphere: Intraterrestrial life on Earth. *Annu. Rev. Earth Planet. Sci.* 40, 551-568.

Edwards, K. J.; Backert, N.; Bach, W.; Becker, K.; Klaus, A.; Griffin, D. W.; Anderson, L.; Haddad, A. G.; Harigane, Y.; Campion, P. L.; Hirayama, H.; Mills, H. J.; Hulme, S. M.; Nakamura, K.; Jorgensen, S. L.; Orcutt, B.; Insua, T. L.; Park, Y. -S.; Rennie, V.; Salas, E. C.; Rouxel, O.; Wang, F.; Russel, J. A.; Wheat, C. G.; Sakata, K.; Brown, M.; Magnusson, J. L.; Ettlinger, Z. (2013) Mid-atlantic ridge microbiology: initiation of long-term coupled microbiological, geochemical, and hydrological experimentation within the seafloor at North Pond, western flank of the Mid-Atlantic Ridge *Integrated Ocean Drilling Program: Preliminary Reports* 336. d*oi*:10.2204/iodp.sd.14.05.2012.

Edwards, K. J.; Backert, N.; Bach, W.; Becker, K.; Klaus, A.; Griffin, D. W.; Anderson, L.; Haddad, A. G.; Harigane, Y.; Campion, P. L.; Hirayama, H.; Mills, H. J.; Hulme, S. M.; Nakamura, K.; Jorgensen, S. L.; Orcutt, B.; Insua, T. L.; Park, Y. -S.; Rennie, V.; Salas, E. C.; Rouxel, O.; Wang, F.; Russel, J. A.; Wheat, C. G.; Sakata, K.; Brown, M.; Magnusson, J. L.; Ettlinger, Z. (2012) Initiation of long-term coupled microbiological, geochemical, and hydrological experimentation within the seafloor at North Pond, western flank of the Mid-Atlantic Ridge. *Integrated Ocean Drilling Program: Preliminary Reports* 336. doi:10.2204/iodp.pr.336.2012

Ferris J. P., Hill Jr A. R., Liu R. and Orgel L. E. (1996) Synthesis of long prebiotic oligomers on mineral surfaces. *Nature* 381, 59-61.

Ferris J. P. (1992) Chapter 6 Chemical markers of prebiotic chemistry in hydrothermal systems. *Orig. Life Evol. Biosph.* **22**, 109-134.

Ferris J. P., Joshi P. C., Edelson E. H. and Lawless J. G. (1978) HCN: a plausible source of purines, phyrimidines and amino acids on the primitive earth. *J. Mol. Evol.*

11, 293-311.

Fisher A. T., Davis E. E., Hutnak M., Spiess V., Zuhlsdorff L., Cherkaoul A. Christiansen L., Edwards K. J., Macdonald R., Villinger H. Mottl M. J., Wheat C. G. and Becker K. (2003) Hydrothermal recharge and discharge across 50 km guided by seamounts on a young ridge flank. *Nature* 421, 618-621.

Fisher A. T. (2005) Marine hydrogeology: recent accomplishments and future opportunities. *Hydorogeol. J.* 13, 69-97.

Fisher C. R., Takai K. and Bris N. L. (2007) Hydrothermal vent ecosystems. *Oceanography* 20, 14-23.

Fisk M. R., Giovannoni S. J. and Thorseth I. H. (1998) Alteration of oceanic volcanic glass: textual evidence of microbial activity. *Science* 281, 978-980.

Fox S. W. and Harada K. (1958) Thermal copolymerization of amino acids to a product resembling protein. *Science* 128, 1214.

Furukawa Y., Sekine T., Oba M., Kakegawa T. and Nakazawa H. (2009) Biomolecule formation by oceanic impacts on early Earth. *Nature Geoscience* 2, 62-66.

Gao Q., Xu W., Xu Y., Wu D., Sun Y., Deng F. and Shen W. (2008) Amino acid adsorption on mesoporous materials: Influence of types of amino acids, modification of mesoporous materials, and solution conditions. *J. Phys. Chem. B* **112**, 2261-2267.

Harada K. and Fox S. W. (1964) The thermal copolymerization of amino acids common to protein. *Nature,* **201**, 355-356.

Holm N. G. (1992) Chapter 1 Why are hydrothermal systems proposed as plausible environments for the origin of life? *Orig. Life Evol. Biosph.* **22**, 5-14.

Holm N. G. and Andersson E. (2005) Hydrothermal simulation experiments as a tool for studies of the origin of life on Earth and other terrestrial planets: A review. *Astrobiology*, 5, 444-460.

Huber C. and Wächtershäuser G. (2003) A possible primordial peptide cycle. *Science* **301**, 938-940.

Huber C. and Wächtershäuser G. (1998) Peptides by Activation of Amino Acids with CO on (Ni,Fe)S Surfaces: Implications for the Origin of Life. *Science* **281**, 670-672.

Hulme S. M., Wheat C. G., Fryer P. and Mottl M. (2010) Pore water chemistry of the Mariana serpentinite mud volcanoes: A window to the seismogenic zone. *Geochem. Geophys. Geosyst*. **11**, 2009GC002674.

Imai E., Honda H., Hatori K., Brack A. and Matsuno K. (1999) Elongation of oligopeptides in a simulated submarine hydrothermal system. *Science* **283**, 831-833.

Irwin L. N. and Schulze-Makuch (2011) Aquatic life in perpetual darkness on an ice-covered water world like Europa. *Cosmic Biology: How life could evolve on other worlds* Springer Praxis Books, DPI 10.1007/978-1-4419-1647-1_8.

Kawamura K., Nishi T. and Sakiyama T. (2004) Consecutive elongation of alanine oligopeptides at the second tine range under hydrothermal conditions using a microfloe reactor system. *J. Am. Chem. Soc.* 127, 522-523.

Kelley D. S., Karson J. A., Blackman D. K., Früh-Green G. L., Butterfield D. A., Lilley M. D., Olson E. J., Schrenk M. O., Roe K. K., Lebon G. T., Rivizzigno P. and the AT3-60 Shipboard Party (2001) An off-axis hydrothermal vent field near the Mid-Atlantic Ridge at 30°N. *Nature* **412**, 145-149.

Kelley D. S., Karson J. A., Fruh-Green G. L., Yoerger D. R., Shank T. M., Butterfield D. A., Hayes J. M., Schrenk M. O., Olson E. J., Proskurowski G., Jakuba M., Bradley A., Larson B., Ludwig K., Glickson D., Buckman K., Bradley A. S., Brazelton W. J., Roe K., Elend M. J., Delacour A., Bernasconi S. M., Lilley M. D., Baross J. A., Summons R. E. and Sylva S. P. (2005) A serpentinite-hosted ecosystem: The lost city hydrothermal field. *Science* **307**, 1428-1434.

Kitadai N., Yokoyama N. and Nakashima S. (2009) ATR-IR spectroscopic study of L-lysine adsorption on amorphous silica. *J. Colloid. Interface Sci.* **329**, 31-37.

Konn C., Charlou J. L., Donval J. P., Holm N. G., Dehairs F. and Bouillon S. (2009) Hydrocarbons and oxidized organic compounds in hydrothermal fluids from Rainbow and Lost City ultramafic-hosted vents. *Chemical Geology* **258**, 299-314.

Lahav N., White D. and Chang S. (1978) Peptide formation in the prebiotic era: thermal condensation of glycine in fluctuating clay environments. *Science* **201**, 67-69.

Lambert J. (2008) Adsorption and polymerization of amino acids on mineral surfaces: A review. *Orig. Life Evol. Biosph.* **38**, 211-242.

Lang S. Q,, Butterfield D. A., Schulte M., Kelley D. S. and Lilley M. D. (2010) Elevated concentration of formate, acetate and dissolved organic carbon found at the Lost City hydrothermal field. *Geochim. Cosmochim. Acta* **74**, 941-952.

Lawless J. G. and Levi N. (1979) The role of metal ions in chemical evolution: polymerization of alanine and glycine in a cation-exchanged clay environment. *Journal of Molecular Evolution,* **13**, 281-286.

Lawrence L. and Moore W. (1951) Kinetics of the hydrolysis of simple glycine peptides. *J. Am. Chem. Soc.* **73**, 3973-3977.

Lemke K. H., Rosenbauer R. J., Bird D. K. (2009) Peptide synthesis in early earth hydrothermal systems. *Astrobiology* **9**, 141-146.

Lever M. A., Rouxel O., Alt J. C., Shimizu N. Ono S., Coggon R. M., Shanks III W. C., Lapham L., Elvert M., Prieto-Mollar X., Hinrichs K., Inagaki F. and Teske A. (2013) Evidence for microbial carbon and sulfur cycling in deeply buried ridge flank basalt. *Science* 339, 1305-1308.

Li J. and Brill T. B. (2003) Spectroscopy of hydrothermal reactions. 27. Simultaneous determination of hydrolysis rate constants of glycylglycine to glycine and glycylglycine-Diketopiperazine equilibrium constants at 310-330°C and 275 bar. *J. Phys. Chem. A* **107**, 8575-8577.

Macleod G., McKeown C., Hall A. J. and Russell M. J. (1994) Hydrothermal and oceanic pH conditions of possible relevance to the origin of life. *Orig. Life Evol. Biosph.* **24**, 19-41.

Marshall W. L. (1994) Hydrothermal synthesis of amino acids. *Geochim. Cosmochim. Acta* **58**, 2099-2106.

Martin W., Baross J., Kelley D. and Russell M. J. (2008) Hydrothermal vents and the origin of life. *Nature Rev. Microbiol.* **6**, 805-814.

Mason O.U.. Stingl U., Whilhelm L. J., Moeseneder M. M., Di Meo-Savoie C. A., Fisk M. R. and Giovannoni S. J. (2007) The phylogeny of endolithic microbes associated with marine basalts. *Enviromental Microbiology* 9, 2539-2550.

McCollum T. M. (1999) Methanogenesis as a potential source of chemical energy for primary biomass production by autotrophic organisms in hydrothermal systems on Europa. *J. Geophys. Res.* 104, 30729-30742.

McCollom T. M. and Bach W. (2009) Thermodynamic constraints on hydrogen generation during serpentinization of ultramafic hosted deep-sea hydrothermal systems. *Astrobiology*, **7**, 933-950.

Meng M., Stievano L. and Lambert J. (2004) Adsorption and thermal condensation mechanism of amino acids on oxide supports. 1. Glycine on silica. *Langmuir*, **20**, 914-923.

Miller S. L. (1953) A production of amino acids under possible primitive earth conditions. *Science* **117**, 528-529.

Mitsuzawa S. and Yukawa T. (2004) A reaction network for triglycine synthesis under hydrothermal conditions. *Bull. Chem. Soc. Jan.* **77**, 965-973.

Mottl M. J., Komor S. C., Fryer P. and Moyer C. L. (2003) Deep-slab fluids fuel extremophilic archaea on a Mariana forearc serpentinite mud volcano: ocean drilling program Leg 195. *Geochem. Geophys. Geosys.* 4, doi: 10.1029/2003GC000588

Mojzsis S. J., Harrison T. M. and Pidgeon (2001) Oxygen-isotope evidence from ancient zircons for liquid water at the Earth's surface 4,300Myr ago. *Nature* **409**, 178-181.

Mojzsis S. J.,Arrhenius G., McKeegan K. D., Harrison T. M., Nutman A. P. and Friend C. R. L. (1996) *Nature* **384**, 55-59.

Ohara S., Kakegawa T. and Nakazawa H. (2007) Pressure effects on the abiotic polymerization of glycine. *Orig. Life Evol. Biosph.* **37**, 215-223.

Orcutt B. N., Sylvan J. B., Knab N. J. and Edwards K. J. (2011) Microbial ecology of the dark ocean above, at, and below the seafloor. *Microbiology abd molecular biology reviews* 75, 361-422.

Oró J. and Guidry C. L. (1960) A novel synthesis of polypeptides. *Nature* **186**, 156-157.

Oró J. (1960) Synthesis of adenine from ammonium cyanide. *Biochem. Bioph. Res. Commun.* **2**, 407-412.

Oró J. and Kimball A. P. (1961) Synthesis of purines under possible primitive Earth conditions. 1. Adenine from hydrogen cyanide. *Arch. Biochem. Biophys.* **94**, 221-227.

Oró J. and Kimball A. P. (1962) Synthesis of purines under possible primitive Earth conditions. 2. Purine intermediates from hydrogen cyanide. *Arch. Biochem. Biophys.* **96**, 293-313.

Parbhakar A., Cuadros J. Sephton M. A., Dubbin W., Coles B. J. and Weiss D. (2007) Adsorption of L-lysine on montmorillonite. *Colloids and Surfaces A: Physicochem. Eng. Aspects* **307**, 142-149.

Parkes R. J., Cragg B. A., Bale S. J., Getliff J. M., Goodman K., Rochelle P. A., Fry J. C., Welghtman A. J. and Harvey S. M. (1994) Deep bacterial biosphere in pacific ocean sediments. *Nature* 371, 410-413.

Pizzarello S. (2004) Chemical evolution and meteorites: an update. *Orig. Life Evol. Biosph.* **34**, 25-34.

Plankensteiner K., Righi A. and Rode B. M. (2002) Glycine and diglycine as possible catalytic factors in the prebiotic evolution of peptides. *Orig. Life Evol. Biosph.* **32**, 225-236.

Ponnamperuma C. Shimoyama A. and Friebele E. (1982) Clay and the origin of life. *Orig. Life Evol. Biosph.* **12**, 9-40.

Qian Y., Engel M. H., Macko S. A., Carpenter S. and Deming J. W. (1993) Kinetics of peptide hydrolysis and amino acid decomposition at high temperature. *Geochim Cosmochim. Acta* **57**, 3281-3293.

Radzicka A. and Wolfenden R. (1996) Rates of uncatalyzed peptide bond hydrolysis in neutral solution and the transition state affinities of proteases. *J. Am. Chem. Soc.* **118**, 6105-6109.

Rode B. M. and Schwendinger Y. (1990) Copper-catalyzed amino acid condensation in water a simple possible way of prebiotic peptide formation. *Orig. Life Evol. Biosph.* **20**, 401-410.

Remko M. and Rode B. M. (2000) Bivalent cation binding effect on formation of peptide bond. *Chemical Physics Letters*, **316**, 489-494.

Rode B. M. (1999) Peptides and the origin of life. *Peptides* **20**, 773-786.

Rode B. M. and Schwendinger M. G. (1990) Copper-catalyzed amino acid condensation in water – a simple possible way of prebiotic peptide formation. *Orig. Life Evol. Biosph.* **20**, 401-410.

Russell M. J. and Hall A. J. (1997) The emergence of life from iron monosulphide bubbles at a submarine hydrothermal redox and pH front. *J. Geol. Soc.* **154**, 377-402.

Russell M. J. (2003) The importance of being alkaline. *Science* **302**, 580-581.

Saetia S., Liedl K. R., Eder A. H. and Rode B. M. (1993) Evaporation cycle experiments – A simulation of salt-induced peptide synthesis under possible prebiotic conditions. *Orig. Life Evol. Biosph.* **23**, 167-176.

Sakata K., Kitadai N. and Yokoyama T. (2010) Effects of pH and temperature on dimerization rate of glycine: Evaluation of favorable environmental conditions for chemical evolution of life. *Geochim Cosmochim. Acta* **74**, 6841-6851.

Sakata K., Yabuta H. and Kondo T. Effects of metal ions and pH on the formation and decomposition rates of di- and tri-peptides in aqueous solution. *Geochemical Journal*, in press.

Sanchez R. A., Ferris J. P. and Orgel L. E. (1967) Studies in prebiotic synthesis II. Synthesis of purine precursors and amino acids from aqueous hydrogen cyanide. *J. Mol. Biol.* 30, 223-253.

Schwendinger M. G. and Rode B. M. (1989) Possible role of copper and sodium chloride in prebiotic evolution of peptides. *Analytical Sciences*, **5**, 411-414.

Schwendinger M. G. and Rode B. M. (1991) Salt-induced formation of mixed peptides under possible prebiotic conditions. *Inorgica Chimica Acta* 186, 247-251.

Schwendinger M. G. and Rode B. M. (1992) Investigation on the mechanism of the salt-induced peptide formation. *Orig. Life Evol. Biosph.* **22**, 349-359.

Shapiro R. (1995) The prebiotic role of adenine: a critical analysis. *Orig. Life Evol. Biosph.* **25** 83-98.

Shibuya T., Komiya T., Nakamura K., Takai K. and Maruyama S. (2010) Highly alkaline, high-temperature hydrothermal fluids in the early Archean ocean. *Precambrian Res.* 182, 230-238.

Singer E., Emerson D., Webb E. A. and Edwards K. J. (2010) Genomic insights into the first cultured member of the Zetaproteobacteria, the Fe-oxidizing Mariprofundus ferrooxydans PV-1. *ISME*, Seattle.

Son H. L., Suwannachot Y. Bujdak J. and Rode B. M. (1998) Salt-induced peptide formation from amino acids in the presence of clays and related catalysts. *Inorgica Chimica Acta* 272, 89-94.

Stievano L., Piao L. Y., Lopes I. Meng M. Costa D. and Lambert J. (2007) Glycine and lycine adsorption and reactivity on the surface of amorphous silica. *Eur. J. Mineral.* **19**, 321-331.

Suwannachot Y. and Rode B. M. (1999) Mutual amino acid catalysis in salt-induced peptide formation supports this mechanism's role in prebiotic peptide evolution. *Orig. Life Evol. Biosph.* **29**, 463-471.

Takai K., Nakamura K., Toki K., Tsunogai U., Miyazaki M., Miyazaki J., Hirayama H., Nakagawa S., Nunoura T. and Horikoshi K. (2008) Cell proliferation at 122°C and isotopically heavy CH4 production by hyperthermophilic methanogen under high-pressure cultivation. *PNAS* **105**, 10949-10954.

Tauler R. and Rode B. M. (1990) Reactions of Cu(II) with glycine and glycylglycine in aqueous solution at high concentration of sodium chloride. *Inorgica Chimica Acta* 173, 93-98.

Tivey M. K. (2007) Generation of seafloor hydrothermal vent fluids and associated mineral deposits. *Oceanography* **20**, 50-65.

Tivey M. K., Humphris S. E., Thompson G. and Hannington M. D. (1995) Deducing patterns of fluid flow and mixing within the TAG active hydrothermal mound using mineralogical and geochemical data. *J. Geophys. Res.* **100**, 12527-12555.

Yanagawa H. and Kobayashi K. (1992) Chapter 8 An experimental approach to chemical evolution in submarine hydrothermal systems. *Orig. Life Evol. Biosph.* **22**, 147-159.

Yanagawa H., Makino Y., Sato K., Nishizawa K. and Egami F. (1984) Novel formation of alpha-amino-acids from alpha-oxo acids and anmonia in an aqueous-medium. *Orig. Life Evol. Biosph.* **14**, 163-169.

Wheat C. G., Elderfield H., Mottl M. J. and Monnin C. (2000) Chemical composition of basement fluids within an oceanic ridge flank: Implications for along-strike and across-strike hydrothermal circulation. *Journal of Geophysical Research* 105, 13437-13447.

Wheat C. G., Fryer P., Takai K. and Hulme S. (2010) South Chamorro seamount. *Oceanography* 23, 174-175.

Whitman W. B., Coleman D. C. and Wiebe W. J. (1998) Prokaryotes: The unseen majority. *Proc. Natl. Acad. Sci.* 95, 6578-6583.

Chapter 2

Effects of pH and temperature on dimerization rate of glycine: Evaluation of favorable environmental conditions for chemical evolution of life

Sakata K., Kitadai N. and Yokoyama T. Effects of pH and temperature on dimerization rate of glycine: Evaluation of favorable environmental conditions for chemical evolution of life. Geochimica et Cosmochimica Acta 74 (2010) 6841–6851.

2.1. Introduction

Chemical evolution of life is the process by which complex organic molecules were formed from simpler organic and inorganic molecules through chemical reactions in Earth's early history. Hydrothermal vents have been suggested as an environment where chemical evolution may have occurred (e.g., Corliss, 1990; Holm, 1992; Macleod et al., 1994; Russell and Hall, 1997; Russell, 2003; Martin et al., 2008). A hydrothermal vent was first discovered at Galapagos Rift in 1977 (Corliss et al., 1979), and to date, about 150 hydrothermal activities have been found at various locations on the seafloor. In many cases seawater percolates into oceanic crust in these hydrothermal vents and is heated, reacts with surrounding rocks, and the resultant hot reductive fluid issues from the seafloor (Tivey, 2007). The temperatures of the hydrothermal fluids can reach about 400 °C, in contrast to a typical temperature of 2 °C for deep seawater (Tivey et al., 1995). The pH of the hydrothermal fluids ranges from less than 1 to 11. pH values of 2−4 are most common (Fisher et al., 2007; Tivey, 2007), but values as high as 10−11 have been reported at the Lost City site (Kelley et al., 2001, 2005). At hydrothermal vents, organic matter such as aliphatic hydrocarbon, aromatic carbon, carboxylic acids (Konn et al., 2009), formate, and acetate (Lang et al., 2010), which might act as primary materials of life, have been found. In addition to the possibility that the primary materials were formed by hydrothermal activities, it has been proposed that meteorites are a potential source of organic matters (Chyba and Sagan, 1992; Pizzarello, 2004). Experimental studies that address the syntheses of amino acids and carboxylic acid and the polymerization of amino acids under hydrothermal conditions have also been conducted (e.g., Oró and Guidry, 1960; Ferris 1992; Marshall, 1994; Imai et al., 1999; Cody et al., 2000; Lemke et al., 2009).

Among various reactions that might occur during the chemical evolution of life, polymerization of amino acids (formation of peptide bonds) is one of the most important reactions because amino acids are essential components of proteins, which are fundamental to life. An amino acid consists of a basic amino group, an acidic carboxyl group, and a characteristic side chain. The degree of protonation of these functional groups changes depending on solution pH ($-NH_3^+ \leftrightarrow -NH_2 + H^+$, $-COOH \leftrightarrow -COO^- + H^+$), and accordingly, the net charge of the amino acid molecule changes. Fig. 2.1 shows the changes in the dissociation states of glycine (Gly: NH_2-CH_2-COOH) as a function of pH. Amino acids generally show the highest polymerization reactivity

under an anionic state (Zamaraev et al., 1997; Bujdák and Rode, 1999a). Because the molar fraction of the anionic state increases with pH, the polymerization rates of amino acids are expected to be higher at higher pH. On the other hand, the hydrolysis of peptide bonds is also accelerated at higher pH because OH^- catalyzes the hydrolysis (Smith and Hansen, 1998; Zahn, 2004). As a result of these conflicting mechanisms, it is likely that an optimum pH for polymerization exists. Although experiments on the polymerization of amino acids have been conducted under several different pH (e.g., Rode and Schwendinger, 1990; Zamaraev et al., 1997; Huber and Wächtershäuser, 1998), the pH range was limited and experimental conditions differed. Given that there are large variations in pH and temperature in natural environments, it is important to examine the polymerization rates of amino acids under a wide range of pH and temperature to consider favorable environments for the chemical evolution of life.

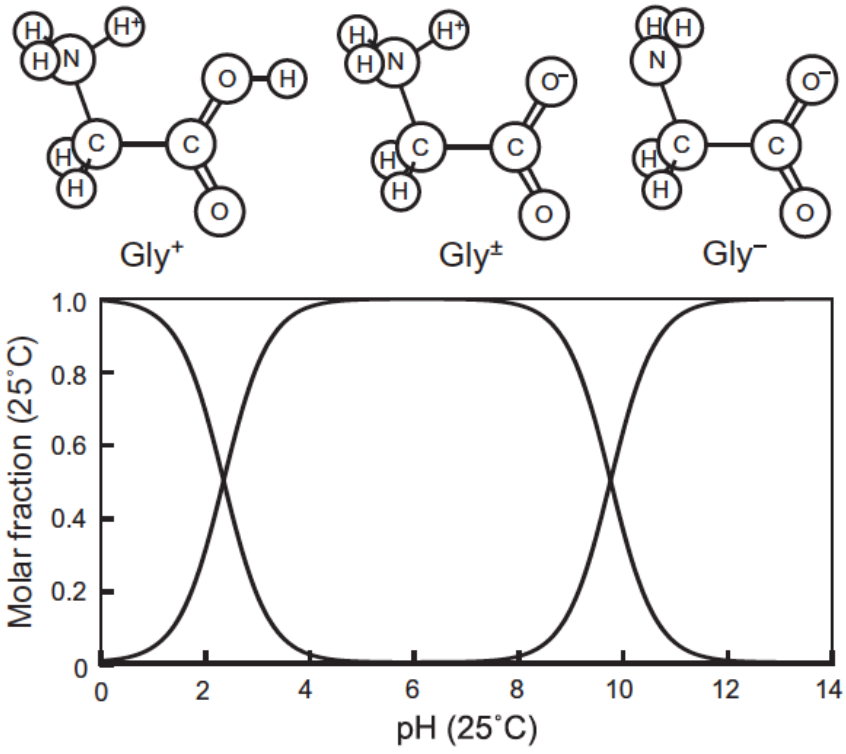

Fig. 2.1. Changes in the molar fractions of different dissociation states of Gly as function of pH at 25 °C, determined on the basis of published dissociation constants (Marshall and Franck, 1981; Goldberg et al., 2002; Clarke et al., 2005).

In this study, hydrothermal experiments were conducted at 140 °C for pH values ranging from 3.1 to 10.9. At pH 9.8, the experiments were also performed at

temperatures ranging from 120 to 180 °C. Gly was used because it is the simplest amino acid, and it is often the most abundant product in hydrothermal synthesis experiments of amino acids (Yanagawa and Kobayashi, 1992; Marshall, 1994). Fig. 2.2 shows the reaction pathways for the dimerization of Gly, which dimerizes to glycilglycine (GlyGly) and GlyGly further reversibly changes to diketopiperazine (DKP) (Qian et al., 1993). First, we determined the pH dependences of the reaction rates of Gly to GlyGly (k_1), GlyGly to Gly (k_{-1}), GlyGly to DKP (k_2), and DKP to GlyGly (k_{-2}). The dimerization rate of Gly significantly changed with pH. Since Gly has three dissociation states (Gly^+, $Gly^{\pm}$, and Gly^-) and the molar fraction of each dissociation state changes with pH, the dimerization rates were also evaluated for each dissociation state. We show that the pH dependence of the dimerization rate of Gly can be explained by the change in dissociation states of Gly and discuss favorable pH and temperature values for the dimerization of Gly.

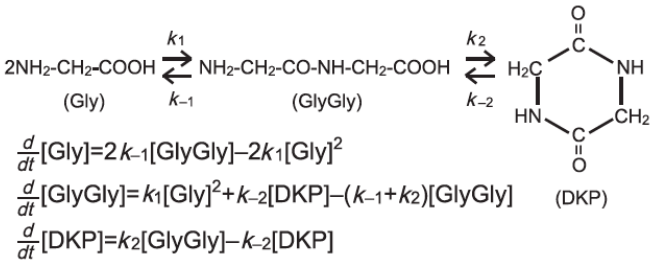

Fig. 2.2. Reaction pathways between Gly, GlyGly, and DKP and relevant rate equations. k_1, k_{-1}, k_2 and k_{-2} are the rate constants for the polymerization of Gly, decomposition of GlyGly, formation of DKP, and decomposition of DKP, respectively.

2.2. Methods

Powdered Gly (99.9%; Peptide Institute) was dissolved in deionized water (18.2 MΩ) to prepare solutions having Gly concentrations of 100 mM and 200 mM. The 100 mM Gly solution had pH 6.0. NaOH was added to the 200 mM Gly solutions to make 100 mM Gly solutions having pH 7.1, 8.4, 9.0, 9.4, 9.8, 10.2, 10.4, and 10.9. For the acid pH range, HCl was added to the 200 mM Gly solutions to make 100 mM Gly solutions having pH 5.0, 3.9, and 3.1. Then 8.0 ml of each solution was inserted into a 10-ml Teflon vessel and shielded in a screw-capped stainless steel outer vessel. The solutions were then heated in an electric oven at 140 °C for 1–14 days. The pH 9.8 solutions were also heated at 120, 160, and 180 °C for 1–5 days to evaluate the temperature dependence of the reaction rates. Before and after the experiment, the pH of

the solutions was measured at 25 °C by a pH meter (B-212; HORIBA). Changes in the pH values before and after the heating were small (<5.0% increase).

The concentrations of Gly, GlyGly, and DKP were determined by a liquid chromatograph (ICA-2000; TOA DKK) equipped with a UV detector (UV-2075; Jasco) operated at a wavelength of 200 nm. In the chromatograph measurement, a reverse-phase type column (Hydrosphere C18; YMC; Ohara et al., 2007) was used at 37 °C. A 10 mM $C_6H_{13}SO_3Na$ solution with pH 2.5 was used as an eluent (adjusted by H_3PO_4; Bujdák and Rode, 1999b), at a flow rate of 1.0 ml min^{-1}. Measurement errors in the concentrations of Gly, GlyGly, and DKP were estimated to be less than 3.0%.

2.3. Results and Discussion

2.3.1. Reaction rate constants without considering dissociation states

Fig. 2.3 shows a chromatogram of the solution obtained after heating at 140 °C for 3 days at pH 9.8. The signals of Gly, GlyGly, and DKP are apparent. A trimer of Gly and potential decomposition components of Gly including formic acid, acetic acid, and glycolic acid can be detected in a chromatogram, but they were not. Fig. 2.4 shows changes in the amount of GlyGly under pH 3.1−10.9 with experimental time. With increasing pH, the rate of the formation of GlyGly increased from pH 5.0 to 9.8 and then decreased from pH 9.8 to 10.9. Note that the heating time at the highest pH values (Fig. 2.4c) is shorter than that of the lower ones (Figs. 2.4a and 2.4b). Fig. 2.5 shows changes in the amount of DKP under pH 3.1−10.9 with time. With increasing pH, the rate of the formation of DKP increased from pH 5.0 to 8.4 and then decreased as pH increased.

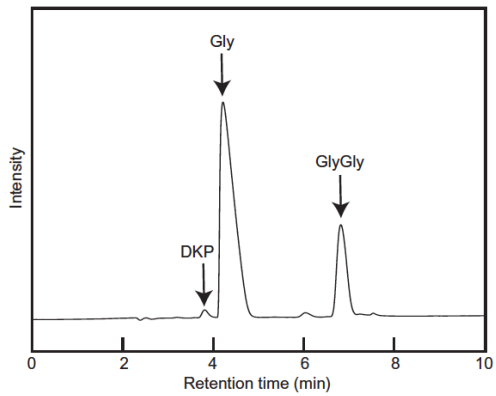

Fig. 2.3. A chromatogram obtained after heating the Gly solution at pH 9.8 for 2 days at 140 °C.

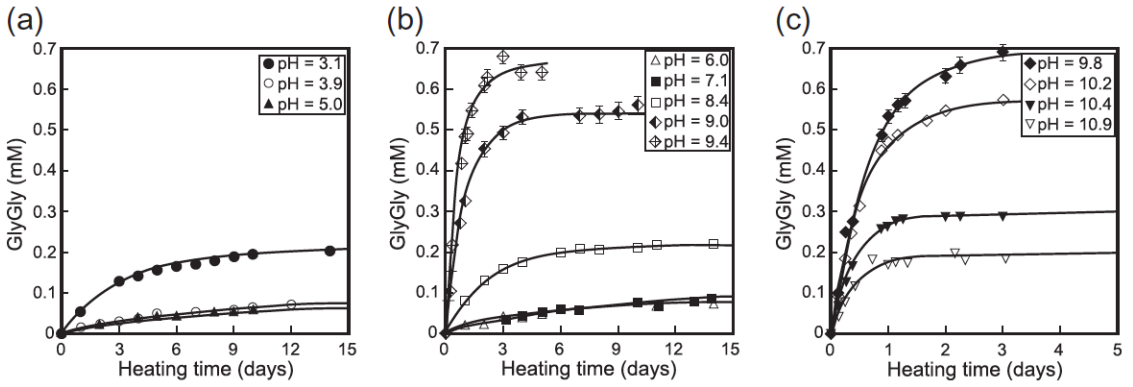

Fig. 2.4. Changes in the concentration of GlyGly with time in the hydrothermal reaction of Gly at 140 °C under (a) pH 3.1-5.0, (b) pH 6.0-9.4, and (c) pH 9.8-10.9. Solid lines are the results of fitting to determine the rate constants of the formation of GlyGly.

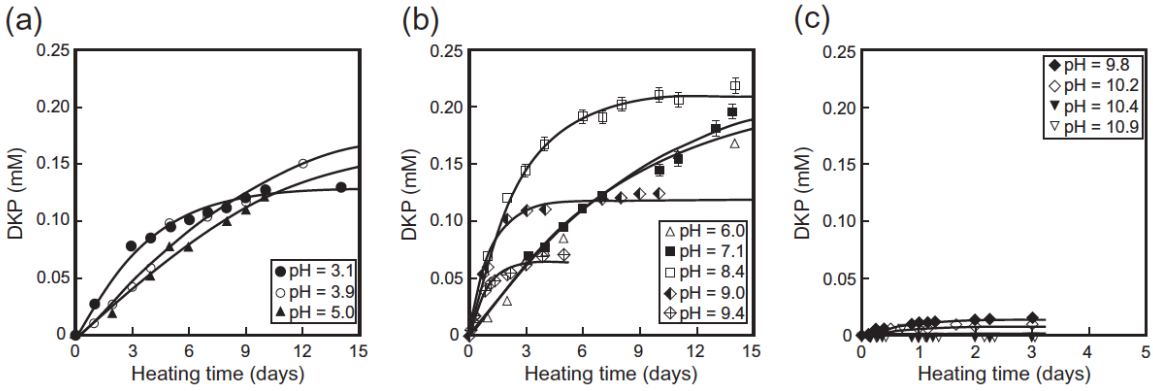

Fig. 2.5. Changes in the concentration of DKP with time in the hydrothermal reaction of Gly at 140 °C under (a) pH 3.1-5.0, (b) pH 6.0-9.4, and (c) pH 9.8-10.9. Solid lines are the results of fitting to determine the rate constants of the formation of DKP.

To analyze the experimental results, we need to consider the following reactions (Fig. 2.2): Gly to GlyGly (second-order reaction; k_1), GlyGly to DKP (first-order reaction; k_2), GlyGly to Gly (first-order reaction; k_{-1}), and DKP to GlyGly (first-order reaction; k_{-2}) (Qian et al., 1993; Li and Brill, 2003), where k_1, k_{-1}, k_2 and k_{-2} are the rate constants. The rate equations for these reactions can be written as (Fig. 2.2):

$$\frac{d}{dt}[\mathrm{Gly}] = 2k_{-1}[\mathrm{GlyGly}] - 2k_1[\mathrm{Gly}]^2 \qquad (1)$$

$$\frac{d}{dt}[\mathrm{GlyGly}] = k_1[\mathrm{Gly}]^2 + k_{-2}[\mathrm{DKP}] - (k_{-1} + k_2)[\mathrm{GlyGly}] \qquad (2)$$

$$\frac{d}{dt}[\mathrm{DKP}] = k_2[\mathrm{GlyGly}] - k_{-2}[\mathrm{DKP}] \qquad (3)$$

To obtain the rate constants, the above rate equations were fitted to the experimental results by the least-squares method using the numerical software Scilab. The results of fitting for the formation of GlyGly and DKP are shown in Figs. 2.4 and 2.5, respectively, and the rate constants obtained are plotted against pH in Fig. 2.6. Errors were estimated from the maximum error in concentration measurements (3%), and the adjusted fitting results were evaluated. All of the rate constants changed with pH, and the rate constant of the polymerization of Gly (k_1) reached a maximum at about pH 9.8 (Fig. 2.6a).

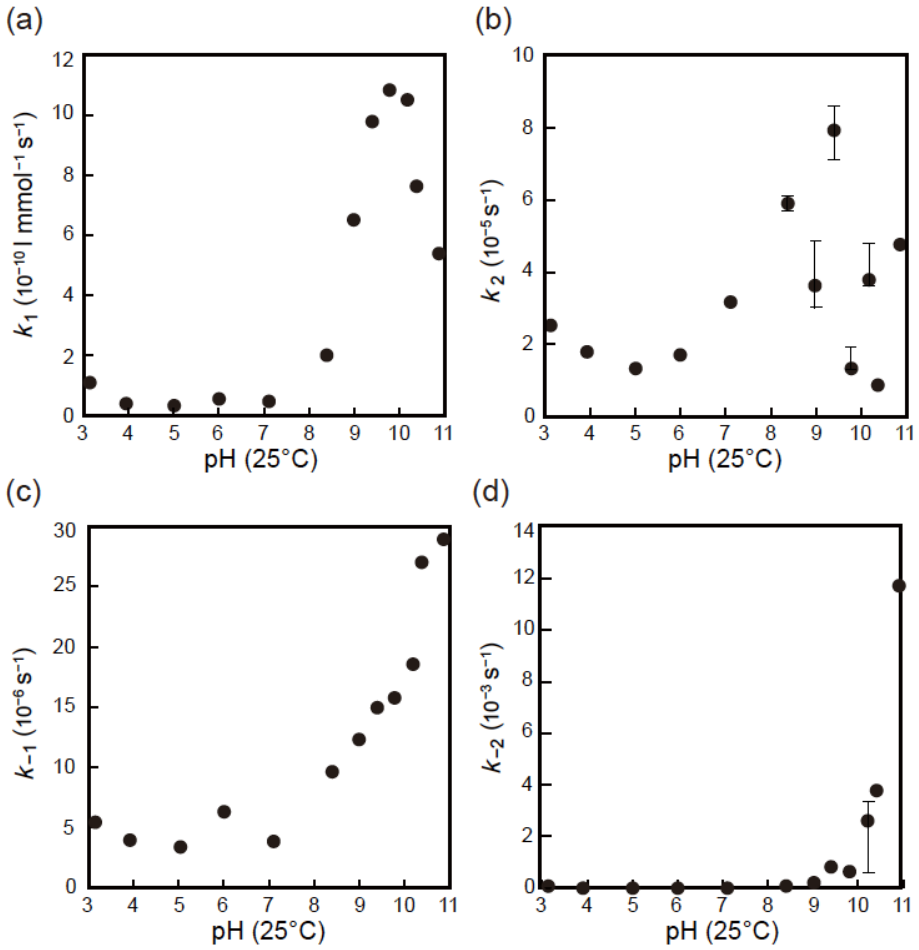

Fig. 2.6. Rate constants as function of pH (25 °C) for the reactions of (a) Gly to GlyGly (k_1), (b) GlyGly to DKP (k_2), (c) GlyGly to Gly (k_{-1}), and DKP to GlyGly (k_{-2}).

Figs. 2.7a, 2.7b, 2.7c, and 2.7d are Arrhenius plots of k_1, k_{-1}, k_2, and k_{-2} at pH 9.8, respectively. The activation energies obtained were 88, 93, 82, and 134 kJ mol^{-1} for the reactions of Gly to GlyGly, GlyGly to DKP, GlyGly to Gly, and DKP to GlyGly, respectively.

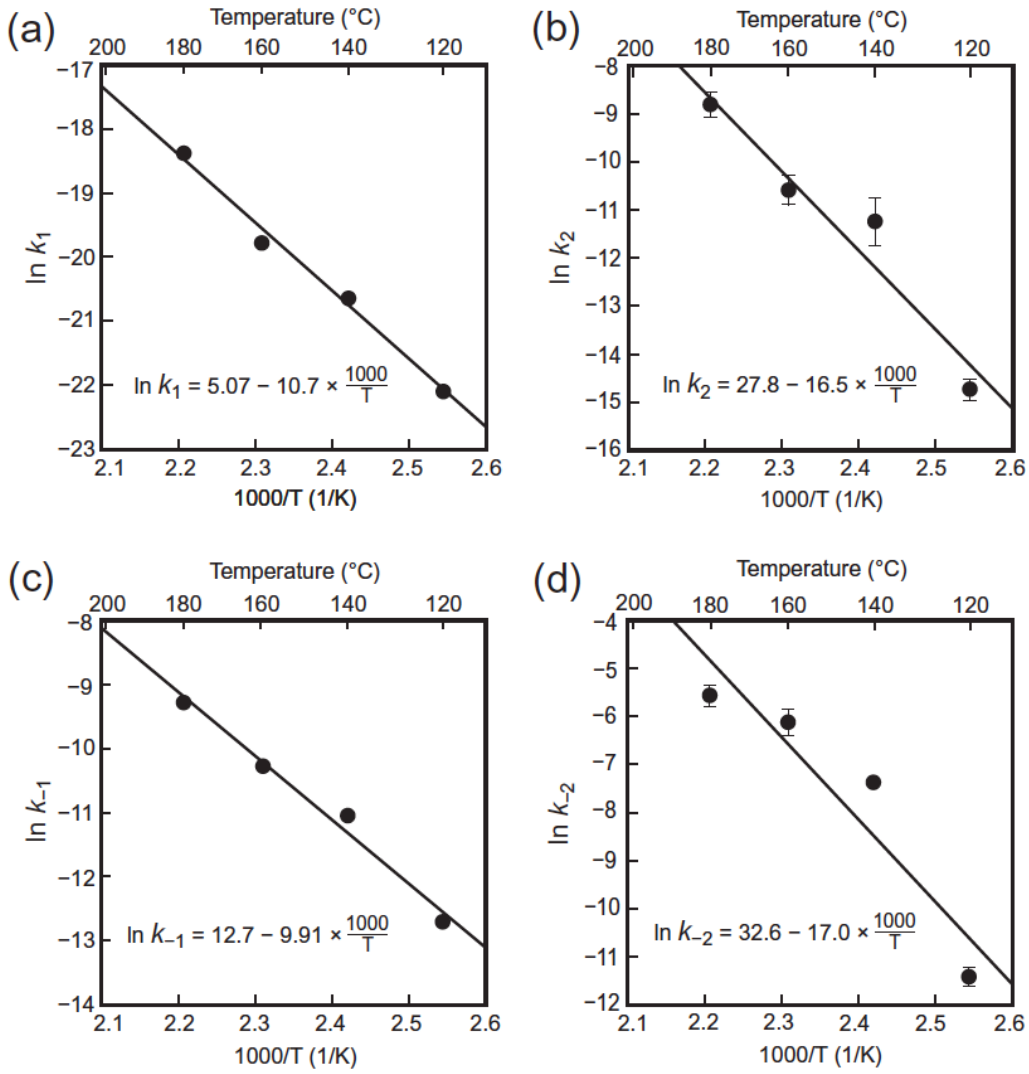

Fig. 2.7. Arrhenius plots for the reactions of (a) Gly to GlyGly (k_1), (b) GlyGly to DKP (k_2), (c) GlyGly to Gly (k_{-1}), (d) DKP to GlyGly (k_{-2}).

2.3.2. Reaction rate constants considering dissociation states

Gly has three dissociation states (Gly^+, $Gly^\pm$, and Gly^-), and GlyGly also has three dissociation states ($GlyGly^\pm$, $GlyGly^-$, and $GlyGly^+$). This means that the reaction of Gly + Gly → GlyGly can be separated into several reactions, such as $Gly^+ + Gly^- \rightarrow GlyGly^\pm$ and $Gly^\pm + Gly^- \rightarrow GlyGly^-$. To evaluate the rates of individual reactions, the

molar fractions of each dissociation state during the experiment need to be known. In our experiment, pH was adjusted at 25 °C and the solution was heated to 140 °C. The pH dependence of the molar fractions of each dissociation state of Gly at 140 °C can be evaluated from the following equations:

$$[H^+][OH^-] = K_w \quad (4)$$

$$[Gly^+] + [Gly^-] + [Gly^\pm] = [Gly] \quad (5)$$

$$K_a = \frac{[Gly^\pm][H^+]}{[Gly^+]} \quad (6)$$

$$K_{a'} = \frac{[Gly^-][H^+]}{[Gly^\pm]} \quad (7)$$

K_w in Eq. (4) is the dissociation constant of water at 140 °C, determined from the known temperature dependence of K_w (Marshall and Franck, 1981). Eq. (5) indicates that the sum of each dissociation state of Gly is equal to total concentration of Gly (= 100 mM). The total concentration of Gly was approximately constant during the hydrothermal experiment because the amounts of GlyGly and DKP formed in the experiment were very small as compared with that of Gly. Eqs. (6) and (7) are related to the reactions of $Gly^+ \leftrightarrow Gly^\pm + H^+$ and $Gly^\pm \leftrightarrow Gly^- + H^+$, respectively. K_a and $K_{a'}$ at 140 °C were calculated by the van't Hoff model using the standard partial molar heat capacity (−120.9 J K^{-1} mol^{-1} for Eq. (6) and −172.9 J K^{-1} mol^{-1} for Eq. (7)), enthalpy at 25 °C (4.54 kJ mol^{-1} for Eq. (6) and 44.4 kJ mol^{-1} for Eq. (7)), and dissociation constant at 25 °C ($10^{-2.35}$ for Eq. (6) and $10^{-9.78}$ for Eq. (7)) (Clarke et al., 2005). The pH dependence of the dissociation states of Gly at 140 °C calculated from Eqs. (4)–(7) differs from that at 25 °C (Fig. 2.8). The conservation of charge equation can be used to evaluate how the pH, which was adjusted at 25 °C, changes as the temperature increases to 140 °C:

$$[Gly^+] + [Na^+] + [H^+] = [Gly^-] + [OH^-] \quad (8)$$

Because the amount of NaOH added to the solution is known, the concentration of Na^+ is known. By combining Eqs. (4)–(8), the changes in pH and the dissociation states of Gly with increasing temperature could be evaluated, and some examples are shown in Fig. 2.8 (arrows). The molar fractions of each dissociation state of GlyGly at 140 °C were determined in the same manner. Dissociation constants for the reactions of $GlyGly^+ \rightarrow GlyGly^\pm + H^+$ and $GlyGly^\pm \rightarrow GlyGly^- + H^+$ at 140 °C were calculated by the van't Hoff model using the standard partial molar heat capacities (−128 J K^{-1} mol^{-1}

and −16 J K^{-1} mol^{-1}), enthalpies at 25 °C (0.11 kJ mol^{-1} and 43.4 kJ mol^{-1}), and dissociation constants at 25 °C ($10^{-3.140}$ and $10^{-8.265}$) (Goldberg et al., 2002). The molar fractions of each dissociation state of Gly and GlyGly determined in this manner are used in the following discussion.

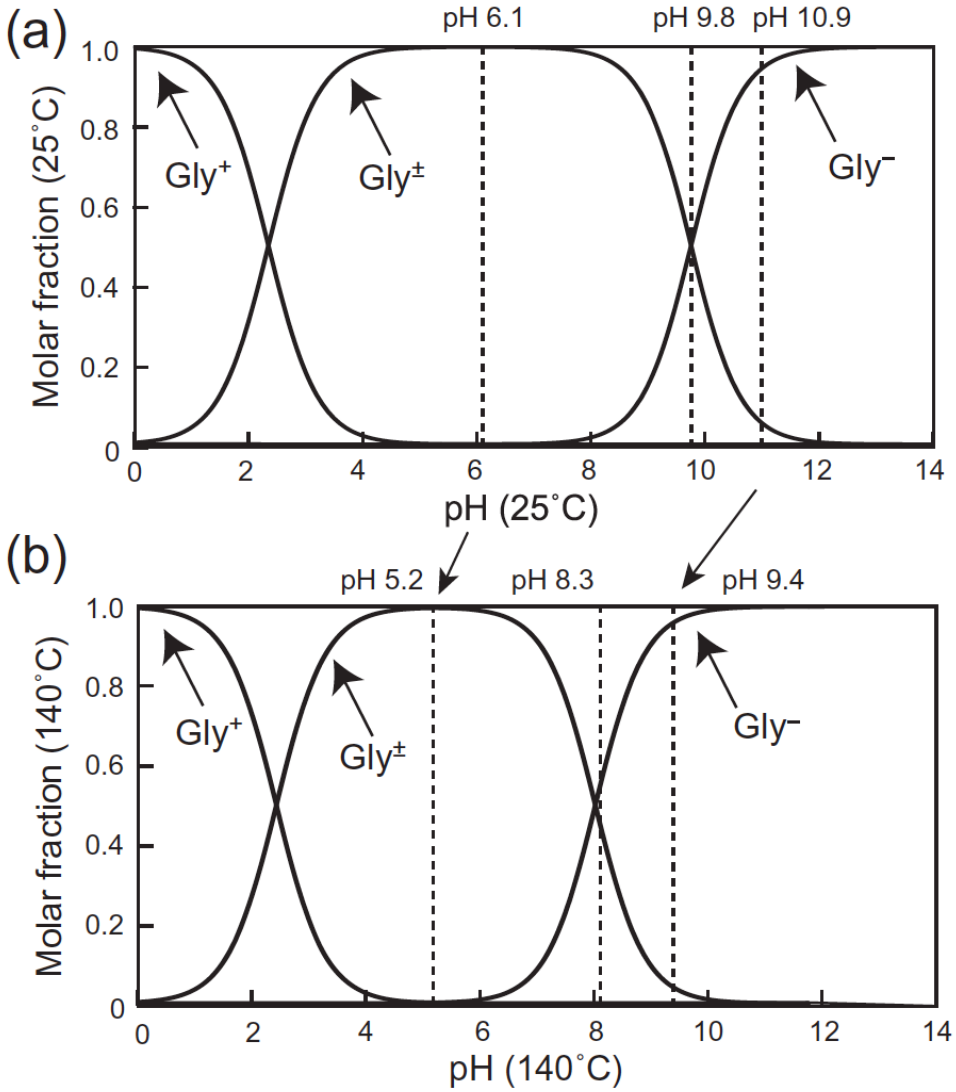

Fig. 2.8. Comparison of the pH dependences of the molar fractions of different dissociation states of Gly at (a) 25 °C and (b) 140 °C.

The rate of dimerization of Gly reached a maximum at about pH 9.8 (Fig. 2.6a). In alkaline pH, Gly is mainly present as $Gly^{\pm}$ and Gly^{-}, and the amount of Gly^{+} is approximately zero (<0.1%) (Fig. 2.8b). Likewise, GlyGly is mainly present as $GlyGly^{\pm}$ and $GlyGly^{-}$, and the amount of $GlyGly^{+}$ is approximately zero. DKP does not change its protonation state depending on pH. Therefore, in alkaline solution, the reaction

pathways involving Gly, GlyGly, and DKP can be reasonably written by the combination of $Gly^{\pm}$, Gly^{-}, $GlyGly^{\pm}$, $GlyGly^{-}$, and DKP. We focused on the reactivity of these chemical species to evaluate the fast dimerization of Gly at about pH 9.8.

First, we examined the reaction of Gly + Gly → GlyGly. The overall dimerization of Gly can be separated into the following three reactions: $Gly^{\pm} + Gly^{\pm} \rightarrow GlyGly^{\pm} + H_2O$ ($k_{1,a}$), $Gly^{\pm} + Gly^{-} \rightarrow GlyGly^{-} + H_2O$ ($k_{1,b}$), and $Gly^{-} + Gly^{-} \rightarrow GlyGly^{-} + OH^{-}$ ($k_{1,c}$), where $k_{1,a}$, $k_{1,b}$, and $k_{1,c}$ are the rate constants (Fig. 2.9a). The change in total concentration of GlyGly with time can be expressed as:

$$\frac{d}{dt}[GlyGly] = k_a[Gly^{\pm}]^2 + k_b[Gly^{\pm}]\left[Gly^{-}\right] + k_c\left[Gly^{-}\right]^2 \qquad (9)$$

The sum of $[Gly^{-}]$ and $[Gly^{\pm}]$ should be equal to [Gly], and if the molar fractions of Gly^{-} and $Gly^{\pm}$ are expressed as α_1 and β_1, respectively (i.e., $[Gly^{-}] = \alpha_1[Gly]$ and $[Gly^{\pm}] = \beta_1[Gly]$), $\alpha_1 + \beta_1 = 1$. Eq. (9) can then be rewritten as:

$$\frac{d}{dt}[GlyGly] = \{(k_a - k_b + k_c)\alpha^2 + (-2k_a - 2k_b)\alpha + k_a\}[Gly]^2 \qquad (10)$$

This means that:

$$k_1 = (k_a - k_b + k_c)\alpha^2 + (-2k_a + k_b)\alpha + k_a \qquad (11)$$

Fig. 2.9b shows k_1 plotted against the molar fraction of Gly^{-} ($=\alpha_1$). Note that k_1 was determined for each pH and the molar fraction of Gly^{-} at the pH is known. By fitting Eq. (11) to the data (the solid curve in Fig. 2.9b), $k_{1,a}$, $k_{1,b}$, and $k_{1,c}$ can be evaluated. The result of the fitting revealed that k_1 has a maximum value of 1.55×10^{-9} l mmol^{-1} s^{-1} at a Gly^{-} fraction of 0.55. Table 1 shows the values of $k_{1,a}$, $k_{1,b}$, and $k_{1,c}$ obtained by this method. The rate constant of the fastest reaction $Gly^{\pm} + Gly^{-} \rightarrow GlyGly$ ($k_{1,a}$) is about 98 times the size of the slowest reaction $Gly^{\pm} + Gly^{\pm} \rightarrow GlyGly$ ($k_{1,b}$). The kinetically most advantageous condition for the dimerization of Gly is therefore that $Gly^{\pm}$ and Gly^{-} exist in approximately equal amounts. This condition is achieved at about pH 9.8 at 25 °C. These results clearly show that $Gly^{\pm}$ and Gly^{-} have different reactivities. Since Gly^{-} has an uncharged amino group (NH_2) with nucleophilicity, Gly^{-} is advantageous to attack the charged carboxylic group of other molecules (Bujdák and Rode, 2001). Reactivity between Gly^{-} and Gly^{-} is less than that between Gly^{-} and $Gly^{\pm}$ because coulombic repulsion works between Gly^{-} and Gly^{-}. Reactivity of $Gly^{\pm}$ and $Gly^{\pm}$ is much lower because $Gly^{\pm}$ has an intramolecular electrical interaction between a charged amino group and a charged carboxyl group and this leads to low reactivity to other $Gly^{\pm}$ molecules.

The reaction of GlyGly to DKP can be separated into the following two reactions: $GlyGly^{\pm} \rightarrow DKP + H_2O$ ($k_{2,a}$) and $GlyGly^{-} \rightarrow DKP + OH^{-}$ ($k_{2,b}$) (Fig. 2.9c). The change in total concentration of DKP with time can be expressed as:

$$\frac{d}{dt}[DKP] = k_a[GlyGly^{\pm}] + k_b\left[GlyGly^{-}\right] \quad (12)$$

By expressing the molar fractions of $GlyGly^{-}$ and $GlyGly^{\pm}$ as α_2 and β_2, respectively (thus, $\alpha_2 + \beta_2 = 1$), Eq. (12) can be rewritten as:

$$\frac{d}{dt}[DKP] = \{(-k_a + k_b)\alpha + k_a\}[GlyGly] \quad (13)$$

Thus,

$$k_2 = (-k_a + k_b)\alpha + k_a \quad (14)$$

Fig. 2.9d shows k_2 plotted against α_2. By fitting Eq. (14) to the data (the solid line in Fig. 2.9d), $k_{2,a}$ and $k_{2,b}$ were estimated to be similar (Table 2.1). The data in Fig. 2.9d do not lie along the fitted line. It appears that $k_{2,a}$ and $k_{2,b}$ are almost equal and k_2 is independent of α_2, and the dispersion of measurement points reflects the variation of $k_{2,a}$. Although the variation of $k_{2,a}$ looks large, $k_{2,a}$ ranges from 8×10^{-6} s^{-1} to 7×10^{-5} s^{-1}. The similarity between $k_{2,a}$ and $k_{2,b}$ indicates that $GlyGly^{-}$ and $GlyGly^{\pm}$ have similar reactivities.

The reaction of GlyGly to Gly can be separated into the following three reactions: $GlyGly^{\pm} + H_2O \rightarrow 2Gly^{\pm}$ ($k_{-1,a}$), $GlyGly^{-} + H_2O \rightarrow Gly^{\pm} + Gly^{-}$ ($k_{-1,b}$), and $GlyGly^{-} + OH^{-} \rightarrow 2Gly^{-}$ ($k_{-1,c}$) (Fig. 2.9e). The change in overall concentration of Gly with time can be expressed as:

$$\frac{d}{dt}[Gly] = 2\left\{k_a[GlyGly^{\pm}] + k_b\left[GlyGly^{-}\right] + k_c\left[GlyGly^{-}\right]\left[OH^{-}\right]\right\} \quad (15)$$

By expressing the molar fraction of $GlyGly^{-}$ and $GlyGly^{\pm}$ as α_3 and β_3, respectively (thus, $\alpha_3 + \beta_3 = 1$), Eq. (15) can be rewritten as

$$\frac{d}{dt}[Gly] = 2\left\{\left(-k_a + k_b + k_c\left[OH^{-}\right]\right)\alpha + k_a\right\}[GlyGly] \quad (16)$$

Since the dissociation constant of the reaction of $GlyGly^{\pm} \rightarrow GlyGly^{-} + H^{+}$ is known,

$$K_a = \frac{\left[GlyGly^{-}\right][H^{+}]}{[GlyGly^{\pm}]} \quad (17)$$

Also, from the definition of α_3 and β_3, $\left[GlyGly^{-}\right] + [GlyGly^{\pm}] = \alpha[GlyGly] + \beta[GlyGly] = [GlyGly]$ (18)

From Eqs. (4), (17), and (18), the concentration of OH^{-} can be expressed as:Fig.

$$[OH^{-}] = \frac{K_w}{K_a}\frac{\alpha_3}{1-\alpha_3} \quad (19)$$

Then, Eq. (16) can be rewritten as:

$$k_{-1}\left[\mathrm{GlyGly}\right] = \{(-k_{-1,a} + k_{-1,b})\alpha_3 + k_{-1,c}\frac{K_w}{K_a}\frac{\alpha_3^2}{1-\alpha_3} + k_{-1,a}\}[\mathrm{GlyGly}] \quad (20)$$

Thus,

$$k_2 = 2\left\{(-k_a + k_b)\alpha + k_c\frac{K_w}{K_a}\frac{\alpha^2}{1-\alpha} + k_a\right\} \quad (21)$$

Fig. 2.9f shows k_{-1} plotted against α_3. By fitting Eq. (21) to the data (the solid curve in Fig. 2.9f), $k_{-1,a}$, $k_{-1,b}$, and $k_{-1,c}$ can be evaluated (Table 2.1). The reaction rate of $GlyGly^{-}$ + OH^{-} → $2Gly^{-}$ ($k_{-1,c}$) is faster than those of $GlyGly^{\pm}$ + H_2O → $2Gly^{\pm}$ ($k_{-1,a}$) and $GlyGly^{-}$ + H_2O → $Gly^{\pm}$ + Gly^{-} ($k_{-1,b}$), which appears to indicate that OH^{-} is more reactive than H_2O, probably because OH^{-} has nucleophilicity owing to its negative charge. Similar values were obtained for $k_{-1,a}$ and $k_{-1,b}$, and GlyGly reacts with H_2O in both reactions. This result again indicates that $GlyGly^{\pm}$ and $GlyGly^{-}$ have similar reactivities.

The reaction of DKP to GlyGly can be separated into the following two reactions: DKP + H_2O → $GlyGly^{\pm}$ ($k_{-2,a}$) and DKP + OH^{-} → $GlyGly^{-}$ ($k_{-2,b}$) (Fig. 2.9g). The change in overall concentration of GlyGly with time can be expressed as:

$$\frac{d}{dt}[\mathrm{GlyGly}] = \left(k_a + k_b\left[OH^-\right]\right)[\mathrm{DKP}] \quad (22)$$

Thus,

$$k_{-2} = k_{-2,a} + k_{-2,b}[OH^-] \quad (23)$$

Fig. 2.9h shows k_{-2} plotted against $[OH^{-}]$. By fitting Eq. (23) to the data (the solid curve in Fig. 2.9h), $k_{-2,a}$ and $k_{-2,b}$ can be estimated. The reaction of DKP + OH^{-} → $GlyGly^{-}$ ($k_{-2,b}$) is faster than that of DKP + H_2O → $GlyGly^{\pm}$ ($k_{-2,a}$) (Table 2.1), ensuring again that OH^{-} is more reactive than H_2O.

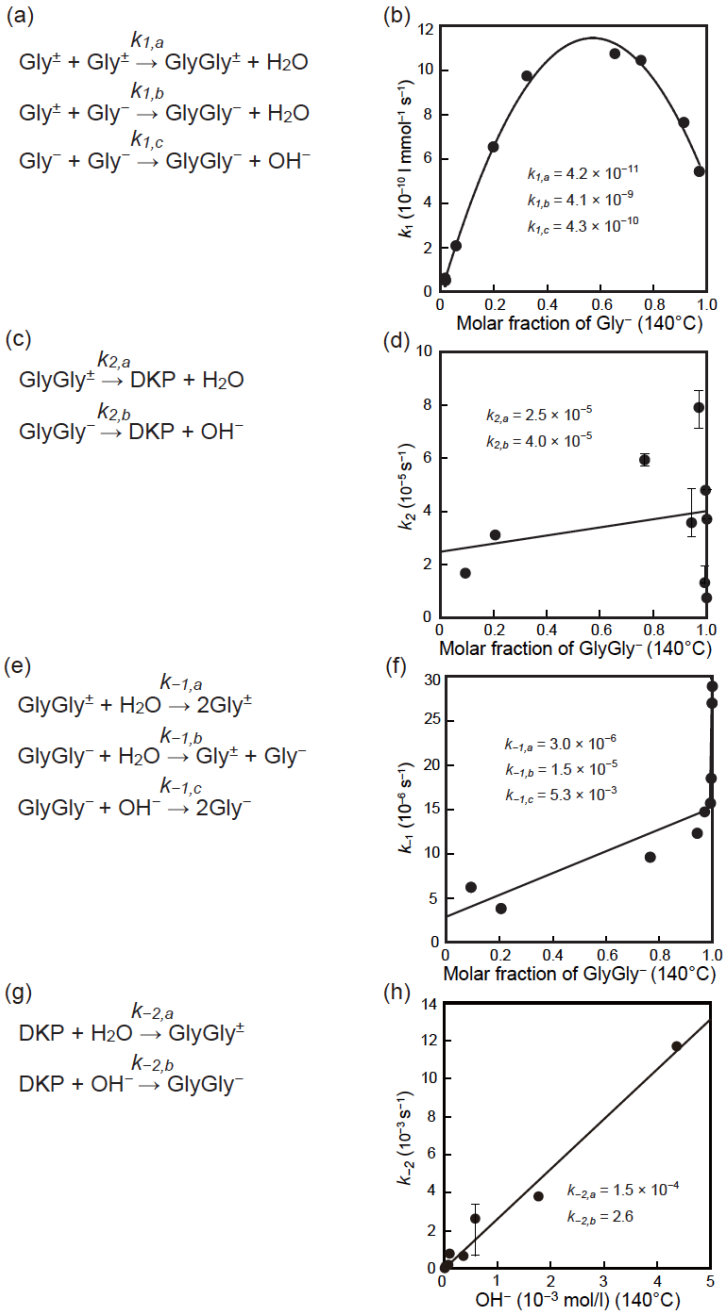

Fig. 2.9. Reaction pathways taking account of the dissociation states of Gly and GlyGly at 140 °C for the reactions of (a) Gly to GlyGly, (c) GlyGly to DKP, (e) GlyGly to Gly, and (g) DKP to GlyGly. Plots of (b) rate constant of Gly to GlyGly (k_1) vs. molar fraction of Gly^{-} with a fitted curve for determining $k_{1,a}$, $k_{1,b}$, and $k_{1,c}$; (d) rate constant of GlyGly to DKP (k_2) vs. molar fraction of $GlyGly^{-}$ with a fitted line for determining $k_{2,a}$ and $k_{2,b}$; (f) rate constant of GlyGly to Gly (k_{-1}) vs. molar fraction of $GlyGly^{-}$ with a fitted curve for determining $k_{-1,a}$, $k_{-1,b}$, and $k_{-1,c}$; and (h) rate constant of DKP to GlyGly (k_{-2}) vs. molar fraction of OH^{-} with a fitted line for determining $k_{-2,a}$ and $k_{-2,b}$.

Table 2.1. Rate constants for the reactions of Gly to GlyGly, GlyGly to DKP, GlyGly to Gly, and DKP to GlyGly at 140 °C. Reference rate constants correspond to values at 140 °C, which were estimated from the reported temperature dependences of the reaction rates.

Reaction	Rate constant (this study)	Reference rate constant
$Gly^{\pm} + Gly^{-} \rightarrow GlyGly^{-} + H_2O$	$4.1 (\pm 0.11) \times 10^{-9}$ (l mmol^{-1} s^{-1}) ($k_{1,b}$)	
$Gly^{-} + Gly^{-} \rightarrow GlyGly^{-} + OH^{-}$	$4.3 (\pm 0.30) \times 10^{-10}$ (l mmol^{-1} s^{-1}) ($k_{1,c}$)	
$Gly^{\pm} + Gly^{\pm} \rightarrow GlyGly^{\pm} + H_2O$	$4.2 (\pm 2.0) \times 10^{-11}$ (l mmol^{-1} s^{-1}) ($k_{1,a}$)	
$GlyGly^{-} \rightarrow DKP + OH^{-}$	$4.0 (\pm 0.96) \times 10^{-5}$ (s^{-1}) ($k_{2,b}$)	
$GlyGly^{\pm} \rightarrow DKP + H_2O$	$2.5 (\pm 2.0) \times 10^{-5}$ (s^{-1}) ($k_{2,a}$)	4.6×10^{-5} (s^{-1}) (Radzicka and Wolfenden, 1996)
$GlyGly^{-} + OH^{-} \rightarrow 2Gly^{-}$	$5.3 (\pm 1.2) \times 10^{-3}$ (mmol l^{-1} s^{-1}) ($k_{-1,c}$)	1.4×10^{-2} (mmol l^{-1} s^{-1}) (Lawrence and Moore, 1951)
$GlyGly^{-} + H_2O \rightarrow Gly^{\pm} + Gly^{-}$	$1.5 (\pm 0.15) \times 10^{-5}$ (mmol l^{-1} s^{-1}) ($k_{-1,b}$)	
$GlyGly^{\pm} + H_2O \rightarrow 2Gly^{\pm}$	$3.0 (\pm 2.6) \times 10^{-6}$ (mmol l^{-1} s^{-1}) ($k_{-1,a}$)	1.5×10^{-6} (mmol l^{-1} s^{-1}) (Qian et al., 1993) 6.1×10^{-6} (mmol l^{-1} s^{-1}] (Radzicka and Wolfenden, 1996)
$DKP + OH^{-} \rightarrow GlyGly^{-}$	2.6 (± 0.14) (s^{-1}) ($k_{-2,b}$)	
$DKP + H_2O \rightarrow GlyGly^{\pm}$	$1.5 (\pm 2.2) \times 10^{-4}$ (s^{-1}) ($k_{-2,a}$)	1.2×10^{-4} (s^{-1}) (Radzicka and Wolfenden, 1996)

2.3.3. Comparison with other rate constants

The rate constants obtained in this study can be compared with the results of several previous studies. Lawrence and Moore (1951) conducted a heating experiment of solutions containing 0.05 mol l^{-1} GlyGly and 0.21 mol l^{-1} NaOH at 54.4, 70.2, and 87.2 °C and evaluated the rate of reaction of GlyGly to Gly. Under the alkaline solution, GlyGly is present as $GlyGly^{-}$. Qian et al. (1993) evaluated the rate of reaction of GlyGly to Gly under unbuffered conditions (pH 5.6−7.9) at 120, 160, and 220 °C; under these conditions we estimate that the main existence forms of Gly and GyGly were $Gly^{\pm}$ and $GlyGly^{\pm}$. Radzicka and Wolfenden (1996) studied the reaction between GlyGly and DKP under hydrothermal conditions at pH 7 at 84−160 °C and evaluated the rate and equilibrium constant for the reaction. They also evaluated the rate of reaction of GlyGly to Gly under hydrothermal conditions at pH 4.2−7.8 and 120−200 °C. Under the experimental conditions of Radzicka and Wolfenden (1996), we presume that Gly and GlyGly mainly existed as $Gly^{\pm}$ and $GlyGly^{\pm}$. Table 1 shows the rate constants at 140 °C estimated from the temperature dependences of the reaction rates reported in the above studies. The rate constants in the current study differ from the values of previous studies by factors of 0.5–3. Thus, the reproducibility of the experiment is reasonably good, although previous studies have not taken the dissociation states of Gly and GlyGly into consideration.

2.3.4. Dimerization rates in hydrothermal environments

The above analyses can be used to estimate a dimerization rate under given pH and temperature conditions. Fig. 2.10 shows the estimated dimerization rates under several hydrothermal environments for which pH and temperature have been reported. The conditions for each hydrothermal environment are as follows: Lost City (pH 10−11, < 91 °C: Kelley et al., 2005), Rainbow (pH 2.8, 365 °C: Douville et al., 2002), Sediment Hosted (pH 5.1−5.9, 100−315 °C: Tivey, 2007), Mid Ocean Ridge (pH 2.8−4.5, < 405 °C: Ding et al., 2005; Tivey, 2007), back arc basins (pH <1−5.0, 278−334 °C: Fouquest et al., 1991; Tivey, 2007), and sea-water (pH 8, 2 °C: Tivey, 2007), where all pH values are those at 25 °C. Since activation energies are assumed to be equal at all pH (88 kJ mol^{-1} at pH 9.8, derived from Fig. 7a), lines for each pH in Fig. 10 have the same slope. The dimerization rate increases with rising temperature in an Arrhenius plot. However, Shock (1990) conducted the thermodynamic calculation on

synthesis of organic materials that are important for the origin of life and showed that the amounts of production of amino acids became greatest at about 150 °C. In addition, according to Ito et al. (2006), when amino acids contained in submarine sediments from Hawaii (depth 3438 m) were heated in NaCl solution with sediments, the amounts of degraded amino acids were 90% at 200 °C, 60% at 150 °C, and 25% at 100 °C. Thus, amino acids are unstable at > 200 °C. Our results in combination with those from other studies indicate therefore that Gly dimerizes most efficiently under alkaline pH (~9.8) at about 150°C. Although the ranges of pH and temperature on the early Earth are unclear, among the hydrothermal vents presented in Fig. 2.10, Lost City has the most favorable condition for the dimerization of Gly.

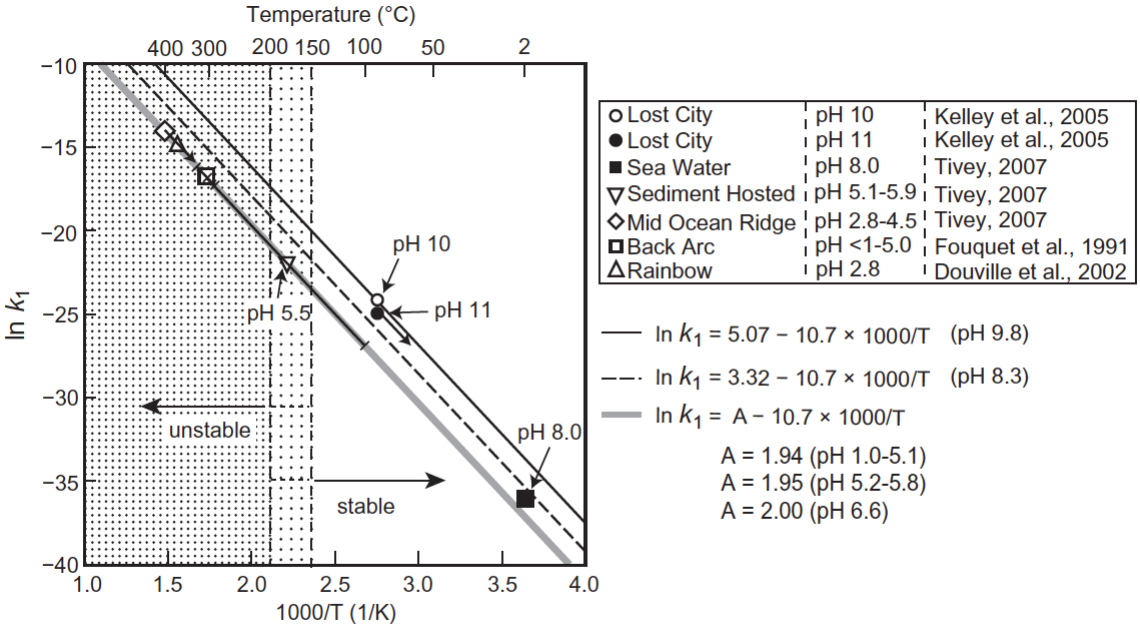

Fig. 2.10. Dimerization rate constants estimated for several hydrothermal vents.

Amino acids have different polar side chain characteristics and different numbers of amino and carboxylic groups. Despite the variation, all amino acids have at least one amino group and one carboxylic group whose protonation states change with pH. It is thus presumed that the polymerization rates of amino acids other than Gly are also affected by pH, although the degree to which pH affects the rate of polymerization may change depending on the amino acid. Because the amino acid concentration is also important for polymerization in addition to pH and temperature, it is difficult to specify

where the polymerization of amino acids actually occurred from our results alone. Although our experiment was performed taking hydrothermal conditions in consideration, the dissociation states of amino acids may also play important roles in the reactions not necessarily related to hydrothermal conditions, such as at the surfaces of minerals or salt-induced peptide formation (e.g., Eder and Rode, 1994; Rode, 1999; Bujdák and Rode, 1999a; Bujdák and Rode, 1999b; Bujdák and Rode, 2001). For example, in the case of the reaction between Gly and $CuCl_2$, it has been suggested that peptide formation is promoted because Gly^+ and Gly^- bind to Cu^{2+} (Eder and Rode, 1994). Such a reaction may be affected by the molar fractions of each of Gly's dissociation states. Thus, the effect of the dissociation state of Gly on polymerization rate revealed in this study seems to be useful to evaluate a suitable environment for the chemical evolution of life under various conditions.

2.4. Conclusion

We studied the effects of pH and temperature on the dimerization rate of Gly. The rate significantly changed with pH and reached a maximum at about pH 9.8. Since Gly has three dissociation states (Gly^+, $Gly^\pm$, and Gly^-), the dimerization of Gly can be separated into reactions for each dissociation state. The rates decreased in the order of $Gly^\pm + Gly^- \rightarrow$ GlyGly (fast), $Gly^- + Gly^- \rightarrow$ GlyGly (medium), and $Gly^\pm + Gly^\pm \rightarrow$ GlyGly (slow), and the rate constants differed by as much as a factor of 98. Thus, each dissociation state of Gly has a different reactivity, and the pH dependence of the dimerization rate can be explained by the change of the dissociation states of Gly with pH. The dimerization rate became greatest at pH 9.8 because the fractions of $Gly^\pm$ and Gly^- are approximately equal at this pH. The revealed relationship between pH, dissociation state, polymerization rate, and temperature seems to be useful for the evaluation of favorable conditions for chemical evolution of life.

2.5. References

Bujdák J. and Rode B. M. (1999a) Silica, alumina and clay catalyzed peptide bond formation: enhanced efficiency of alumina catalyst. *Orig. Life Evol. Biosph.* **29**, 451-461.

Bujdák J. and Rode B. M. (1999b) The effect of clay structure on peptide bond formation catalysis. *J. Mol. Catal. A: Chem.* **144**, 129-136.

Bujdák J. and Rode B. M. (2001) Activated alumina as an energy source for peptide bond formation: Consequences for mineral-mediated prebiotic processes. *Amino acids* **21**, 281-291.

Chyba C. and Sagan C. (1992) Endogenous production, exogenous delivery and impact-shock synthesis of organic molecules: an inventory for the origins of life. *Nature* **355**, 125-132.

Clarke R. G. F., Collins C. M., Roberts J. C., Trevani L. N., Bartholomew R. J. and Tremaine P. R. (2005) Ionization constants of aqueous amino acids at temperatures up to 250°C using hydrothermal pH indicators and UV-visible spectroscopy: Glycine, α-alanine, and proline. *Geochim. Cosmochim. Acta* **69**, 3029-3043.

Cody G. D., Boctor N. Z., Filley T. R., Hazen R. M., Scott J. H., Sharma A. and Yoder Jr. H. S. (2000) Primordial carbonylated iron-sulfur compounds and the synthesis of pyruvate. *Science* **289**, 1337-1339.

Corliss J. B. (1990) Hot springs and the origin of life. *Nature* **347**, 624.

Corliss J. B., Dymond J., Gordon L. I., Edmond J. M., von Herzen R. P., Ballard R. D., Green K., Williams D., Bainbridge A., Crane K. and van Andel T. H. (1979) Submarine thermal springs on the Galápagos rift. *Science* **203**, 1073-1083.

Douville E., Charlou J. L., Oelkers E. H., Bienvenu P., Jove Colon C. F., Donval J. P., Fouquet Y., Prieur D. and Appriou P. (2002) The rainbow vent fluids (36°14′N, MAR): the influence of ultramafic rocks and phase separation on trace metal content in Mid-Atlantic Ridge hydrothermal fluids. *Chemical Geology* **184**, 37-48.

Eder A. and Rode B. M. (1994) Influence of alkali- and alkaline-earth-metal cations on the 'salt-induced peptide formation' reaction. *J. Chem. Soc. Dalton Trans.* 1125-1130.

Ferris J. P. (1992) Chapter 6 Chemical markers of prebiotic chemistry in hydrothermal systems. *Orig. Life Evol. Biosph.* **22**, 109-134.

Fisher C. R., Takai K. and Bris N. L. (2007) Hydrothermal vent ecosystem. *Oceanography* **20**, 14-23.

Fouquet Y., Von Stackelberg U., Charlou J. L., Donval J. P., Erzinger J., Foucher J. P., Herzig P., Mühe R., Soakai S., Wiedicke M. and Whitechurch H. (1991) Hydrothermal activity and metallogenesis in the Lau back-arc basin. *Nature* **349**, 778-781.

Goldberg R. N., Kishore N. and Lennen R. M. (2002) Thermodynamic quantities for the ionization reactions of buffers. *J. Phys. Chem. Ref. Data* **31**, 231-370.

Holm N. G. (1992) Chapter 1 Why are hydrothermal systems proposed as plausible environments for the origin of life? *Orig. Life Evol. Biosph.* **22**, 5-14.

Huber C. and Wächtershäuser G. (1998) Peptides by Activation of Amino Acids with CO on (Ni,Fe)S Surfaces: Implications for the Origin of Life. *Science* **281**, 670-672.

Imai E., Honda H., Hatori K., Brack A. and Matsuno K. (1999) Elongation of oligopeptides in a simulated submarine hydrothermal system. *Science* **283**, 831-833.

Ito M., Gupta L. P., Masuda H. and Kawahata H. (2006) Thermal stability of amino acids in sea floor sediment in aqueous solution at high temperature. *Org. Geochem.* **37**, 177-188.

Kelley D. S., Karson J. A., Blackman D. K., Früh-Green G. L., Butterfield D. A., Lilley M. D., Olson E. J., Schrenk M. O., Roe K. K., Lebon G. T., Rivizzigno P. and the AT3-60 Shipboard Party (2001) An off-axis hydrothermal vent field near the Mid-Atlantic Ridge at 30°N. *Nature* **412**, 145-149.

Kelley D. S., Karson J. A., Fruh-Green G. L., Yoerger D. R., Shank T. M., Butterfield D. A., Hayes J. M., Schrenk M. O., Olson E. J., Proskurowski G., Jakuba M., Bradley A., Larson B., Ludwig K., Glickson D., Buckman K., Bradley A. S., Brazelton W. J., Roe K., Elend M. J., Delacour A., Bernasconi S. M., Lilley M. D., Baross J. A., Summons R. E. and Sylva S. P. (2005) A serpentinite-hosted ecosystem: The lost city hydrothermal field. *Science* **307**, 1428-1434.

Konn C., Charlou J. L., Donval J. P., Holm N. G., Dehairs F. and Bouillon S. (2009) Hydrocarbons and oxidized organic compounds in hydrothermal fluids from Rainbow and Lost City ultramafic-hosted vents. *Chemical Geology* **258**, 299-314.

Lang S. Q,, Butterfield D. A., Schulte M., Kelley D. S. and Lilley M. D. (2010) Elevated concentration of formate, acetate and dissolved organic carbon found at the Lost City hydrothermal field. *Geochim. Cosmochim. Acta* **74**, 941-952.

Lawrence L. and Moore W. (1951) Kinetics of the hydrolysis of simple glycine peptides. *J. Am. Chem. Soc.* **73**, 3973-3977.

Lemke K. H., Rosenbauer R. J., Bird D. K. (2009) Peptide synthesis in early earth hydrothermal systems. *Astrobiology* **9**, 141-146.

Li J. and Brill T. B. (2003) Spectroscopy of hydrothermal reactions. 27. Simultaneous determination of hydrolysis rate constants of glycylglycine to glycine and

glycylglycine-Diketopiperazine equilibrium constants at 310-330°C and 275 bar. *J. Phys. Chem. A* **107**, 8575-8577.

Macleod G., McKeown C., Hall A. J. and Russell M. J. (1994) Hydrothermal and oceanic pH conditions of possible relevance to the origin of life. *Orig. Life Evol. Biosph.* **24**, 19-41.

Marshall W. L. and Franck E. U. (1981) Ion product of water substance, 0-1000°C, 1-10,000 bars new international formulation and its background. *J. Phys. Chem. Ref. Data* **10**, 295-304.

Marshall W. L. (1994) Hydrothermal synthesis of amino acids. *Geochim. Cosmochim. Acta* **58**, 2099-2106.

Martin W., Baross J., Kelley D. and Russell M. J. (2008) Hydrothermal vents and the origin of life. *Nature Rev. Microbiol.* **6**, 805-814.

Ohara S., Kakegawa T. and Nakazawa H. (2007) Pressure effects on the abiotic polymerization of glycine. *Orig. Life Evol. Biosph.* **37**, 215-223.

Oró J. and Guidry C. L. (1960) A novel synthesis of polypeptides. *Nature* **186**, 156-157.

Pizzarello S. (2004) Chemical evolution and meteorites: an update. *Orig. Life Evol. Biosph.* **34**, 25-34.

Qian Y., Engel M. H., Macko S. A., Carpenter S. and Deming J. W. (1993) Kinetics of peptide hydrolysis and amino acid decomposition at high temperature. *Geochim Cosmochim. Acta* **57**, 3281-3293.

Radzicka A. and Wolfenden R. (1996) Rates of uncatalyzed peptide bond hydrolysis in neutral solution and the transition state affinities of proteases. *J. Am. Chem. Soc.* **118**, 6105-6109.

Rode B. M. (1999) Peptides and the origin of life. *Peptides* **20**, 773-786.

Rode B. M. and Schwendinger M. G. (1990) Copper-catalyzed amino acid condensation in water – a simple possible way of prebiotic peptide formation. *Orig. Life Evol. Biosph.* **20**, 401-410.

Russell M. J. (2003) The importance of being alkaline. *Science* **302**, 580-581.

Russell M. J. and Hall A. J. (1997) The emergence of life from iron monosulphide bubbles at a submarine hydrothermal redox and pH front. *J. Geol. Soc.* **154**, 377-402.

Shock E. L. (1990) Geochemical constraints on the origin of organic compounds in hydrothermal systems. *Orig. Life Evol. Biosph.* **20**, 331-367.

Smith R. M. and Hansen D. E. (1998) The pH-rate profile for the hydrolysis of a peptide bond. *J. Am. Chem. Soc.* **120**, 8910-8913.

Tivey M. K. (2007) Generation of seafloor hydrothermal vent fluids and associated mineral deposits. *Oceanography* **20**, 50-65.

Tivey M. K., Humphris S. E., Thompson G. and Hannington M. D. (1995) Deducing patterns of fluid flow and mixing within the TAG active hydrothermal mound using mineralogical and geochemical data. *J. Geophys. Res.* **100**, 12527-12555.

Yanagawa H. and Kobayashi K. (1992) Chapter 8 An experimental approach to chemical evolution in submarine hydrothermal systems. *Orig. Life Evol. Biosph.* **22**, 147-159.

Zahn D. (2004) On the role of water in amide hydrolysis. *Eur. J. Org. Chem.* 4020-4023.

Zamaraev K. I., Romannikov V. N., Salganik R. I., Wlassoff W. A. and Khramtsov V. V. (1997) Modelling of the prebiotic synthesis of oligopeptides: silicate catalyses help to overcome the critical stage. *Orig. Life Evol. Biosph.* **27**, 325-337.

Chapter 3

Effects of metal ions and pH on the formation and decomposition rates of di- and tri-peptides in aqueous solution

This chapter is in press as:
Sakata K., Yabuta H. and Kondo T. Effects of metal ions and pH on the formation and decomposition rates of di- and tri-peptides in aqueous solution. Geochemical Journal, in press.

3.1. Introduction

Deep-sea hydrothermal systems have been suggested as a suitable environment for chemical evolution in the early Earth (e.g., Corliss, 1990; Holm, 1992; Yanagawa and Kobayashi, 1992; Macleod et al., 1994; Russell and Hall, 1997; Russell, 2003; Holm and Andersson, 2005; Martin et al., 2008). In terrestrial hydrothermal systems, seawater percolates into the deep oceanic crust; reacts with the surrounding rocks at high temperatures; and changes into hot, reduced fluids (up to 400°C) (Tivey et al., 1995; Tivey, 2007). Water–rock interaction produces a broad range of pH and redox conditions in seafloor hydrothermal fluids (e.g., East Pacific Rise, Lucky Strike hydrothermal field, Rainbow plume, and Trans-Atlantic Geotraverse area), and might have controlled the prebiotic chemistry.

Recently, hydrothermal systems eructing basic and low-temperature fluids were discovered in the south Chamorro seamount (Mottl et al., 2003) and Lost City hydrothermal field (Kelley et al., 2001). The high pH values of the fluids at these sites have been attributed to the serpentinization of olivine (Kelley et al., 2001; Kelley et al., 2005; Hulme et al., 2010; Wheat et al., 2010). Serpentinization yields H_2-rich fluids that can facilitate organic chemical synthesis (Horita and Berndt, 1999; McCollom and Seewald, 2007; McCollom and Bach, 2009). Therefore, basic hydrothermal systems are regarded as suitable environments for the origin of life (Russell, 2003; Holm et al., 2006; Holm and Neubeck, 2009). Based on the petrological analysis of Archean basalt (Shibuya et al., 2010), it was proposed that the Archean subseafloor hydrothermal systems were characterized by high-pH fluids. In addition, there have been several studies that experimentally demonstrate prebiotic chemistry at high pH (e.g., Huber and Wächtershäuser, 1998; Russell, 2003; Holm et al., 2006; Sakata et al., 2010). For example, in a previous study, we reported a maximum dimerization rate for glycine (Gly) in aqueous solution at 150°C and pH 9.8 (Sakata et al., 2010).

The metal ions produced by the hydrothermal alteration of rocks are also important in prebiotic chemistry. Typical hydrothermal systems, including south Chamorro, release fluids that are enriched in a variety of metal ions such as Ca^{2+}, K^{+}, Ba^{2+}, Fe^{2+}, Mn^{2+}, Cu^{2+}, Zn^{2+}, and Pb^{2+} (Mottl et al., 2003; Tivey, 2007; Hulme et al., 2010). Although the concentrations of the metal ions in the Lost City hydrothermal field are low, enrichment in Ca^{2+} characterizes this system (Kelley et al., 2001, 2005). Recently, it has been suggested that the fluxes of organo–metal complexes of organic

carbon and metal ions (e.g., Cu^{2+}, Fe^{2+}) are more abundant in hydrothermal plumes than previously assumed (Sander and Koschinsky, 2011). Toner et al. (2009) has also shown that organic carbon is associated with Fe in hydrothermal plume particles. These reports have forced the revision of the notion that most of the metals released from hydrothermal vents are incorporated in minerals. Fe^{2+} and Mn^{2+} were probably more abundant in ancient oceans than in modern oceans (Anbar, 2008). Thus, the interactions between organic molecules and dissolved metal ions could have been more important in prebiotic chemistry, whereas mineral surface catalysis might have been of lesser importance around hydrothermal vents in the early Earth. In fact, most of the present-day living organisms contain metalloproteins, which may have been derived from the interactions of organic molecules and metal ions in the early terrestrial oceans.

It is well known that divalent metal ions, especially Cu^{2+}, can catalyze the oligomerization of amino acids in acidic and neutral aqueous solutions (e.g., Schwendinger and Rode, 1989; Eder and Rode, 1994; Imai et al., 1999; Rode, 1999; Li et al., 2010). This reaction is called the "salt-induced peptide formation (SIPF)" reaction (Schwendinger and Rode, 1989), and the monochlorocuprate complex is assumed to be the reactive species that leads to the linking of the two amino acids to a peptide (Rode, 1999). The monochlorocuprate complex is very stable and partially charged, causing the nucleophilic attack of the amino group of the chelated amino acid at the protonated carboxyl group of the other amino acids (Rode, 1999). On the other hand, it was reported that other divalent cations such as Mg^{2+}, Ca^{2+}, Mn^{2+}, Co^{2+}, Ni^{2+}, Fe^{2+}, Zn^{2+}, and Cd^{2+} have little effect on the polymerization of Gly (Schwendinger and Rode, 1989; Rode and Schwendinger, 1990). Zn^{2+} catalyzes the formation and hydrolysis of diketopiperazines (DKP) (Cronin et al., 1971) and the hydrolysis of Glycylglycine (GlyGly) (Long et al., 1971).

To date, most of the prebiotic peptide synthesis have been conducted under acidic and neutral conditions to simulate the typical hydrothermal environment. However, because of the recent discovery of basic hydrothermal systems, greater chemical diversity in the hydrothermal systems of the early Earth is expected. Therefore, in this study, systematic heating experiments of Gly with various metal ions (Ca^{2+}, Mg^{2+}, Zn^{2+}, Fe^{2+}, Mn^{2+}, and Cu^{2+}) in aqueous solution under a broad range of pH conditions were conducted to determine the most favorable conditions for the formation of peptides. Variations in the reaction rate constants of the formation and decomposition of

dipeptides, tripeptides, and DKP under different conditions were studied with respect to the glycine–metal complexation mechanism.

3.2. Methods

Analytical grade Gly, GlyGly, and Glycylglycylglycine (GlyGlyGly) were obtained from the Peptide Institute. DKP was obtained from Tokyo Chemical Industry. HCl, NaOH, $CaCl_2$, $ZnCl_2$, $MnCl_2$, and $FeCl_2$ were obtained from Wako Pure Chemical Industries. $MgCl_2$ and $CuCl_2$ were obtained from Kanto Chemical.

Solutions of 100 mM Gly with pH 2.1–3.4, 100 mM Gly with pH 4.5–6.0, and 5 mM metal chloride (MCl_2, M = Ca, Mg, Cu, Fe, Mn, and Zn) with pH 9.8–9.9 were prepared. The pH of the Gly solutions was adjusted to pH 2.1–2.3 and pH 9.8–9.9 by using HCl and NaOH, respectively. The pH of the solution of Gly and $CuCl_2$ was 3.4, and NaOH was used to adjust the pH of the solutions to 7.1 and 9.8, respectively. The pH of the solutions of Gly and the metal chlorides ranged from 4.5 to 6.0. Each solution (0.5–1.0 ml) was placed in a pyrex glass tube and vacuumed; subsequently, the tube was filled with Ar gas and sealed. To prevent contamination, the pyrex glass tubes were heated at 500°C for 4.5 h before inserting the samples. Finally, the solutions were heated in an electric oven at 140°C from 1 to 74 days. Before and after the experiment, the pH of the solutions was measured at 25°C with a pH meter (B-212; HORIBA). The changes in the pH before and after the experiments were <1.7 (Table 3.1). In the solution of Gly and $FeCl_2$ at pH 2.3 and 5.0, red iron oxides precipitated after heating, and the precipitation was more pronounced at pH 2.3 than at pH 5.0.

Table 3.1. The changes in the pH before and after heating experiments at 140°C.

	pH (before experiments)	pH (after experiments)
No metal ion	2.3	1.8 ~ 2.6
	6.0	7.3 ~ 7.7
	9.8	8.9 ~ 9.6
Ca^{2+}	2.3	2.5 ~ 2.8
	5.7	6.7 ~ 7.4
	9.9	9.6 ~ 9.9
Mg^{2+}	2.3	2.5 ~ 2.6
	5.7	6.7 ~ 7.3
	9.9	8.8 ~ 9.2
Zn^{2+}	2.3	2.6 ~ 2.9
	4.5	4.9 ~ 5.4
	9.8	8.7 ~ 9.8
Fe^{2+}	2.3	1.7 ~ 1.9
	5.0	3.3 ~ 4.3
Mn^{2+}	2.2	1.9 ~ 2.3
	5.7	6.2 ~ 6.8
Cu^{2+}	3.4	3.8 ~ 4.1
	7.1	7.3 ~ 7.7
	9.8	8.7 ~ 9.1

Each sample was diluted 10 or 20 times and analyzed by using a high-performance liquid chromatography (HPLC) system (ICA-2000; TOA DKK) equipped with a Jasco UV-2075 detector at a wavelength of 200 nm. A reversed phase-type HPLC column (Hydrosphere C18; YMC) was used at 37°C. A 10 mM $C_6H_{13}SO_3Na$ solution with pH 2.5 was used as eluent and adjusted using H_3PO_4 (Bujdák and Rode, 1999) at a flow rate of 1.0 ml min^{-1}. Gly, GlyGly, GlyGlyGly, and DKP were identified and quantified by comparing the observed peak retention times and peak areas, respectively, with those of standard compounds. The errors in the concentrations of Gly, GlyGly, GlyGlyGly, and DKP were estimated to be <3.0%.

3.3. Results and Discussion

3.3.1. Yields of GlyGly, DKP, and GlyGlyGly

Figure 3.1 shows the chromatograms of the products obtained from the solutions after the hydrothermal reactions at 140°C under the respective conditions. GlyGly and DKP were produced under all conditions (Fig. 3.1), and GlyGlyGly was only produced from solutions containing Cu^{2+} (Figs. 3.1h, 1p, and 1v). The relative abundances of DKP and GlyGly increased with increasing heating time. Table 3.2 and Fig. 3.2 summarize the GlyGly and DKP yields. The GlyGly, DKP, and GlyGlyGly yields were 0.05%–0.68%, 0.001%–0.11%, and 0.01%–0.05%, respectively (Table 3.2). In this study, the GlyGly yields (0.06%) from the solution containing Cu^{2+} (pH 3.4) are four times lower than the yield (0.25%) reported by Rode and Schwendinger (1990) who heated a solution of 800 mM Gly and 400 mM $CuCl_2$ (pH 2.5) at 80–90°C for 10 days. In this study, the GlyGly yields (0.12%) from the solution containing Fe^{2+} (pH 5.0) are 2–4 times higher than those (0.03%–0.06%) reported by Rode and Schwendinger (1990) who heated a solution of 900 mM Gly and 500 mM $FeCl_2$ (pH 5.0) at 75°C for 11 days. However, GlyGlyGly was not detected in the Rode and Schwendinger (1990) experiments. Thus, these differences observed are attributed to the differences in the concentration, time, and temperature, which are the factors that Cleaves et al. (2009) regard as the major limiting parameters of peptide synthesis under deep-sea hydrothermal conditions.

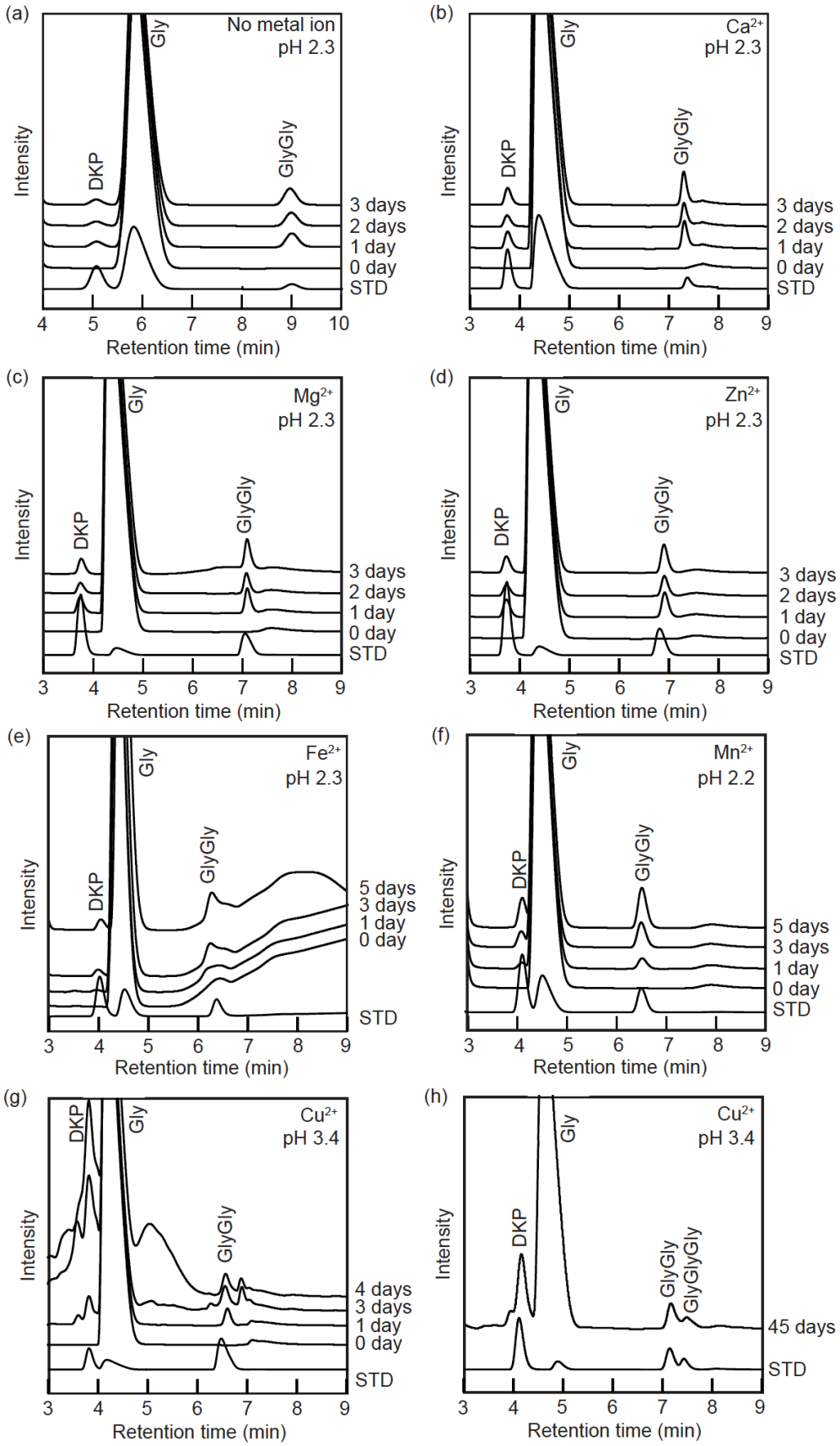
(a)
No metal ion
pH 2.3
Gly
DKP
GlyGly
Intensity
3 days
2 days
1 day
0 day
STD
Retention time (min)
(b)
Ca2+
pH 2.3
(c)
Mg2+
pH 2.3
(d)
Zn2+
pH 2.3
(e)
Fe2+
pH 2.3
5 days
3 days
1 day
0 day
STD
(f)
Mn2+
pH 2.2
(g)
Cu2+
pH 3.4
4 days
(h)
GlyGlyGly
45 days

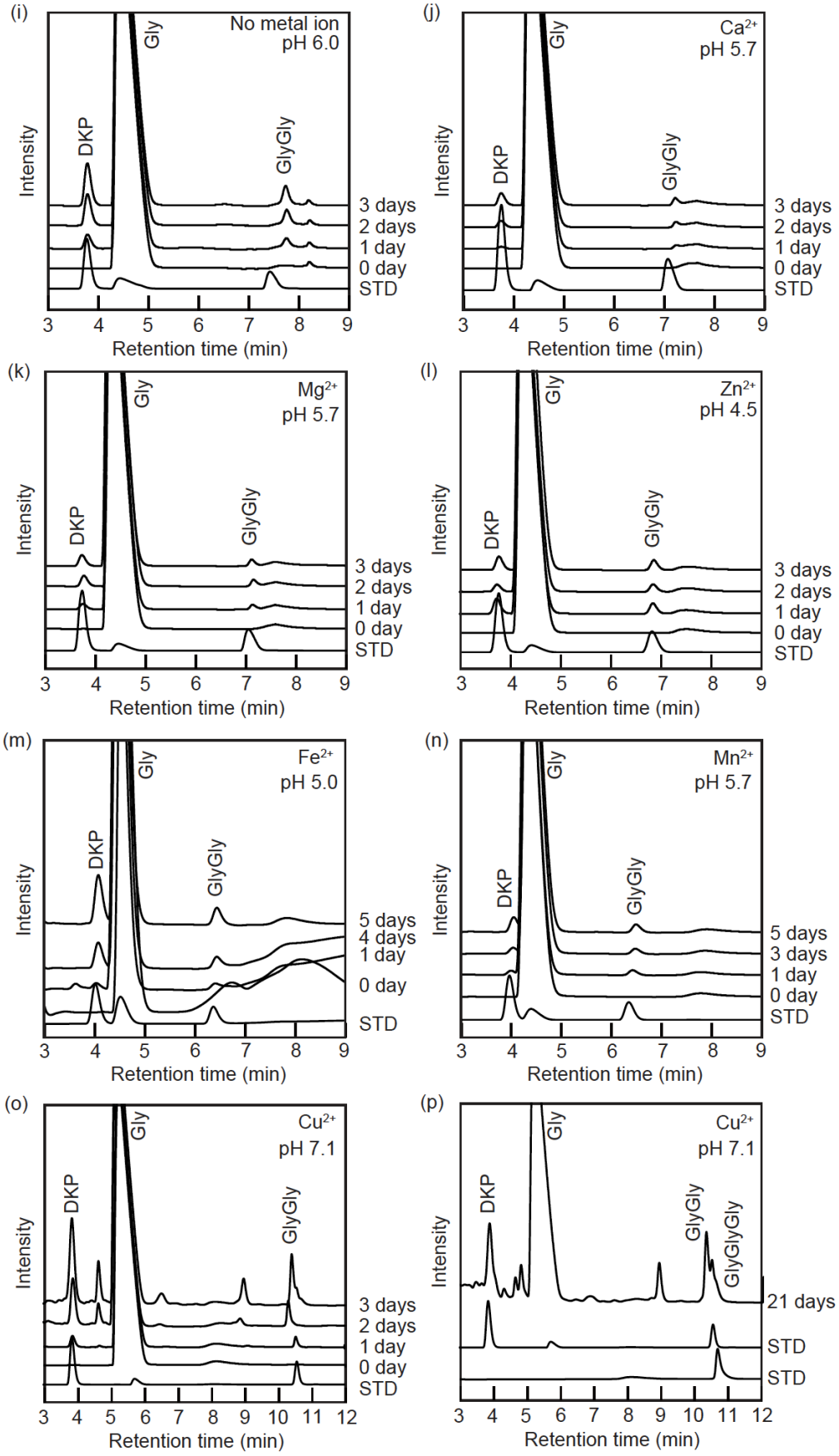
(i)
No metal ion
pH 6.0
Gly
DKP
GlyGly
Intensity
3 days
2 days
1 day
0 day
STD
Retention time (min)
(j)
Ca2+
pH 5.7
(k)
Mg2+
pH 5.7
(l)
Zn2+
pH 4.5
(m)
Fe2+
pH 5.0
5 days
4 days
(n)
Mn2+
pH 5.7
(o)
Cu2+
pH 7.1
(p)
Cu2+
pH 7.1
GlyGlyGly
21 days

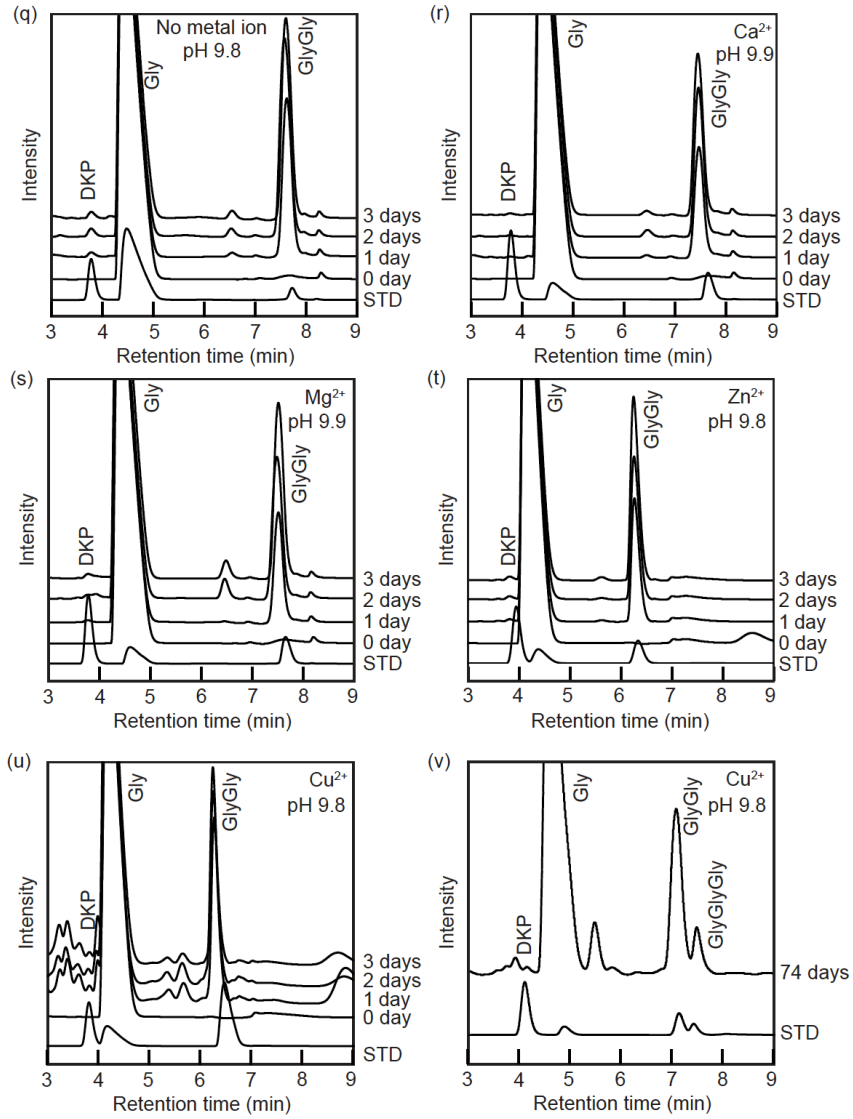

Fig. 3.1. HPLC chromatograms before and after the hydrothermal reactions of glycine in aqueous solution at (a–h) pH 2.2–3.4, (i–p) pH 4.5–7.1, and (q–v) pH 9.8–9.9. (a, i, and q) No metal ions were present, (b, j, and r) with Ca^{2+}, (c, k, and s) with Mg^{2+}, (d, l, and t) with Zn^{2+}, (e and m) with Fe^{2+}, (f and n) with Mn^{2+}, and (g, h, o, p, u, and v) with Cu^{2+}. Individual salts were also added to the standard solutions to inhibit the relative retention time shifts of the components because of the salt effects. Ratios of concentrations of Gly: GlyGly: DKP in the standards were 200: 1: 1 for no metal ions (pH 2.3, pH 9.8) and with Fe^{2+} (pH 2.3 and pH 5.0), 100: 1: 1 for Mn^{2+} (pH 2.2), 40: 1: 1 for Mn^{2+} (pH 5.7), and 20: 1: 1 for no metal ions (pH 6.0), Ca^{2+} (pH 2.3, 5.7, 9.9), Mg^{2+} (pH 2.3, 5.7, 9.9), Zn^{2+} (pH 2.3, 4.5, 9.8), Cu^{2+} (pH 3.4, 7.1, 9.8). The concentrations of GlyGlyGly for the dtandards with Cu^{2+} were 0.01 (pH 3.4 and pH 9.8) or 0.05 mM (pH 7.1).

Table 3.2. Yields of GlyGly, DKP, and GlyGlyGly from solutions without and with metal ions (Ca^{2+}, Mg^{2+}, Zn^{2+}, Fe^{2+}, Mn^{2+}, and Cu^{2+}) at different pH conditions and heating times at 140°C .

	Heating time (days)	GlyGly (%)	DKP (%)	GlyGlyGly (%)
No metal ion (pH 2.3)	74	0.17	0.03	-
Ca^{2+} (pH 2.3)	14	0.15	0.05	-
Mg^{2+} (pH 2.3)	14	0.18	0.07	-
Zn^{2+} (pH 2.3)	14	0.14	0.04	-
Fe^{2+} (pH 2.3)	36	0.15	0.04	-
Mn^{2+} (pH 2.2)	37	0.17	0.06	-
Cu^{2+} (pH 3.4)	45	0.06	0.11	0.01
No metal ion (pH 6.0)	42	0.10	0.10	-
Ca^{2+} (pH 5.7)	15	0.07	0.08	-
Mg^{2+} (pH 5.7)	14	0.05	0.07	-
Zn^{2+} (pH 4.5)	14	0.05	0.07	-
Fe^{2+} (pH 5.0)	30	0.12	0.11	-
Mn^{2+} (pH 5.7)	43	0.06	0.09	-
Cu^{2+} (pH 7.1)	21	0.09	0.09	0.01
No metal ion (pH 9.8)	74	0.62	0.01	-
Ca^{2+} (pH 9.8)	3	0.45	-	-
Mg^{2+} (pH 9.9)	3	0.48	0.001	-
Zn^{2+} (pH 9.8)	37	0.68	0.014	-
Cu^{2+} (pH 9.8)	74	0.62	0.004	0.05

The GlyGly yields from basic solutions (pH 9.8–9.9) are the highest, regardless of the presence or absence of any metal ion (Fig. 3.2a). The yields are 3–10 times higher than those from acidic and neutral solutions. The GlyGly yields from the highly acidic solutions (pH 2.2–3.4) are 2–3 times higher than those from the mildly acidic and neutral solutions (pH 4.3–7.1) except for solutions containing Fe^{2+} and Cu^{2+}. At pH 9.8–9.9, the GlyGly yields from solutions containing Ca^{2+} and Mg^{2+} are 0.7–0.8 times lower than those without metal ions, whereas the GlyGly yields from solutions containing Zn^{2+} and Cu^{2+} are nearly similar to those without metal ions (Fig. 3.2a). At pH 4.3–7.1, the GlyGly yields from solutions containing Fe^{2+} and Cu^{2+} are similar to those without metal ions, whereas the GlyGly yield from solutions containing Ca^{2+}, Mg^{2+}, Zn^{2+}, and Mn^{2+} was nearly two times lower than that without metal ions (Fig. 3.2a). At pH 2.2–3.4, the GlyGly yields from solutions containing Ca^{2+}, Mg^{2+}, Zn^{2+}, Fe^{2+}, and Mn^{2+} are similar to those without metal ions, whereas the GlyGly yield from the solution containing Cu^{2+} was three times lower than that without metal ions (Fig. 3.2a).

In contrast, the DKP yields from basic solutions are much lower than those from acidic and neutral solutions, regardless of the presence or absence of any metal ion (Fig. 3.2b). In most cases, the DKP yields from mildly acidic and neutral solutions (pH 4.3–7.1) are higher than those from highly acidic solutions (pH 2.2–3.4), except for solutions with Mg^{2+} and Cu^{2+}. At pH 2.2–3.4, the DKP yields from solutions with metal ions were 1.2–3.5 times higher than solutions without metal ions (Fig. 3.2b). At pH 4.3–7.1, the DKP yields from solutions with metal ions were slightly smaller than solutions without metal ions (Fig. 3.2b).

GlyGlyGly, which was only produced from the solutions containing Cu^{2+}, is five times more abundant under basic conditions than under acidic and neutral conditions.

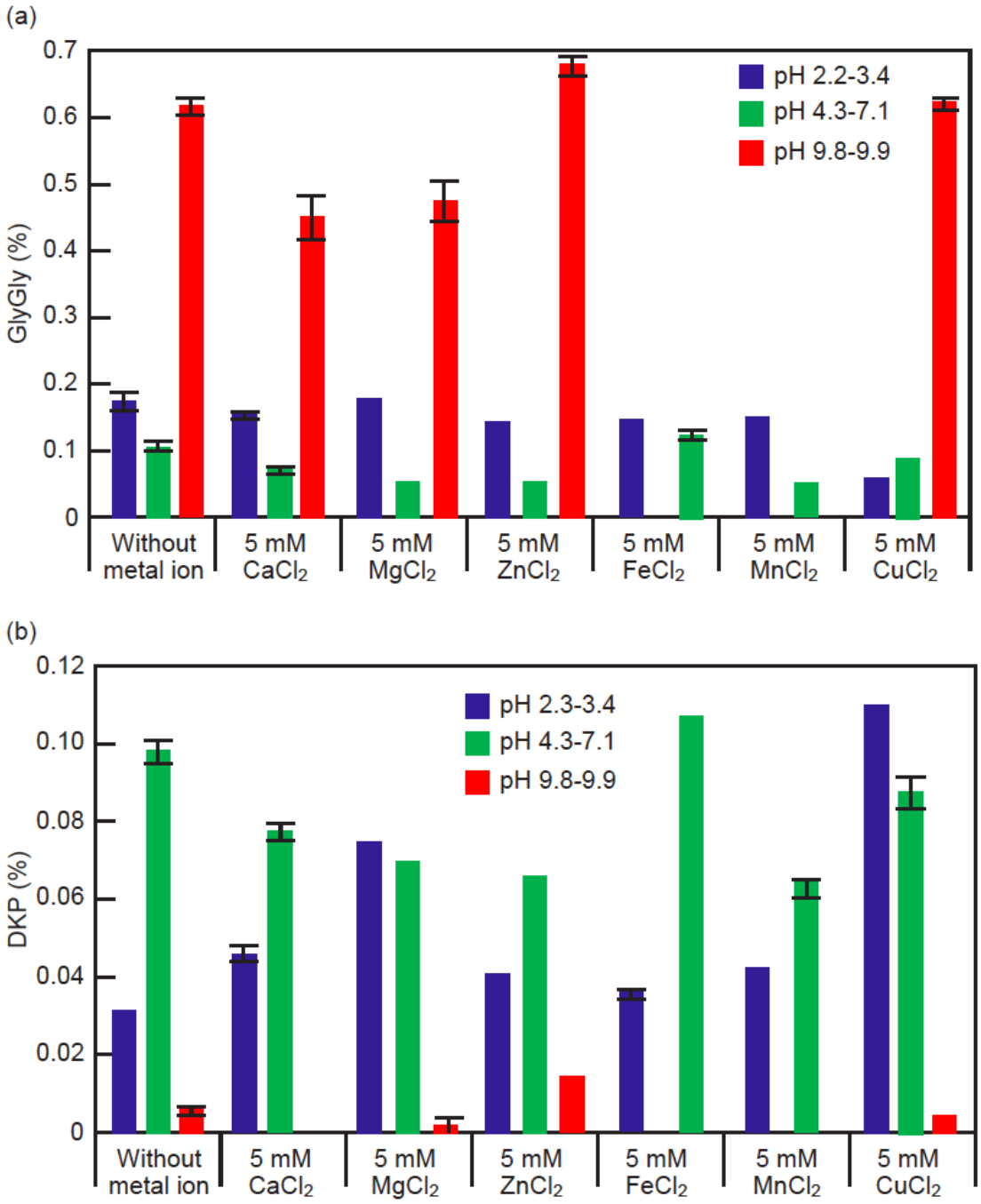

Fig. 3.2. Comparison of the yields of (a) GlyGly and (b) DKP obtained by heating of Gly solutions with or without metal ions at different pH conditions (see Table 3.1). Bar graphs: blue (pH 2.2–3.4), green (pH 4.3–7.1), and red (pH 9.8–9.9).

3.3.2. Estimation of the reaction rate constants

Time profiles of the concentrations of Gly, GlyGly, DKP, and GlyGlyGly are shown in Fig. 3.3. Under all experimental conditions, the reaction rates of GlyGly and

DKP are in the following order of pH 4.3–7.1 < pH 2.2–3.4 < pH 9.8–9.9. To estimate the reaction rates, we considered the following reactions, where k_n is the reaction rate constant, (Fig. 3.4): 1) the formation of GlyGly from Gly (second-order reaction, k_1), 2) the formation of DKP from GlyGly (first-order reaction, k_2), 3) the hydrolysis of GlyGly to produce Gly (first-order reaction, k_{-1}), 4) the hydrolysis of DKP to produce GlyGly (first-order reaction, k_{-2}) (Qian et al., 1993; Li and Brill, 2003), 5) the formation of GlyGlyGly from Gly and GlyGly (second-order reaction, k_3), and 6) the hydrolysis of GlyGlyGly to produce Gly and GlyGly (first-order reaction, k_{-3}).

Except for Cu^{2+}, the rate equations for these reactions can be written as,

$$\frac{d}{dt}[Gly] = 2k_{-1}[GlyGly] - 2k_1[Gly]^2 \qquad (1)$$

$$\frac{d}{dt}[GlyGly] = k_1[Gly]^2 + k_{-2}[DKP] - (k_{-1} + k_2)[GlyGly] \qquad (2)$$

$$\frac{d}{dt}[DKP] = k_2[GlyGly] - k_{-2}[DKP] \qquad (3)$$

At equilibrium, the rate equations for these reactions can be expressed as a function of the equilibrium constant E_n

$$k_{-1} = k_1 \frac{[Gly]^2_{equilibrium}}{[GlyGly]_{equilibrium}} = E_1 k_1 \qquad (4)$$

$$k_{-2} = k_2 \frac{[GlyGly]_{equilibrium}}{[DKP]_{equilibrium}} = E_2 k_2 \qquad (5)$$

Equations (1), (2), and (3) can be rewritten by using E_1 and E_2, as follows:

$$\frac{d}{dt}[Gly] = 2E_1 k_1[GlyGly] - 2k_1[Gly]^2 \qquad (6)$$

$$\frac{d}{dt}[GlyGly] = k_1[Gly]^2 + E_2 k_2[DKP] - (E_1 k_1 + k_2)[GlyGly] \qquad (7)$$

$$\frac{d}{dt}[DKP] = k_2[GlyGly] - E_2 k_2[DKP] \qquad (8)$$

Similarly, for the solution of Gly and Cu^{2+}, the rate equations are as follows:

$$\frac{d}{dt}[Gly] = 2k_{-1}[GlyGly] + k_{-3}[GlyGlyGly] - 2k_1[Gly]^2 - k_3[Gly][GlyGly]$$

(9)

$$\frac{d}{dt}[GlyGly] = k_1[Gly]^2 + k_{-2}[DKP] + k_{-3}[GlyGlyGly] - (k_{-1} + k_2)[GlyGly] - k_3[Gly][GlyGly] \quad (10)$$

$$\frac{d}{dt}[DKP] = k_2[GlyGly] - k_{-2}[DKP] \quad (11)$$

$$\frac{d}{dt}[GlyGlyGly] = k_3[Gly][GlyGly] - k_{-3}[GlyGlyGly] \quad (12)$$

At equilibrium, the rate equations for these reactions can be written as,

$$k_{-2} = k_2 \frac{[GlyGly]_{equilibrium}}{[DKP]_{equilibrium}} = E_2 k_2 \quad (13)$$

$$k_{-3} = k_3 \frac{[Gly]_{equilibrium}[GlyGly]_{equilibrium}}{[GlyGlyGly]_{equilibrium}} = E_3 k_3 \quad (14)$$

Equations (9), (10), and (11) can be rewritten by E_2 and E_3, as follows:

$$\frac{d}{dt}[Gly] = 2k_{-1}[GlyGly] + E_3 k_3[GlyGlyGly] - 2k_1[Gly]^2 - k_3[Gly][GlyGly] \quad (15)$$

$$\frac{d}{dt}[GlyGly] = k_1[Gly]^2 + E_2 k_2[DKP] + E_3 k_3[GlyGlyGly] - (k_{-1} + k_2)[GlyGly] - k_3[Gly][GlyGly] \quad (16)$$

$$\frac{d}{dt}[DKP] = k_2[GlyGly] - E_2 k_2[DKP] \quad (17)$$

$$\frac{d}{dt}[GlyGlyGly] = k_3[Gly][GlyGly] - E_3 k_3[GlyGlyGly] \quad (18)$$

Equations (6)–(8) or (15)–(18) were fitted to the experimental results to estimate the rate constants using least squares method and the numerical software Scilab (Fig. 3.3). The chelation species were not considered in the calculations, and the dominant fitting parameters were k_1 and k_{-1}, which were determined within two significant figures.

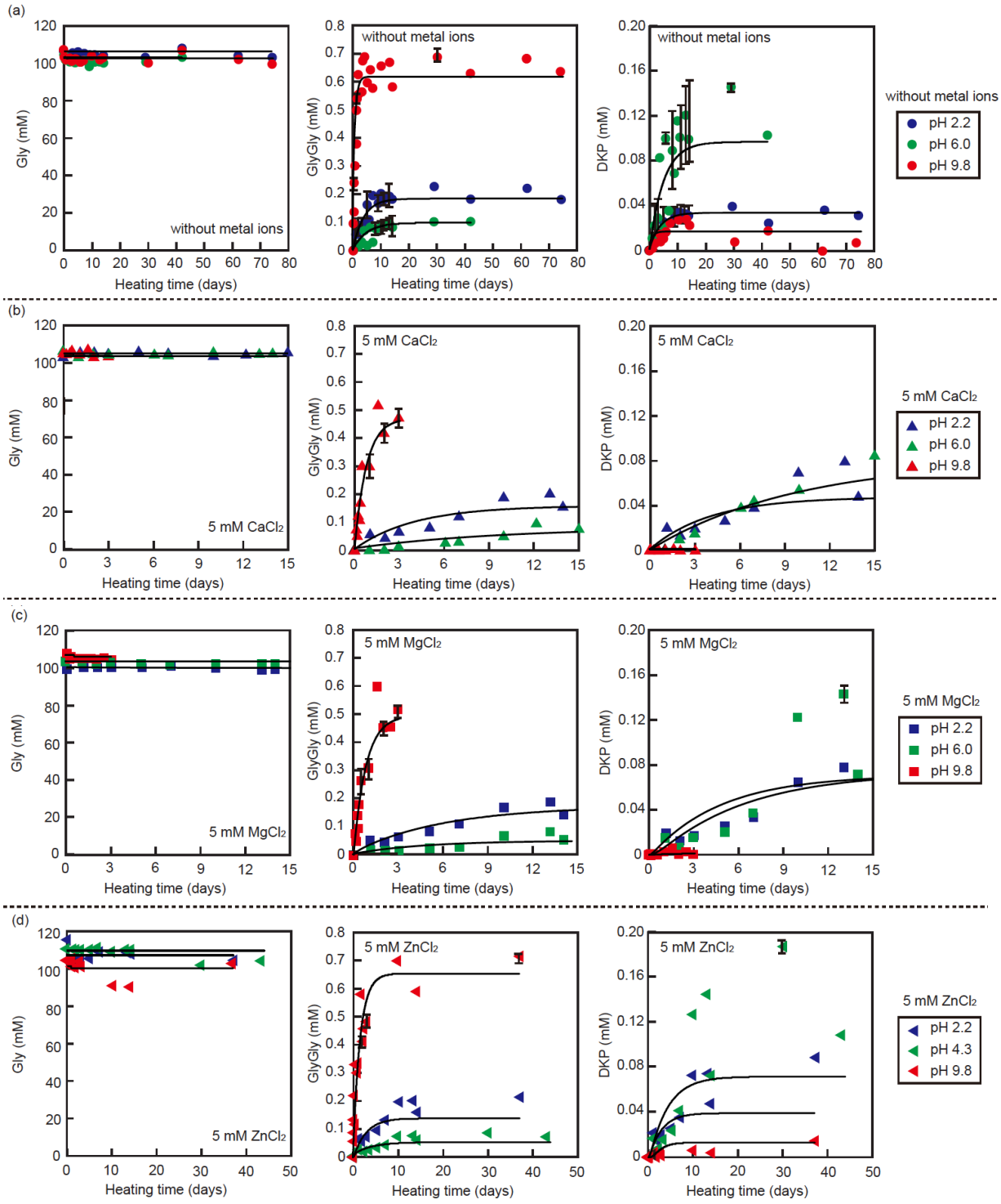
(a)
Gly (mM)
without metal ions
Heating time (days)
GlyGly (mM)
without metal ions
Heating time (days)
DKP (mM)
without metal ions
Heating time (days)
without metal ions
pH 2.2
pH 6.0
pH 9.8
(b)
Gly (mM)
5 mM CaCl2
Heating time (days)
GlyGly (mM)
5 mM CaCl2
Heating time (days)
DKP (mM)
5 mM CaCl2
Heating time (days)
5 mM CaCl2
pH 2.2
pH 6.0
pH 9.8
(c)
Gly (mM)
5 mM MgCl2
Heating time (days)
GlyGly (mM)
5 mM MgCl2
Heating time (days)
DKP (mM)
5 mM MgCl2
Heating time (days)
5 mM MgCl2
pH 2.2
pH 6.0
pH 9.8
(d)
Gly (mM)
5 mM ZnCl2
Heating time (days)
GlyGly (mM)
5 mM ZnCl2
Heating time (days)
DKP (mM)
5 mM ZnCl2
Heating time (days)
5 mM ZnCl2
pH 2.2
pH 4.3
pH 9.8

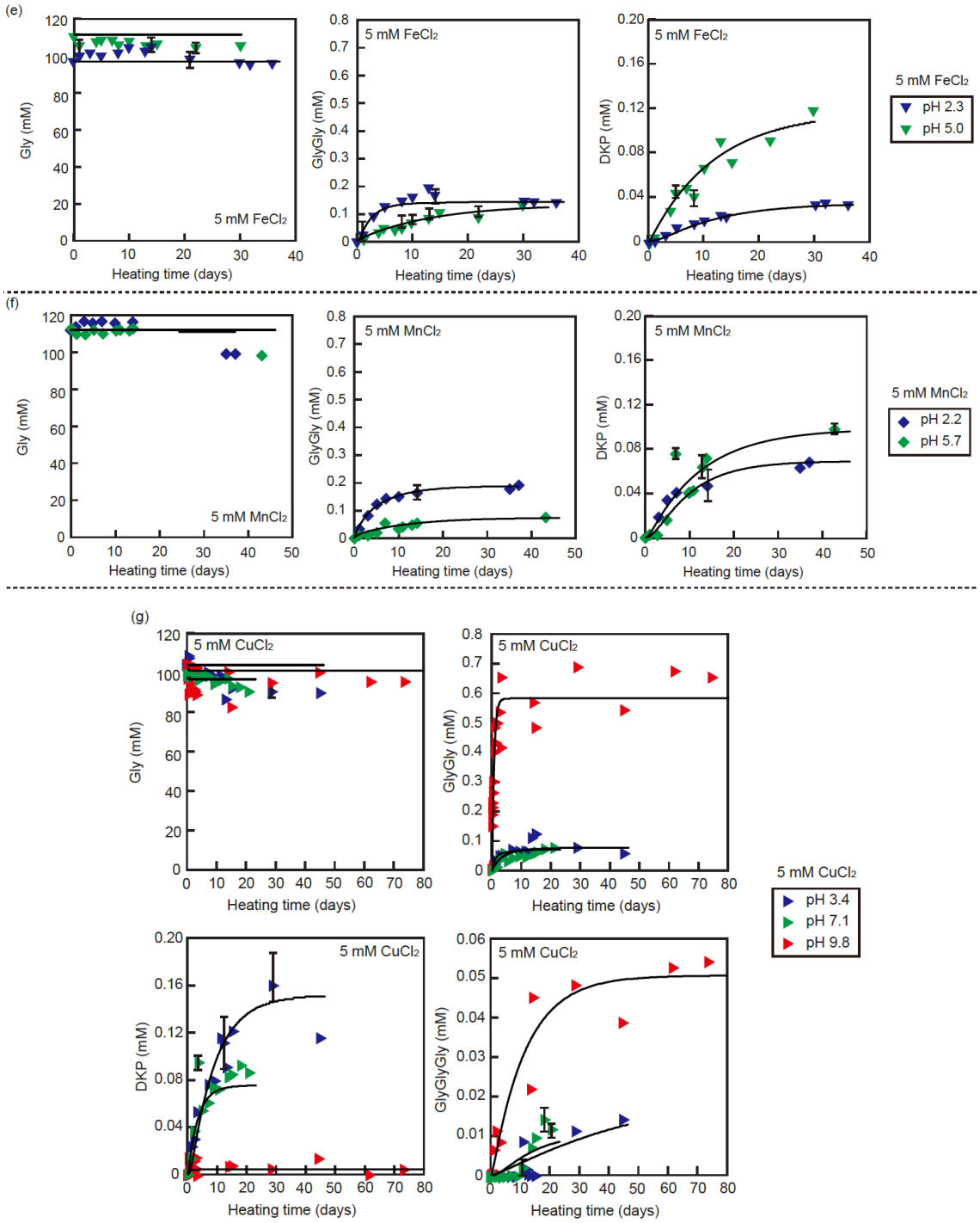

Fig. 3.3. Time profiles of the concentrations of Gly, GlyGly, and DKP in the solutions during heating at 140°C. (a) No metal ions were present, (b) with Ca^{2+}, (c) with Mg^{2+}, (d) with Zn^{2+}, (e) with Fe^{2+}, and (f) with Mn^{2+}. (g) Time profiles of the concentrations of Gly, GlyGly, DKP, and GlyGlyGly in the solutions during heating at 140°C with Cu^{2+}. Blue simboles: pH 2.2–3.4, green simboles: pH 4.3–7.1, and red simbols: pH 9.8–9.9. Solid lines represent the peak fittings for determining the rate constants.

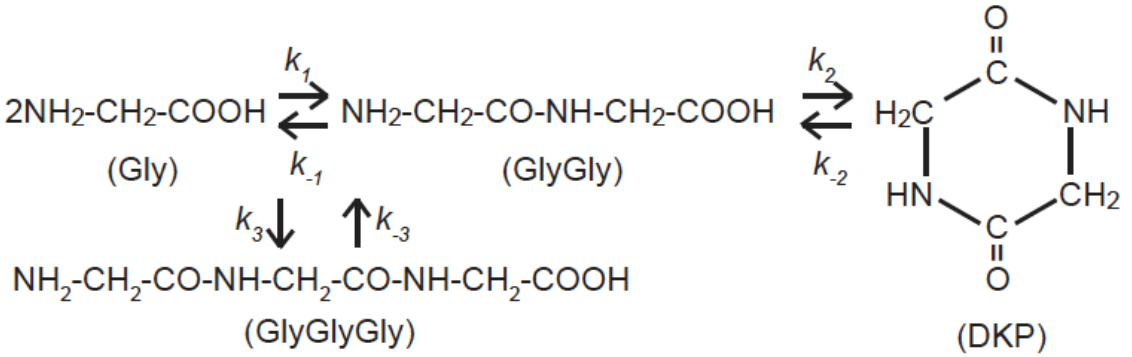

Fig. 3.4. Reaction pathways between Gly, GlyGly, GlyGlyGly, and DKP. The reaction rate constants (k_n) are as follows: dimerization of Gly (k_1), hydrolysis of GlyGly (k_{-1}), formation of DKP (k_2), hydrolysis of DKP (k_{-2}), formation of GlyGlyGly (k_3), and hydrolysis of GlyGlyGly (k_{-3}).

Table 3.3 and Fig. 3.5 summarize the reaction rates (k_1, k_{-1}, k_2, and k_{-2}) for the various conditions. The dimerization rate constants of Gly (k_1) at pH 9.8–9.9 are one order of magnitude higher than those under acidic and neutral conditions, regardless of the presence or absence of metal ions (Table 3.3). This is consistent with the conclusion of Sakata et al. (2010) that the dimerization rate of Gly is the greatest at pH 9.8 because of the presence of a Gly zwitterion and anion in equal molar fractions (Fig. 3.6). Generally, for similar pH ranges, the k_1 values are lower for reactions with metal ions than those without metal ions (Fig. 3.5a). However, the values for reactions with Cu^{2+} (pH 9.8) are 1.2 times higher than those without metal ions (Fig. 3.5a).

The hydrolysis rate constants of GlyGly (k_{-1}) have similar values in most cases (Table 3.3), and the formation rate constants of DKP from GlyGly (k_2) are roughly similar for the different pH values (Table 3.3). On the other hand, the k_2 values for the reactions with metal ions are one order of magnitude lower than those without metal ions (Fig. 3.5c). Hydrolysis rate constants of DKP (k_{-2}) with metal ions are one to three orders of magnitude lower than those without metal ions (Table 3.3). However, the k_{-2} values for reactions with metal ions under basic conditions (pH 9.8–9.9) are not estimated because of the very low yields of DKP and the large calculation errors. Thus, the k_2 and k_{-2} values for reactions with Ca^{2+} under basic conditions (pH 9.8–9.9) were not estimated, because the concentration of DKP was below the detection limit. The formation rate constant of GlyGlyGly (k_3) was only calculated from the reactions with

Cu^{2+}. The value of k_3 in neutral conditions (pH 7.1) is 1.5–2 times higher than that in acidic (pH 3.4) and basic (pH 9.8) conditions.

Table 3.3. Rate constants (k_1, k_2, k_{-1}, k_{-2}, k_3, and k_{-3}) for solutions without and with metal ions (Ca^{2+}, Mg^{2+}, Zn^{2+}, Fe^{2+}, Mn^{2+}, and Cu^{2+}) at different pH conditions and heating times at 140°C.

	k_1 (l mol^{-1} s^{-1})	k_{-1} (s^{-1})	k_2 (s^{-1})	k_{-2} (s^{-1})	k_3 (l mol^{-1} s^{-1})	k_{-3} (s^{-1})
No metal ion (pH 2.3)	6.2×10^{-8}	3.8×10^{-6}	2.7×10^{-4}	1.3×10^{-3}	-	-
Ca^{2+} (pH 2.3)	5.5×10^{-8}	3.7×10^{-6}	5.5×10^{-5}	1.8×10^{-4}	-	-
Mg^{2+} (pH 2.3)	4.9×10^{-8}	2.8×10^{-6}	6.3×10^{-6}	1.5×10^{-5}	-	-
Zn^{2+} (pH 2.3)	6.4×10^{-8}	5.3×10^{-6}	2.9×10^{-5}	9.9×10^{-5}	-	-
Fe^{2+} (pH 2.3)	7.2×10^{-8}	4.7×10^{-6}	2.8×10^{-7}	1.1×10^{-6}	-	-
Mn^{2+} (pH 2.2)	4.1×10^{-8}	2.7×10^{-6}	1.4×10^{-6}	3.8×10^{-6}	-	-
Cu^{2+} (pH 3.4)	6.6×10^{-8}	9.3×10^{-6}	4.2×10^{-6}	9.6×10^{-7}	6.7×10^{-7}	3.5×10^{-8}
No metal ion (pH 6.0)	4.3×10^{-8}	4.0×10^{-6}	1.3×10^{-3}	1.0×10^{-3}	-	-
Ca^{2+} (pH 5.7)	1.7×10^{-8}	2.4×10^{-6}	6.2×10^{-5}	5.9×10^{-5}	-	-
Mg^{2+} (pH 5.7)	2.9×10^{-8}	6.1×10^{-6}	4.8×10^{-5}	3.4×10^{-5}	-	-
Zn^{2+} (pH 4.5)	3.7×10^{-8}	7.9×10^{-6}	1.3×10^{-5}	9.8×10^{-6}	-	-
Fe^{2+} (pH 5.0)	2.0×10^{-8}	1.9×10^{-6}	4.1×10^{-5}	4.6×10^{-5}	-	-
Mn^{2+} (pH 5.7)	1.4×10^{-8}	2.5×10^{-6}	8.1×10^{-6}	5.9×10^{-6}	-	-
Cu^{2+} (pH 7.1)	5.5×10^{-8}	7.1×10^{-6}	9.3×10^{-5}	9.0×10^{-5}	1.4×10^{-6}	1.3×10^{-7}
No metal ion (pH 9.8)	8.3×10^{-7}	1.4×10^{-5}	4.1×10^{-4}	4.5×10^{-2}	-	-
Ca^{2+} (pH 9.8)	6.2×10^{-7}	1.4×10^{-5}	-	-	-	-
Mg^{2+} (pH 9.9)	6.2×10^{-7}	1.4×10^{-5}	3.8×10^{-6}	1.3×10^{-3}	-	-
Zn^{2+} (pH 9.8)	4.8×10^{-7}	7.3×10^{-6}	2.0×10^{-7}	9.8×10^{-6}	-	-
Cu^{2+} (pH 9.8)	9.7×10^{-7}	1.7×10^{-5}	8.3×10^{-5}	3.9×10^{-2}	8.8×10^{-7}	1.5×10^{-5}

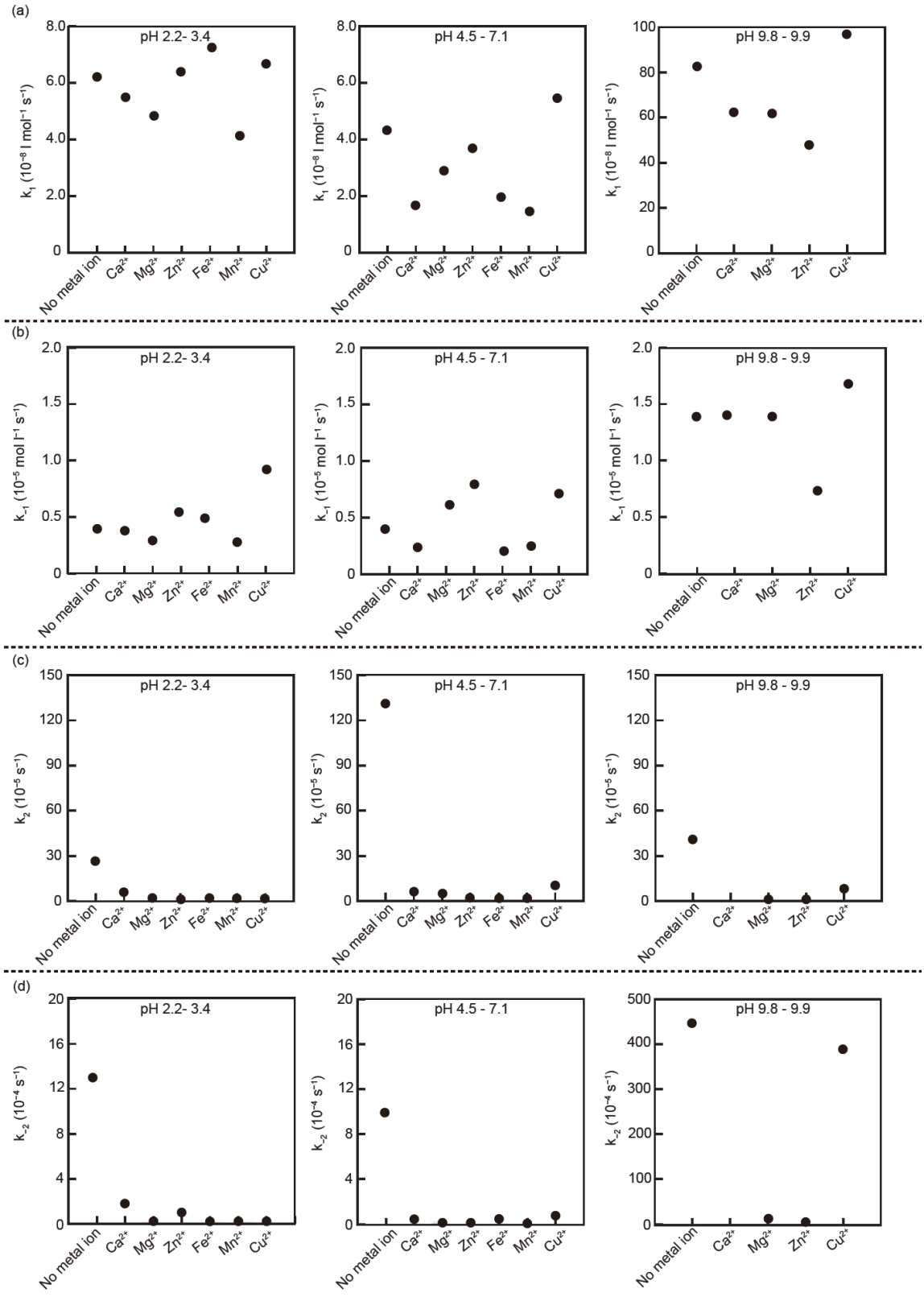

Fig. 3.5. Comparison of the rate constants (a) k_1, (b) k_{-1}, (c) k_2, and (d) k_{-2} for solutions with or without metal ions at different pH conditions.

3.3.3. Stability of the Cu^{2+} complex and the SIPF reaction

Eder and Rode (1994) proposed a scheme for the catalysis of the Salt Induced Peptide Fromation (SIPF) reaction by $CuCl_2$. In this scheme, the hydrated $CuCl_2$ binds one amino acid in the chelate form as well as a second amino acid in its protonated form only through the carbonyl oxygen. In the complex, the amino acids facilitate the nucleophilic attack of the chelated amino group nitrogen to the carboxyl carbon to form peptides (Eder and Rode, 1994). The Cu^{2+} complex is very stable compared to Ca^{2+}, Mg^{2+}, and Zn^{2+} complexes, as verified by Gibbs free energies; the distances between metal ions and the carbonyl oxygen of Gly; and ionic radii (Remko and Rode, 2006). Thus, the higher k_1 values for Cu^{2+} under basic and neutral conditions in this study can be explained by the higher stability of the Cu^{2+} complex with Gly in the SIPF reaction. The Zn^{2+} complex is the second most stable, reflecting the relatively high yields of GlyGly (Fig. 3.2a).

The lower k_1 values for acidic and neutral conditions can be explained by the difference of chemical species of Gly at different pH conditions (Fig. 3.6; Sakata et al., 2010). The dissociation of Gly in the aqueous solutions is independent of temperature (Sakata et al., 2010). For the chelation of the Cu^{2+} complex with Gly, a carboxylate anion and a lone pair of amino nitrogen of one Gly molecule need to bind with Cu^{2+}. Basic conditions are ideal for chelation, because an anionic state of Gly (Gly^-: NH_2–CH_2–COO^-) is present as well as a zwitterionic state ($Gly^{\pm}$: NH_3^+–CH_2–COO^-). Thus, the value of k_1 for basic conditions with Cu^{2+} is very high. Although the chelation is possible because $Gly^{\pm}$ binds with Cu^{2+}, in neutral conditions it is less effective because of the lack of Gly^-. However, chelation is difficult under acidic conditions, because Gly is positively charged (Gly^+: NH_3^+–CH_2–COOH), lowering the k_1 value for acidic conditions with Cu^{2+} compared to conditions without metal ions.

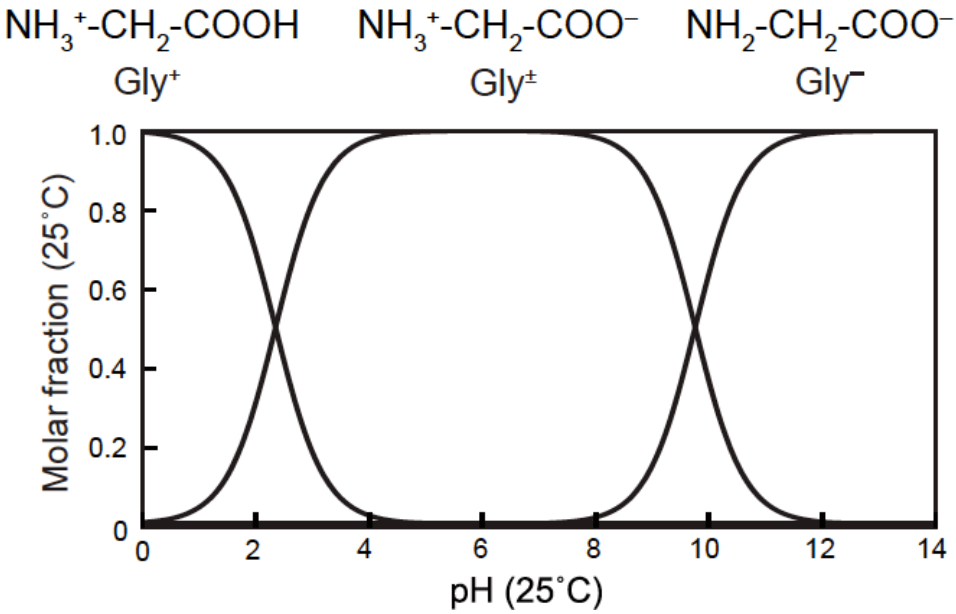

Fig. 3.6. Molar fractions of different dissociation states of Gly as a function of pH at 25 and 140°C. They were determined based on published dissociation constants (Sakata et al., 2010; on the basis of Marshall and Franck, 1981; Goldberg et al., 2002; Clarke et al., 2005).

Similarly, the formation of GlyGlyGly under conditions containing Cu^{2+} (Fig. 3.4) seems to be related to the steric structure of Cu^{2+} complexes with GlyGly (Kaneda and Martell, 1975; Gergely and Nagypál, 1976; Kittl and Rode, 1981; Eder and Rode, 1994; Remko and Rode, 2006). Figure 3.7 shows the molar fractions of the seven chemical species of Cu^{2+} complexes with GlyGly with respect to pH (Kittl and Rode, 1981). Kittl and Rode (1981) determined the formation constants for complexes between Cu^{2+} and GlyGly using potentiometric titration. The concentration of Cu^{2+} and GlyGly were 1 and 5 mM, respectively. The systems were titrated with a 50 mM NaOH solution. All investigations were carried under nitrogen atmosphere at 20ºC and an ionic strength of 200 mM KCl. The systems contained all theoretically possible chemical species of the 1:1 and 1:2 complexes with Cu^{2+} and GlyGly. For the calculation of the formation constants, a Fortran computer program was used. At pH >7.5, the most abundant species is a Cu^{2+} complex with two GlyGly with which another Gly molecule can easily react to yield GlyGlyGly. It is proposed that NaCl also promotes the polymerization of amino acids with Cu^{2+} and increases the formation of di- and tri-peptides (Eder and Rode, 1994; Rode and Schwendinger 1990). Therefore, the yields of di- and tri-peptides

could be higher under subseafloor conditions because of the high concentration of NaCl.

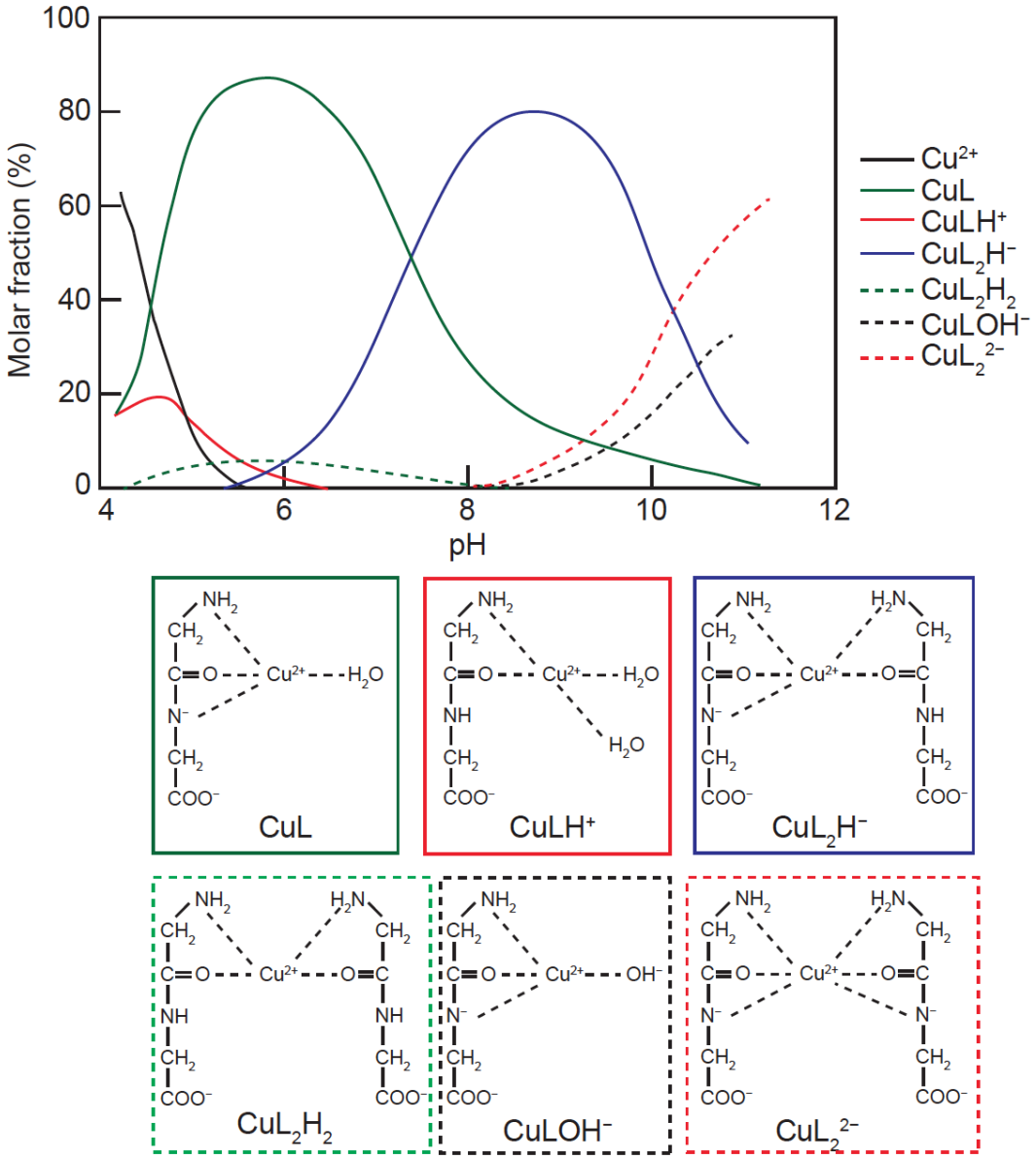

Fig. 3.7. Molar fractions of different Cu^{2+}-chelates to GlyGly as a function of pH at a metal–peptide ratio of 1:5 at 20°C. "L" indicates a ligand of GlyGly (revised Kittl and Rode, 1981).

Hydrothermal fluids are highly reduced and mainly contain Cu^{+} species. Sander and Koschinsky (2011) indicated that dissolved copper species bind as Cu^{2+} with organic compounds in hydrothermal fluids once the redox conditions become oxic because of the mixing of hydrothermal fluids and seawater. Cu^{+} may be less active to

form complexes with amino acids than Cu^{2+}, because the electrons in Cu^{+} occupy all the d orbitals unlike Cu^{2+}. However, Leal and van den Berg (1998) proposed that Cu^{+} forms strong complexes with thiols such as glutathione. Cu^{+} may also effectively polymerize amino acids by forming complexes with amino acids. Mixing of hydrothermal fluids and seawater inevitably occurs; therefore, it is important to consider the effect of Cu^{2+}.

3.3.4. Inhibition of peptide formation by metal ions

This study has demonstrated that most of the metal ions decrease the dimerization rates of Gly and GlyGly yields, except for Cu^{2+} and Zn^{2+} in basic solutions (Figs. 3.2 and 3.5a). In the solutions containing Fe^{2+} that had precipitate of red iron oxides after heating, the oxidation of iron may affect the Gly reactions. Apparently, most of the metal ions promote the hydrolysis of peptides rather than the synthesis. The results are consistent with previous studies (Cronin et al., 1971).

In addition, metal ions may inhibit peptide synthesis by chelation with Gly and GlyGly molecules. The lower formation rates of DKP (k_2) with metal ions than those without metal ions are attributed to the stabilization by chelation with GlyGly (Cronin et al., 1971; Kittl and Rode, 1981; Rainer and Rode, 1982). In a metal–GlyGly complex, the amino or carboxylic group is bound to the metal ion; however, the nucleophilic attack to form DKP is inhibited, although DKP has C=O bonds that can coordinate with metal ions. Complexes with DKP and metal ions have positive charge regardless of pH, because DKP does not dissociate in aqueous solution. Therefore, the hydration of DKP by H^{+} is not favored in acidic (pH 2.2–3.4) and mildly acidic or neutral (pH 4.3–7.1) conditions because of the Coulomb repulsion between the complexes and H^{+}, which is consistent with our results (Fig. 3.2 and Table 3.2). Consequently, prebiotic elongation of peptides is not expected under the experimental conditions of this study. Our conclusion that deep-sea hydrothermal systems are not favorable environments for even simple peptides is in good agreement with Cleaves et al. (2009).

Most previous studies focused on the degree of elongation of the peptide bonds (e.g., Lahav et al., 1978; Lawless and Levi, 1979; Rode, 1999; Bujdák and Rode, 2003). However, it is unclear whether the elongation of the peptide bonds is critical to origin-of-life reactions (Cleaves et al., 2009). Nonetheless, it was proposed that GlyGly promotes the polymerization of amino acids (Plankensteiner et al., 2002). Metal–amino acid or metal–short peptide complexes have various functions, such as self-organization

(e.g., Ohata et al., 1995; 1996), self-recombination (e.g., Mizutani et al., 1998), and catalysis (e.g., Weckhuysen et al., 1996), which could contribute to origin-of-life reactions. In addition, the complexes have high mobility in the oceans without precipitation of metallic ions as minerals (e.g., Toner et al., 2009; Sander and Koschinsky, 2011) and might have facilitated primitive biological functions in the Earth's early oceans.

3.4. Conclusions

In this study, the formation and decomposition rates of diglycine (GlyGly and DKP) and triglycine (GlyGlyGly) were estimated by heating aqueous solutions of glycine at 140°C in the presence of metal ions (Ca^{2+}, Mg^{2+}, Zn^{2+}, Fe^{2+}, Mn^{2+}, and Cu^{2+}) under various pH conditions. High-pH aqueous solutions with Cu^{2+} are the most favorable for prebiotic peptide formation, and triglycine is only produced under these conditions. This observation expands the potential for chemical evolution to new types of deep-sea hydrothermal environments such as the Lost City or south Chamorro sea mount that eruct low-temperature, high-pH fluids because of serpentinization. On the other hand, the other metal ions that we examined promote the hydrolysis rather than the oligomerization of peptides. The metal ions have different effects because of the stability of the complexes (Irving–Williams series) and the pH-dependent dissociation of the chelating amino acid ligands. The results do not support the traditional chemical evolution hypothesis that the oligomerization of amino acids led to the synthesis of proto-proteins (long peptides); however, the formation of short peptides is sufficient to achieve biofunctionality, the next step in prebiotic chemistry. Finally, metal complexes with Cu^{2+} and amino acids or short peptides may have contributed in enzyme catalysis in the early oceans because of higher metal ion concentration.

3.5. References

Anbar A. D. (2008) Elements and evolution. *Science* 322, 1481-1483.

Bujdák J. and Rode B. M. (1999) Silica, alumina and clay catalyzed peptide bond formation: enhanced efficiency of alumina catalyst. *Orig. Life Evol. Biosph.* 29, 451-461.

Bujdák J. and Rode B. M. (2003) Peptide bond formation on the surface of activated alumina: peptide chain elongation. *Catalysis Letters* 91, 149-154.

Clarke R. G. F., Collins C. M., Roberts J. C., Trevani L. N., Bartholomew R. J. and Tremaine P. R. (2005) Ionization constants of aqueous amino acids at temperatures up to 250°C using hydrothermal pH indicators and UV-visible spectroscopy: Glycine, α-alanine, and proline. *Geochim. Cosmochim. Acta* 69, 3029-3043.

Cleaves H. J., Aybrey A. D. and Bada J. L. (2009) An evaluation of the critical parameters for abiotic peptide synthesis in submarine hydrothermal systems. *Orig. Life Evol. Biosph.* 39, 109-126.

Corliss J. B. (1990) Hot springs and the origin of life. *Nature* 347, 624.

Cronin J. R., Long D. A. and Truscott T. G. (1971) Part 12–The effect of Zn(II) on the reaction of some glycine-containing dipeptides and substituted diketopiperazines at pH 5.6 and 368.2 K. *Peptide Kinetics* 2096-2100.

Eder A. and Rode B. M. (1994) Influence of alkali- and alkaline-earth-metal cations on the "salt-induced peptide formation" reaction. *J. Chem. Soc. Dalton Trans.* 1125-1130.

Gergely A. and Nagypál I. (1976) Studies on transition-metal-peptide complexes. Part 1. Equilibrium and thermochemical study of the copper(II) complexes of glycylglycine, glycyl-DL-α-alanine, DL-α-alanylglycine, and DL-α-alanyl-DL-α-alanine. *J. C. S. Dalton* 1104-1108.

Goldberg R. N., Kishore N. and Lennen R. M. (2002) Thermodynamic quantities for the ionization reactions of buffers. *J. Phys. Chem. Ref. Data* 31, 231-370.

Holm N. G. (1992) Chapter 1 Why are hydrothermal systems proposed as plausible environments for the origin of life? *Orig. Life Evol. Biosph.* 22, 5-14.

Holm N. G. and Andersson E. (2005) Hydrothermal simulation experiments as a tool for studies of the origin of life on Earth and other terrestrial planets: a review. *Astrobiology* 5, 444-460.

Holm N. G. and Neubeck A. (2009) Reduction of nitrogen compounds in oceanic basement and its implications for HCN formation and abiotic organic synthesis. *Geochemical Transactions* 10:9, doi: 10.1186/1467-4866-10-9.

Holm N. G., Dumont M., Ivarsson M. and Konn C. (2006) Alkaline fluid circulation in ultramafic rocks and formation of nucleotide constituents: a hypothesis. *Geochemical Transactions* 7:7, doi: 10.1186/1467-4866-7-7.

Horita J. and Berndt M. E. (1999) Abiotic methane formation and isotopic fractionation under hydrothermal conditions. *Science* 285, 1055-1057.

Huber C. and Wächtershäuser G. (1998) Peptides by activation of amino acids with CO on (Ni,Fe)S surfaces: implications for the origin of life. *Science* 281, 670-672.

Hulme S. M., Wheat C. G., Fryer P. and Mottl M. (2010) Pore water chemistry of the Mariana serpentinite mud volcanoes: A window to the seismogenic zone. *Geochem. Geophys. Geosyst.* 11, 2009GC002674.

Imai E., Honda H., Hatori K., Brack A. and Matsuno K. (1999) Elongation of oligopeptides in a simulated submarine hydrothermal system. *Science* 283, 831-833.

Kaneda A. and Martell A. E. (1975) Aqueous equilibria of copper(II)- and nickel(II)-polyglycine complexes. *J. Coord. Chem.* 4, 137-151.

Kelley D. S., Karson J. A., Blackman D. K., Früh-Green G. L., Butterfield D. A., Lilley M. D., Olson E. J., Schrenk M. O., Roe K. K., Lebon G. T., Rivizzigno P. and the AT3-60 Shipboard Party. (2001) An off-axis hydrothermal vent field near the Mid-Atlantic Ridge at 30°N. *Nature* 412, 145-149.

Kelley D. S., Karson J. A., Fruh-Green G. L., Yoerger D. R., Shank T. M., Butterfield D. A., Hayes J. M., Schrenk M. O., Olson E. J., Proskurowski G., Jakuba M., Bradley A., Larson B., Ludwig K., Glickson D., Buckman K., Bradley A. S., Brazelton W. J., Roe K., Elend M. J., Delacour A., Bernasconi S. M., Lilley M. D., Baross J. A., Summons R. E. and Sylva S. P. (2005) A serpentinite-hosted ecosystem: The lost city hydrothermal field. *Science* 307, 1428-1434.

Kittl W. S. and Rode B. M. (1981) Complex formation of copper ion with aliphatic dipeptides. *Inorg. Chim. Acta.* 55, 21-27.

Lahav N., White D. and Chang S. (1978) Peptide formation in the prebiotic era: Thermal condensation of glycine in fluctuating clay environments. *Science* 201, 67-69.

Lawless J. M. and Levi N. (1979) The role of metal ions in chemical evolution: polymerization of alanine and glycine in a cation-exchanged clay environment. *Orig. Life Evol. Biosph.* 13, 281-286.

Leal M. F. C. and van den Berg C. M. G. (1998) Evidence for strong copper(I) complexation by organic ligands in seawater. *Aquat. Geochem.* 4, 49-75.

Li F., Fitz D., Fraser D. G. and Rode B. M. (2010) Catalytic effects of histidine enantiomers and glycine on the formation of dileucine and dimethionine in the salt-induced peptide formation reaction. *Amino Acids* 38, 287-294.

Li J. and Brill T. B. (2003) Spectroscopy of hydrothermal reactions. 27. Simultaneous determination of hydrolysis rate constants of glycylglycine to glycine and glycylglycine-Diketopiperazine equilibrium constants at 310-330°C and 275 bar. *J. Phys. Chem. A* 107, 8575-8577.

Long D. A., Truscott T. G., Cronin J. R. and Lee R. G. (1971) Part 11–Influence of divalent metal ions on rate of reaction of glycyl-glycine in the pH range 0.3-1.0 and 3.8-6.0. *Peptide Kinetics* 1094-1103.

Macleod G., McKeown C., Hall A. J. and Russell M. J. (1994) Hydrothermal and oceanic pH conditions of possible relevance to the origin of life. *Orig. Life Evol. Biosph.* 24, 19-41.

Marshall W. L. and Franck E. U. (1981) Ion product of water substance, 0-1000°C, 1-10,000 bars new international formulation and its background. *J. Phys. Chem. Ref. Data* 10, 295-304.

Martin W., Baross J., Kelley D. and Russell M. J. (2008) Hydrothermal vents and the origin of life. *Nature Rev. Microbiol.* 6, 805-814.

McCollom T. M. and Bach W. (2009) Thermodynamic constraints on hydrogen generation during serpentinization of ultramafic hosted deep-sea hydrothermal systems. *Astrobiology* 7, 933-950.

McCollom T. M. and Seewald J. S. (2007) Abiotic synthesis of organic compounds in deep-sea hydrothermal environments. *Chem. Rev.* 107, 382-401.

Mizutani M., Maejima N., Jitsukawa K., Masuda H. and Einaga H. (1998) An infinite chiral single-helical structure formed in Cu(II)-L-/D-glutamic acid system. *Inorg. Chim. Acta.* 283, 105-110.

Mottl M. J., Komor S. C., Fryer P. and Moyer C. L. (2003) Deep-slab fluids fuel extremophilic on a Mariana forearc serpentinite mud volcano: Ocean Drilling Program Leg 195. *Geochem. Geophys. Geosyst.* 4, 9009, doi: 10.1029/2003GC000588

Ohata N., Masuda H., Odani A. and Yamauchi O. (1995) Unprecedented double helical structure highly self-organized through hydrogen bonds between copper (II)-coordinated L-arginine and dicarboxylate motifs. *J. Inorg. Biochem.* 59, 721.

Ohata N., Masuda H. and Yamauchi O. (1996) Programmed self-assembly of copper(II)-L- and–D-arginine complexes chiral double-helical structures. *Angew. Chem. Int. Ed. Engl.* 35, 531-532.

Plankensteiner K., Righi A. and Rode B. M. (2002) Glycine and diglycine as possible catalytic factors in the prebiotic evolution of peptides. *Orig. Life Evol. Biosph.* 32, 225-236.

Qian Y., Engel M. H., Macko S. A., Carpenter S. and Deming J. W. (1993) Kinetics of peptide hydrolysis and amino acid decomposition at high temperature. *Geochim. Cosmochim. Acta* 57, 3281-3293.

Rainer M. J. A. and Rode B. M. (1982) The complex formation of calcium with aliphatic dipeptides. *Monatshefte für Chemie* 113, 399-407.

Remko M. and Rode B. M. (2006) Effect of metal ions (Li^+, Na^+, K^+, Mg^{2+}, Ca^{2+}, Ni^{2+}, Cu^{2+}, and Zn^{2+}) and water coordination on the structure of glycine and zwitterionic glycine. *J. Phys. Chem. A* 110, 1960-1967.

Rode B. M. (1999) Peptides and the origin of life. *Peptides* 20, 773-786.

Rode B. M. and Schwendinger M. G. (1990) Copper-catalyzed amino acid condensation in water–a simple possible way of prebiotic peptide formation. *Orig. Life Evol. Biosph.* 20, 401-410.

Russell M. J. (2003) The importance of being alkaline. *Science* 302, 580-581.

Russell M. J. and Hall A. J. (1997) The emergence of life from iron monosulphide bubbles at a submarine hydrothermal redox and pH front. *J. Geol. Soc.* 154, 377-402.

Sakata K., Kitadai N. and Yokoyama T. (2010) Effects of pH and temperature on dimerization rate of glycine: Evaluation of favorable environmental conditions for chemical evolution of life. *Geochim. Cosmochim. Acta* 74, 6841-6851.

Sander S. G. and Koschinsky A. (2011) Metal flux from hydrothermal vents increased by organic complexation. *Nature Geoscience* 4, 145-150.

Schwendinger M. G. and Rode B. M. (1989) Possible role of copper and sodium chloride in prebiotic evolution of peptides. *Analytical Sciences* 5, 411-414.

Shibuya T., Komiya T., Nakamura K., Takai K. and Maruyama S. (2010) Highly alkaline, high-temperature hydrothermal fluids in the early Archean ocean. *Precambrian Res.* 182, 230-238.

Tivey M. K. (2007) Generation of seafloor hydrothermal vent fluids and associated mineral deposits. *Oceanography* 20, 50-65.

Tivey M. K., Humphris S. E., Thompson G. and Hannington M. D. (1995) Deducing patterns of fluid flow and mixing within the TAG active hydrothermal mound using

mineralogical and geochemical data. *J. Geophys. Res.* 100, 12527-12555.

Toner B. M., Santelli C. M., Marcus M. A., Wirth R., Chan C. S., McCollom T., Bach W. and Edwards K. J. (2009) Biogenic iron oxyhydroxide formation at mid-ocean ridge hydrothermal vents: Juan de Fuca Ridge. *Geochim. Cosmochim. Acta* 73, 388-403.

Weckhuysen B. M., Verberckmoes A. A., Fu L. and Schoonheydt R. A. (1996) Zeolite-encapsulated copper (II) amino acid complexes: synthesis, spectroscopy, and catalysis. *J. Phys. Chem.* 100, 9456-9461.

Wheat C. G., Fryer P., Takai K. and Hulme S. (2010) Spotlight 9 South Chamorro Seamount. *Oceanography* 23, 174-175.

Yanagawa H. and Kobayashi K. (1992) Chapter 8 An experimental approach to chemical evolution in submarine hydrothermal systems. *Orig. Life Evol. Biosph.* 22, 147-159.

Chapter 4

Effects of basalt, pressure, and temperature on the reactions of glycine in aqueous solution

4.1. Introduction

Deep-sea hydrothermal systems have attracted attention of many scientists as a suitable environment for chemical evolution in the early Earth (e.g., Corliss, 1990; Holm, 1992; Yanagawa and Kobayashi, 1992; Macleod et al., 1994; Russell and Hall, 1997; Russell, 2003; Holm and Andersson, 2005; Martin et al., 2008). A lot of experiments for abiotic synthesis of various organic molecules under the simulating hydrothermal conditions have been conducted (e.g., Ferris et al., 1978; Yanagawa et al., 1984; Harada and Fox, 1964; Imai et al., 1999; Rode, 1999; Huber and Wächetershäuser, 2003; Lambert, 2008; Lemke et al., 2009). In hydrothermal systems, seawater percolates into the deep oceanic crust and reacts with the surrounding rocks at high temperatures. As a result, hot and reduced fluids were eructed from hydrothermal vents (up to 400°C) (Tivey et al., 1995; Tivey, 2007). Water–rock interaction produces a broad range of pH and redox conditions in seafloor hydrothermal fluids (e.g., East Pacific Rise, Lucky Strike hydrothermal field, Rainbow plume, and Trans-Atlantic Geotraverse area), and might have controlled the prebiotic chemistry. In our previous studies, we evaluated the effects of pH and metal ions on polymerization of glycine in aqueous conditions without minerals or rocks. We proposed that basic solutions containing Cu^{2+} at 150°C is the best condition to polymerize amino acids (Sakata et al., 2010; Sakata et al., in press). Effects of metal ions were less than those of pH and pH condition is critical aqueous condition for polymerization of amino acids. However, the yields of GlyGly and GlyGlyGly were 0.62 and 0.05 % after heating at 140°C and pH 9.8 with Cu^{2+} (Sakata et al., in press). The other catalyst activations, such as pressure, condensation or presence of minerals and rocks, are necessary to promote polymerization of amino acids.

It has proposed that the effects of catalysis of clay minerals to synthesis and polymerization of amino acids (e.g., Lahav et al., 1978; Lahav and White 1978; Ponnamperuma et al., 1982; Bujdák and Rode, 2003; Lambert, 2008; Marshall-Bowman et al., 2010). Surfaces of clay minerals are elementally charged in aqueous solution. As a result, amino acids are adsorbed on the surface of clay minerals and polymerization reactions are promoted. To date, the effects of silica, alumina, hectorite, and montmorillonite on the polymerization of amino acids were actively studied (e.g., Yoshino et al., 1971; Bujdák et al., 1997; Bujdák and Rode, 1999a; Bujdák and Rode, 1999b; Bujdák and Rode, 2001; Bujdák and Rode, 2002; Bujdák and Rode, 2003). The

adsorption mechanisms of amino acids and clay minerals are also studied (Meng et al., 2004; Parbhakar et al., 2007; Stievano et al., 2007; Gao et al., 2008; Lambert 2008; Kitadai et al., 2009). While, oceanic crust are mainly composed basalts and has been widely spread from the formation of the earth and has been noticed as one of the possible environments including the earliest ecosystems in the earth (Edwards et al., 2012). Basalt might have catalyzed polymerization of amino acids. However, to date, the effects of basalt on the polymerization of amino acids have not been studied yet.

High-pressure (~10-30 MPa) is also one of the most important environmental conditions under hydrothermal systems. To date, polymerization of amino acids simulating hydrothermal systems have been studied (e.g., Imai et al., 1999; Mitsuzawa and Yukawa, 2004). Imai et al. (1999) heated 100 mM Gly solution containing 10 mM $CuCl_2$ at 250°C and 24.0 MPa using flow reactor and obtained hexa-glycine. Mitsuzawa and Yukawa (2004) heated 100 mM Gly solution at 200°C and 25.0 MPa for 25 minutes using flow reactor and obtained di-glycine. Polymerization of powdered amino acids under high-pressure conditions have been also studied (Ohara et al., 2007; Otake et al., 2011). Ohara et al (2007) heated powdered glycine at 150°C and 100 MPa for 8 days and obtained hexa-glycine. Otake et al (2011) heated powdered glycine and alanine at 250°C and 2.5-5.5 GPa for 24 hours and obtained hexa-glycine. Otake et al (2011) also proposed that stability of amino acids at 5.5 GPa are higher than those at 2.5GPa. It is prospect that pressure also catalyzes polymerization of amino acids in the aqueous conditions. However, the effects of pressure on polymerization of amino acids have not been studied systematically under the aqueous solution.

In this study, systematic heating experiments of Gly solution containing powdered basalts under various pressure (10-35 MPa) to determine the effects of pressure and basalt on the formation of peptides.

4.2. Methods

Analytical grade Gly, GlyGly, and Glycylglycylglycine (GlyGlyGly) were obtained from the Peptide Institute. DKP was obtained from Tokyo Chemical Industry. We used mid ocean ridge basalt collected from North Pond at the 184.2 meter below sea floor (mbsf) on the western flank of the Mid-Ocean Ridge that composed relatively young (~8 Ma) subseafloor (~ 4000 meter water depth) basaltic crust. The basaltic sample was fresh basalt altered only by low-temperature (<20 °C) alteration by seawater

(Expedition 336 Scientists 2012).

Solutions of 100 mM Gly with pH 6.0 were prepared. Basaltic samples were poedered by stainless mortar. The surface areas of basaltic powder were measured by BET multipoint isotherm analysis (Flow Sorb III; Shimadzu) and the value was 0.33 ± 0.01 (m^2/g). Each Gly solution (~ 0.7-0.9 ml) and powdered basalt was placed in a heat-shrinkable teflon tube (~ 40 mm length and 8 mm in diameter) and sealed the sides with teflon rods (~ 10 mm length and 8 mm in diameter). The ratio by weight of Gly solution and basalt in the tubes was 10:1 and tubes were filled with samples. To seal the sides of heat-shrinkable tubes, heat gun were used with careful heating only sides of tubes and teflon rods. Finally, the solutions were inserted by high-pressure container heated in an electric oven at 100-200°C and 10-35 MPa within 12 hours (Fig. 3.1). For comparison, Gly solutions without basalts were heated at 200 °C, 35 MPa and 6 hours. Maximum temperature of this methods is 200 °C. Most samples were heated at 200 °C because except for basic fluids, hydrothermal fluids are < 400 °C. Temperature and pressure were contained within an accuracy of 3°C and 0.34 MPa. Heating experiments were run twice at each experimental condition. Before and after the experiment, the pH of the solutions was measured at 25°C with a pH meter (B-212; HORIBA). The changes in the pH before and after the experiments were <2.7.

Each sample filtrated by filter syringe (0.2 μm) was diluted 10 times and analyzed by using a high-performance liquid chromatography (HPLC) system (ICA-2000; TOA DKK) equipped with a Jasco UV-2075 detector at a wavelength of 200 nm. A reversed phase-type HPLC column (Hydrosphere C18; YMC) was used at 37°C. A 10 mM $C_6H_{13}SO_3Na$ solution with pH 2.5 was used as eluent and adjusted using H_3PO_4 (Bujdák and Rode, 1999a) at a flow rate of 1.0 ml min^{-1}. Gly, GlyGly, GlyGlyGly, and DKP were identified and quantified by comparing the observed peak retention times and peak areas, respectively, with those of standard compounds. The errors in the concentrations of Gly, GlyGly, GlyGlyGly, and DKP were estimated to be <3.0%.

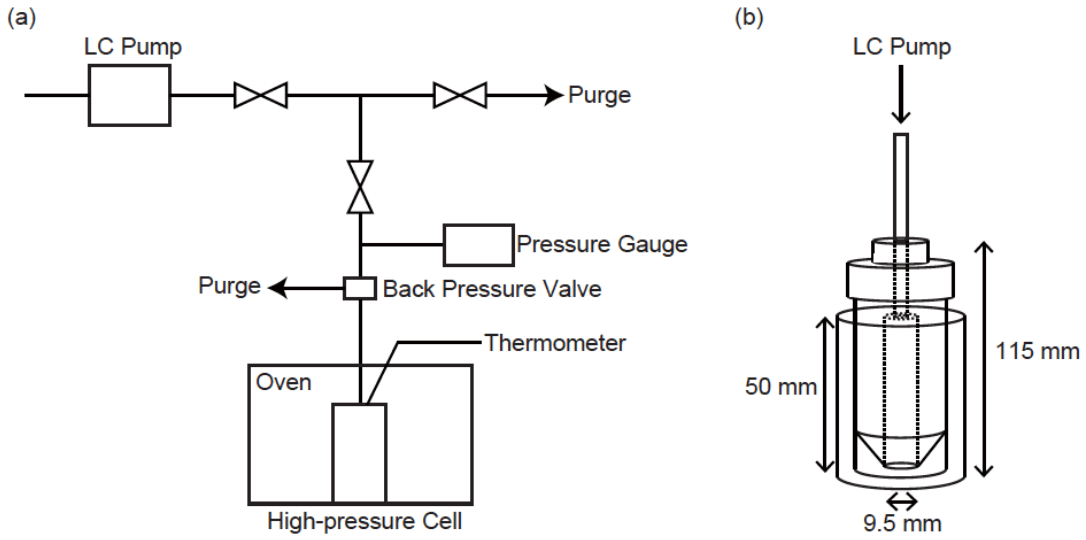

Fig. 4.1. (a) Scheme of experimental apparatus for heating experiments. (b) Scheme of a high-pressure container.

4.3. Results and Discussion

4.3.1. Yields of GlyGly, DKP, and GlyGlyGly

Figure 4.2 shows the chromatograms of the products obtained from the solutions after the hydrothermal reactions under the respective conditions. GlyGly, DKP and GlyGlyGly were produced under all conditions (Fig. 4.2), however GlyGlyGly detected after only first heating experiments. The relative abundances of GlyGly, DKP, and GlyGly increased with increasing heating time, while those of Gly were almost constant (Fig. 4.2).

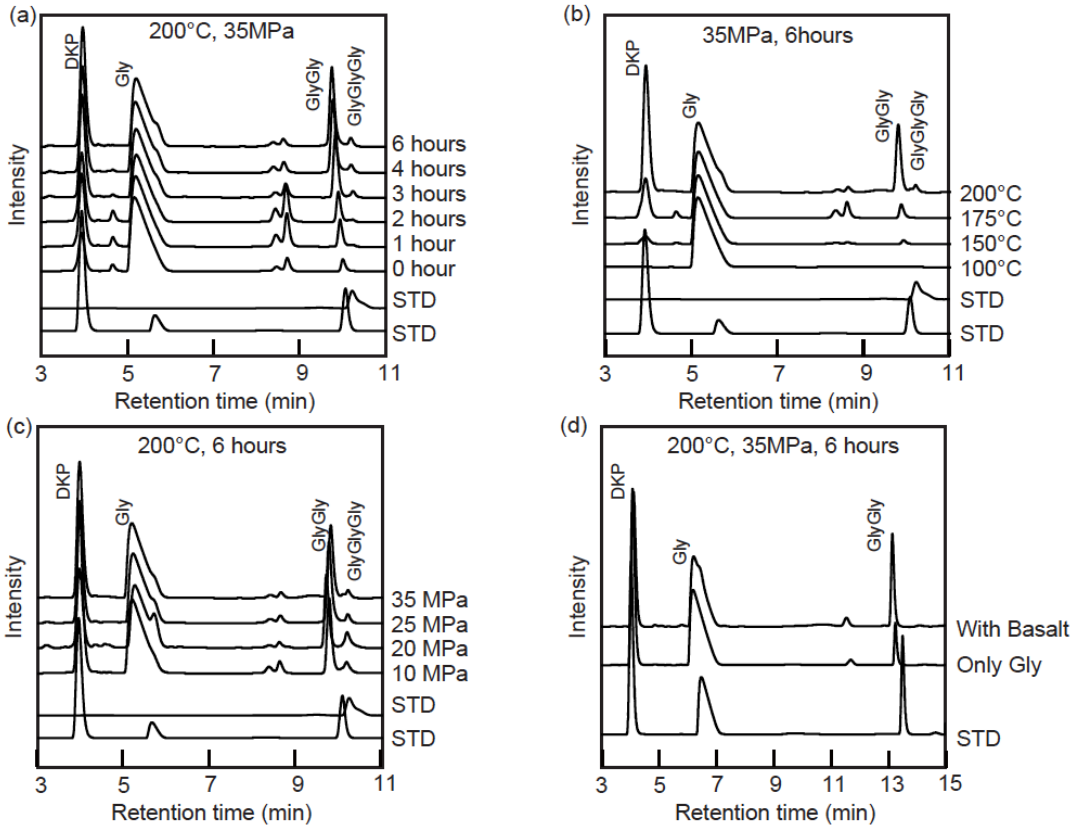

Fig. 4.2. HPLC chromatograms before and after the hydrothermal reactions of glycine in aqueous solution at (a) 200°C and 35 MPa with basalts (b) 35 MPa for 6 hours with basalts (c) 200°C for 6 hours with basalts, and (d) 200°C, 35 MPa for 6 hours with or without basalts. STD shows standards for Gly, GlyGly, GlyGlyGly, and DKP.

Fig. 4.3 and Table 4.1 summarize the yields of GlyGly and DKP. We conducted twice experiments for each experimental condition. Plots mean average values and maximum and minimum values are evaluated as errors. The concentrations of GlyGly and DKP increased with increasing heating time (Fig. 4.3 (a)). The concentration of GlyGly and DKP heated for 12 hours were slightly smaller than those heated for 6 hours. Adsorption of Gly, GlyGly, DKP may be actively occur in the samples heated for 12 hours. The yields of GlyGly and DKP was depend on temperature and those increased as temperature increased within 100-200 °C (Fig. 4.3 (b)). While, the yields of GlyGly and DKP did not depend on pressure and those were almost similar within 10-35 MPa (Fig. 4.3 (c)). Phase transition of water does not occur under the experimental conditions in this study, therefore physical properties of water are constant and yields of GlyGly and DKP were not depend on pressure. The yield of GlyGly from

solutions containing basalts was 2.6 times higher than those from solutions without basalts, while the yield of DKP from solutions containing basalts was 0.84 times lower than those without basalts (Table 4.1).

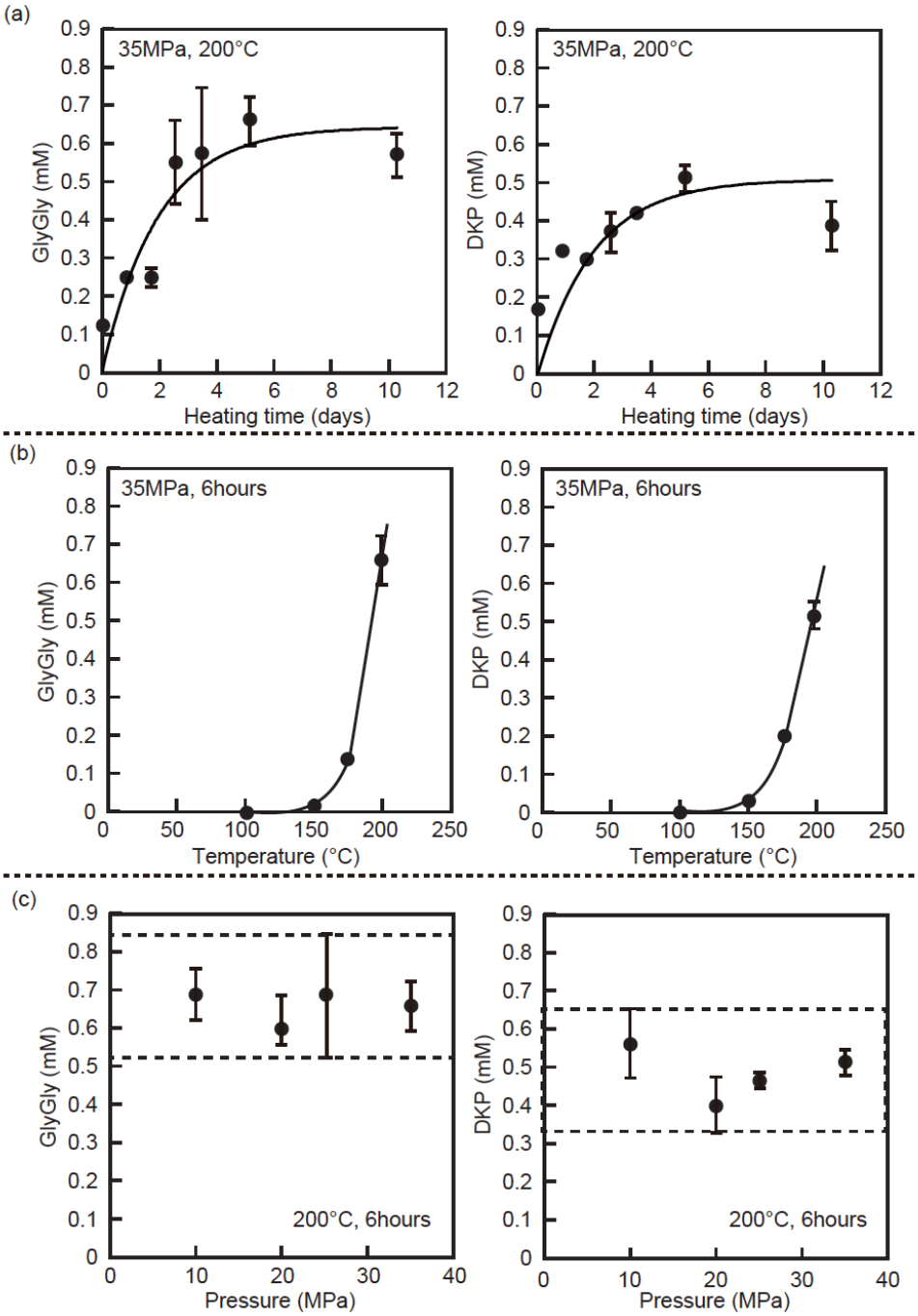

Fig. 4.3. Concentrations of GlyGly, and DKP in the solutions during heating at (a) 200°C and 35 MPa (b) 35 MPa for 6 hours, and (c) 200°C for 6 hours with basalt, respectively. Solid lines in (a) are the results of fitting to determine the rate constants.

Table 4.1. Yields of GlyGly and DKP in the solution during heating at 200°C and 35 MPa for 6 hours with and without basalt, respectively.

	GlyGly (mM)	DKP (mM)
Without basalt	0.25 (±0.02)	0.62 (±0.01)
With Basalt	0.66 (±0.06)	0.52 (±0.04)

4.3.2. Estimation of the reaction rate constants

To analyze the experimental results, we need to consider the following reactions: Gly to GlyGly (second-order reaction; k_1), GlyGly to DKP (first-order reaction; k_2), GlyGly to Gly (first-order reaction; k_{-1}), and DKP to GlyGly (first-order reaction; k_{-2}) (Qian et al., 1993; Li and Brill, 2003), where k_1, k_{-1}, k_2 and k_{-2} are the rate constants. The rate equations for these reactions can be written as:

$$\frac{d}{dt}[\mathrm{Gly}] = 2k_{-1}[\mathrm{GlyGly}] - 2k_1[\mathrm{Gly}]^2 \qquad (1)$$

$$\frac{d}{dt}[\mathrm{GlyGly}] = k_1[\mathrm{Gly}]^2 + k_{-2}[\mathrm{DKP}] - (k_{-1} + k_2)[\mathrm{GlyGly}] \qquad (2)$$

$$\frac{d}{dt}[\mathrm{DKP}] = k_2[\mathrm{GlyGly}] - k_{-2}[\mathrm{DKP}] \qquad (3)$$

To obtain the rate constants, the above rate equations were fitted to the experimental results by the least-squares method using the numerical software Scilab. The results of fitting for the formation of GlyGly and DKP are shown in Figs. 4.3(a). The rate constants obtained in this study and the dimerization rate constant determined on the published Arrenius plots of k_1 (Sakata et al., 2010) are shown in Table 4.2. The dimerization rate with basalt was 13 times higher than that without basalt.

Table 4.2. Rate constants (k_1, k_2, k_{-1} and k_{-2}) for solutions with basalt and dimerization reaction rate determined on the published Arrenius plots of k_1 (Sakata et al., 2010) at at 200 °C.

	k_1 (l mol^{-1} s^{-1})	k_{-1} (s^{-1})	k_2 (s^{-1})	k_{-2} (s^{-1})
Without basalt	1.1×10^{-6}	-	-	-
With Basalt	1.4×10^{-5}	3.8×10^{-3}	2.1×10^{-4}	4.8×10^{-3}

4.3.3. Promotion of peptide bond formation by basalt

Formation of GlyGly from solutions containing basalt was higher than those without basalt, while formation of DKP was similar regardless of presence of basalt (Table 4.1). Metal ions dissolved from basalts after heating experiments are low, for example, concentration of Na, K, Ca, Fe and Al after heating experiments of basalt glass and seawater (initial seawater/rock mass ratio was 10) at 150°C and 500 bars (50 MPa) were 5, 1200, 0.35, 0.06 ppm (Seyfried and Bisschoff, 1979). The catalyzing effects of basalt on polymerization of amino acids are caused by adsorption between basaltic surface and Gly.

It was proposed that alumina is the most actively promote polymerization of glycine among alumina, silica, and hectorite (Bujdák and Rode, 1999b). The mechanisms of polymerization of amino acids by alumina were following (Fig. 4.4); the catalytically active sites are formed through the condensation reactions of hydroxyl groups bound to the neighboring aluminum atoms (Fig. 4.4 (a)), carboxylic groups are attracted to surface of alumina and form Al-OCO bonds (Fig. 4.4 (b)), and finally peptide bonds are formed through nucleophilic reaction by positively charged amino groups (NH_3^+) (Fig. 4.4 (c)) (Bujdák and Rode, 1999d). The catalytic effects of alumina are (1) the removal of intramolecular interaction between $–COO^-$ and $–NH_3^+$ groups within amino acid molecules (2) increasing of the electrophilicity of carbonyl carbon in the amino acids (Bujdák and Rode, 1999b).

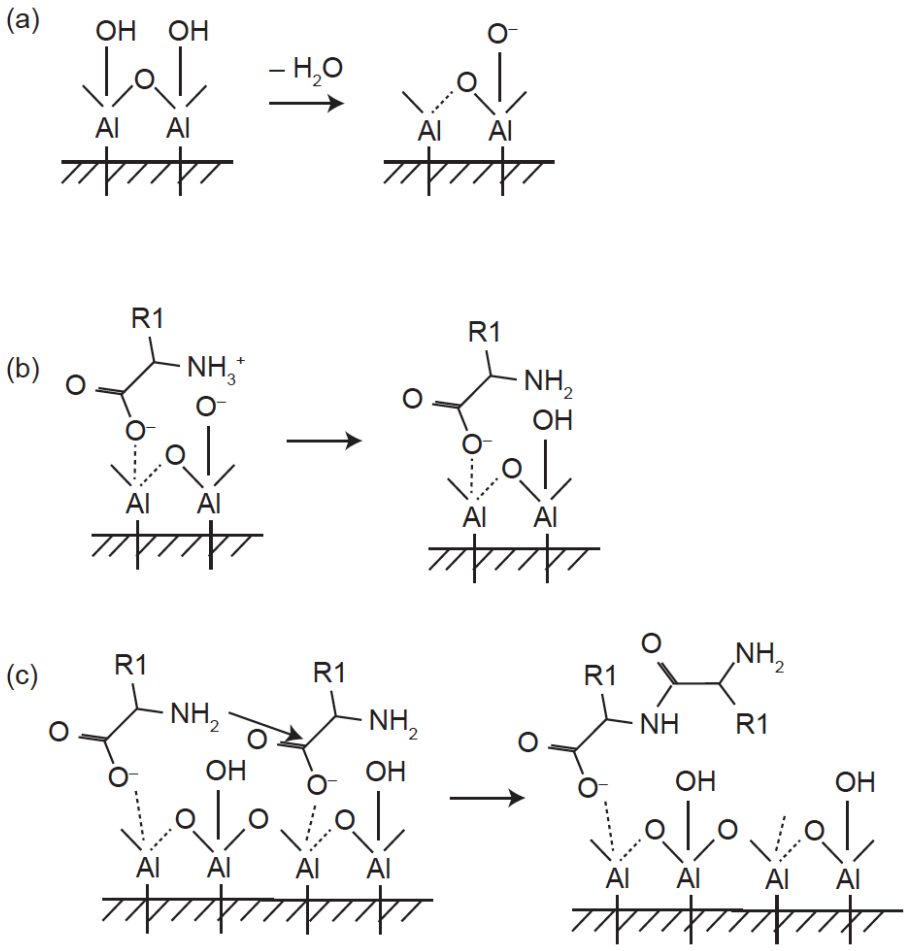

Fig. 4.4. Interaction of alumina and amino acids (zwitterions) leading to peptide bond formation. (a) The formation of catalytically active sited on alumina surface. (b) The activation of functional groups of amino acids at alumina surface. (c) Assumed mechanism of peptide bond formation on alumina surface. (Modified from Bujdák and Rode, 1999b).

In addition to alumina surface, the surface of silica, titania (TiO_2), and kaolinite surface also adsorb carboxylic groups of amino acids through the interaction between Si-O^-, Ti^{4+}, and S-OH_2 (Collins et al., 1988; Ikhsan et al., 2004; Qiu and Barteau, 2007; Lambert 2008). Basalt also contain silica, alumina, and TiO_2, therefore these adsorption between amino acids and these minerals probably catalyze polymerization of amino acids. Chimneys at hydrothermal systems contain much of sulfur oxide and this sulfur also may promote polymerization of amino acids. Basalt composes the oceanic crusts and widely prevails under the subseafloor. The uppermost about 500 m of basaltic

oceanic crust is permeable and fluid flow is focused in specific areas at the contacts of lava flows or in brecciated zones (Fisher 2005). The flow paths beneath the hydrothermal vents are probably one of the most suitable environments for polymerization of amino acids. In these flow paths, the amino acids can adsorb to the surface of basalts and prevent dilution until hydrothermal fluids eruct at hydrothermal vents. In addition to amino acids, hydrogen cyanide (HCN) can be formed from CO and NH_3 in the basement environments (Holm and Neubeck, 2009). HCN is suspected precursor for abiotic synthesis of organic matters. HCN are reactive and easily react to formamide (Saladino et al., 2012). Silica, TiO_2, iron sulfur minerals also promotes synthesis of amino acids and nucleobases from formamide (Saladino et al., 2012). Both of amino acids and nucleobases might have been syntheszed and polymerized in the basement environments. At the present days, in these areas, sea water oxidizes basaltic crust and it has been estimated that these interaction effects on the microbial ecosystems (Bach and Edwards, 2003; Edwards et al., 2005). Chemical reaction between basalts and sea water release energy for supporting chemosynthetic microbes. Oceanic crust is the largest potential habitat in the earth and may support a significant fraction of total biomass (Edwards et al., 2005). In the primitive earth, abundant ecosystems might have prevailed under the hydrothermal systems.

4.4. Conclusion

We studied the effects of basalts, pressure, and temperature on the reaction of Gly. The yields of GlyGly and DKP was depend on temperature and those increased as temperature increased within 100-200 °C. The yields of GlyGly and DKP were similar at 10-35 MPa and formation of GlyGly and DKP did not depend on pressure. While, basalts promoted the formation of GlyGly and the yields of GlyGly with basalt were 2.6 times larger than those without basalt. The dimerization rate with basalt was 13 times higher than that without basalt. These catalytic effects of basalts result from the removal of intramolecular interaction between $–COO^-$ and $–NH_3^+$ groups within amino acid molecules and increasing of the electrophilicity of carbonyl carbon in the amino acids. It is difficult to promote the polymerization of amino acids in the aqueous solution and interaction of amino acids and surface of solids are one of the prospective catalysts. The flow paths beneath the hydrothermal vents flowing hydrothermal fluids around 200°C are probably one of the most suitable environments for polymerization of amino acids.

4.5. References

Bach W. and Edwards K. J. (2003) Iron and sulfide oxidation within the basaltic ocean crust: Implications for chemolithoautotrophic microbial biomass production. *Geochim. Cosmochim. Acta* 67, 3871-3887.

Bujdák J. and Rode B. M. (1997) Glycine oligomerization on silica and alumina. *Reaction kinetics and catalysis letters* 62, 281-286.

Bujdák J. and Rode B. M. (2001) Activated alumina as an energy source for peptide bond formation: Consequences for mineral-mediated prebiotic processes. *Amino acids* 21, 281-291.

Bujdák J. and Rode B. M. (2002) Preferential amino acid sequences in alumina-catalyzed peptide bond formation. *J. Inorg. Biochem.* 90, 1-7.

Bujdák J. and Rode B. M. (1999a) The effect of clay structure on peptide bond formation catalysis. *Journal of Mplecular Catalysis A.* 144, 129-136.

Bujdák J. and Rode B. M. (1999b) Silica, alumina and clay catalyzed peptide bond formation: enhanced efficiency of alumina catalyst. *Orig. Life Evol. Biosph.* 29, 451-461.

Bujdák J. and Rode B. M. (2003) Peptide bond formation on the surface of activated alumina: peptide chain elongation. *Catalysis Letters* 91, 149-154.

Collins J. R., Loew G. H., Luke B. T. and White D. H. (1988) Theoretical investigation of the role of clay edges in prebiotic peptide bond formation. *Orig. Life Evol. Biosph.* 18, 107-119.

Corliss J. B. (1990) Hot springs and the origin of life. *Nature* 347, 624.

Edwards K. J., Bach W. and McCollom T. M. (2005) Geomicrobiology in oceanography: microbe-mineral interactions at and below the seafloor. *TRENDS in Microbiology* 13, 449-456.

Edwards K. J., Becker K. and Colwell F. (2012) The deep dark energy biosphere: Intraterrestrial life on Earth. *Annu. Rev. Earth Planet. Sci.* 40, 551-568.

Edwards, K. J.; Backert, N.; Bach, W.; Becker, K.; Klaus, A.; Griffin, D. W.; Anderson, L.; Haddad, A. G.; Harigane, Y.; Campion, P. L.; Hirayama, H.; Mills, H. J.; Hulme, S. M.; Nakamura, K.; Jorgensen, S. L.; Orcutt, B.; Insua, T. L.; Park, Y. -S.; Rennie, V.; Salas, E. C.; Rouxel, O.; Wang, F.; Russel, J. A.; Wheat, C. G.; Sakata, K.; Brown, M.; Magnusson, J. L.; Ettlinger, Z. (2013) Mid-atlantic ridge microbiology: initiation of long-term coupled microbiological, geochemical, and

hydrological experimentation within the seafloor at North Pond, western flank of the Mid-Atlantic Ridge *Integrated Ocean Drilling Program: Preliminary Reports* 336. d*oi*:10.2204/iodp.sd.14.05.2012.

Edwards, K. J.; Backert, N.; Bach, W.; Becker, K.; Klaus, A.; Griffin, D. W.; Anderson, L.; Haddad, A. G.; Harigane, Y.; Campion, P. L.; Hirayama, H.; Mills, H. J.; Hulme, S. M.; Nakamura, K.; Jorgensen, S. L.; Orcutt, B.; Insua, T. L.; Park, Y. -S.; Rennie, V.; Salas, E. C.; Rouxel, O.; Wang, F.; Russel, J. A.; Wheat, C. G.; Sakata, K.; Brown, M.; Magnusson, J. L.; Ettlinger, Z. (2012) Initiation of long-term coupled microbiological, geochemical, and hydrological experimentation within the seafloor at North Pond, western flank of the Mid-Atlantic Ridge. *Integrated Ocean Drilling Program: Preliminary Reports* 336. doi:10.2204/iodp.pr.336.2012

Ferris J. P., Joshi P. G., Edelson E. H. amd Lawless J. G. (1978) HCN: A plausible source of purines, pyrimidines and amino acids on the primitive earth. *Journal of Molecular Evolutio*n 11, 293-311.

Fisher A. T. (2005) Marine hydrogeology: recent accomplishments and future opportunities. *Hydorogeol. J.* 13, 69-97.

Gao Q., Xu W., Xu Y., Wu D., Sun Y., Deng F. and Shen W. (2008) Amino acid adsorption on mesoporous materials: Influence of types of amino acids, modification of mesoporous materials, and solution conditions. *J. Phys. Chem. B* 112, 2261-2267.

Harada K. and Fox S. W. (1964) The thermal copolymerization of amino acids common to protein. *Nature, 201, 355-356.*

Holm N. G. (1992) Chapter 1 Why are hydrothermal systems proposed as plausible environments for the origin of life? *Orig. Life Evol. Biosph.* 22, 5-14.

Holm N. G. and Andersson E. (2005) Hydrothermal simulation experiments as a tool for studies of the origin of life on Earth and other terrestrial planets: a review. *Astrobiology* 5, 444-460.

Huber C. and Wächtershäuser G. (2003) A possible primordial peptide cycle. *Science* 301, 938-940.

Ikhsan J., Johnson B. B., Wells J. D, and Angove M. J. (2004) Adsorption of aspartic acid on kaolinite. *J Coll Interf Sci.* 273, 1-5.

Imai E., Honda H., Hatori K., Brack A. and Matsuno K. (1999) Elongation of oligopeptides in a simulated submarine hydrothermal system. *Science* 283, 831-833.

Kitadai N., Yokoyama N. and Nakashima S. (2009) ATR-IR spectroscopic study of L-lysine adsorption on amorphous silica. *J. Colloid. Interface Sci.* 329, 31-37.

Lambert J. (2008) Adsorption and polymerization of amino acids on mineral surfaces: A review. *Orig. Life Evol. Biosph.* 38, 211-242.

Lahav N., White D. and Chang S. (1978) Peptide formation in the prebiotic era: Thermal condensation of glycine in fluctuating clay environments. *Science* 201, 67-69.

Lemke K. H., Rosenbauer R. J., Bird D. K. (2009) Peptide synthesis in early earth hydrothermal systems. *Astrobiology* 9, 141-146.

Li J. and Brill T. B. (2003) Spectroscopy of hydrothermal reactions. 27. Simultaneous determination of hydrolysis rate constants of glycylglycine to glycine and glycylglycine-Diketopiperazine equilibrium constants at 310-330°C and 275 bar. *J. Phys. Chem. A* **107**, 8575-8577.

Macleod G., McKeown C., Hall A. J. and Russell M. J. (1994) Hydrothermal and oceanic pH conditions of possible relevance to the origin of life. *Orig. Life Evol. Biosph.* 24, 19-41.

Marshall-Bowman K., Ohara S., Sverjensky D. A., Hazen R. M. and Cleaves H. J. (2010) Catalytic peptide hydrolysis by mineral surface: implications for prebiotic chemistry. *Geochim. Cosmochim. Acta* 74, 5852-5861.

Martin W., Baross J., Kelley D. and Russell M. J. (2008) Hydrothermal vents and the origin of life. *Nature Rev. Microbiol.* 6, 805-814.

Meng M., Stievano L. and Lambert J. (2004) Adsorption and thermal condensation mechanism of amino acids on oxide supports. 1. Glycine on silica. *Langmuir* 20, 914-923.

Mitsuzawa S. and Yukawa T. (2004) A reaction network for triglycine synthesis under hydrothermal conditions. *Bull. Chem. Soc. Jan.* 77, 965-973.

Ohara S., Kakegawa T. and Nakazawa H. (2007) Pressure effects on the abiotic polymerization of glycine. *Orig. Life Evol. Biosph.* 37, 215-223.

Otake T., Taniguchi T., Furukawa Y., Kawamura F., Nakazawa H. and Kakegawa T. (2011) Stability of amino acids and their oligomerization under hugh-pressure conditions: implication for prebiotic chemistry. *Astrobiology* 11, 1-15.

Parbhakar A., Cuadros J. Sephton M. A., Dubbin W., Coles B. J. and Weiss D. (2007) Adsorption of L-lysine on montmorillonite. *Colloids and Surfaces A: Physicochem. Eng. Aspects* 307, 142-149.

Ponnamperuma C., Shimoyama A. and Friebele E. (1982) Clay and the origin of life. *Orig. Life Evol. Biosph.* 12, 9-40.

Qian Y., Engel M. H., Macko S. A., Carpenter S. and Deming J. W. (1993) Kinetics of peptide hydrolysis and amino acid decomposition at high temperature. *Geochim. Cosmochim. Acta* 57, 3281-3293.

Qiu T. and Barteau M. A. (2007) STM study of glycine on TiO_2 (110) single crystal surfaces. *J. Coll. Interf. Sci.* 303, 229-235.

Rode B. M. (1999) Peptides and the origin of life. *Peptides* 20, 773-786.

Russell M. J. (2003) The importance of being alkaline. *Science* 302, 580-581.

Russell M. J. and Hall A. J. (1997) The emergence of life from iron monosulphide bubbles at a submarine hydrothermal redox and pH front. *J. Geol. Soc.* 154, 377-402.

Sakata K., Kitadai N. and Yokoyama T. (2010) Effects of pH and temperature on dimerization rate of glycine: Evaluation of favorable environmental conditions for chemical evolution of life. *Geochim. Cosmochim. Acta* 74, 6841-6851.

Sakata K., Yabuta H. and Kondo T. Effects of metal ions and pH on the formation and decomposition rates of di- and tri-peptides in aqueous solution. *Geochemical Journal*, in press.

Saladino R., Crestini C., Pino S., Costanzo G. and Mauro E. D. (2012) Formamide and the origin of life. *Physics of Life Reviews* 9, 84-104.

Seyfried Jr. W. E. and Bisschoff J. L. (1979) Low temperature basalt alteration by seawater: an experimental study at 70°C and 150°C. *Geochim. Cosmochim. Acta* 43, 1937-1947.

Stievano L., Piao L. Y., Lopes I. Meng M. Costa D. and Lambert J. (2007) Glycine and lycine adsorption and reactivity on the surface of amorphous silica. *Eur. J. Mineral.* 19, 321-331.

Tivey M. K. (2007) Generation of seafloor hydrothermal vent fluids and associated mineral deposits. *Oceanography* 20, 50-65.

Tivey M. K., Humphris S. E., Thompson G. and Hannington M. D. (1995) Deducing patterns of fluid flow and mixing within the TAG active hydrothermal mound using mineralogical and geochemical data. *J. Geophys. Res.* 100, 12527-12555.

Yanagawa H., Makino Y., Sato K., Nishizawa K. and Egami F. (1984) Novel formation of alpha-amino-acids from alpha-oxo acids and anmonia in an aqueous-medium. *Orig. Life Evol. Biosph.* 14, 163-169.

Yanagawa H. and Kobayashi K. (1992) Chapter 8 An experimental approach to chemical evolution in submarine hydrothermal systems. *Orig. Life Evol. Biosph.* 22, 147-159.

Yoshino D., Hayatsu K. and Anders E. (1971) Origin of organic matter in early solar system—III. Amino acids: Catalytic synthesis *Geochim. Cosmochim. Acta* 35, 927-938.

Appendix

Carbon isotopic analyses of basalts and sediments in North Pond for research of deep subseafloor biosphere

A.1. Introduction

The majority of habitable environments in the earth are dark biosphere separated from sunlight. It is estimated that about one third of all biomass, and about three forth of all prokaryotic cells on the earth are in the sediments buried in oceanic subsurface (Whitman et al., 1998). In 1979, the hydrothermal system and the ecosystems supported by hydrothermal fluids were discovered around Galapagos Rift (Corliss et al., 1979). In 1994, it was first proposed that microorganisms exist in deep sea sediment cores from several hundreds of meters obtained during the Ocean Drilling Program (Parkes et al., 1994). In addition, basaltic ocean crust has been focused as a new deep submarine biosphere (Edwards and Bach, 2003). The uppermost about 500 m of basaltic oceanic crust is permeable and fluid flow is focused in specific areas at the contacts of lava flows or in brecciated zones (Fisher 2005). In these areas, sea water oxidizes young basaltic crust (< 10 Ma) and it has been estimated that this interaction effects on the microbial ecosystems (Edwards and Bach 2003; Edwards et al., 2005).

Chemical reaction between basalts and sea water release energy for supporting chemosynthetic microbes. Oceanic crust beneath the sediment is the largest potential habitat in the earth and may support a significant fraction of total biomass (Edwards et al., 2005). However the biosphere of basaltic oceanic crust has been poorly understood because of difficulty to access and return the samples.

Oceanic crust has been widely spread from the formation of the earth and has been noticed as one of the possible environments including the earliest ecosystems in the earth (Edwards et al., 2012). Understanding about ecosystems in the basaltic oceanic crust, such as metabolic systems, activity, abundance, derivation of microbes living there, leads to understanding origin of life or habitability in the primitive terrestrial and extraterrestrial deep biosphere.

In the past, Juan de Fuca Ridge in the eastern Pacific has been mainly studied because Juan de Fuca Ridge was an only site to observe clearly the water-rock reactions in basaltic crusts (e.g., Wheat et al., 2000; Fisher et al., 2003). In these basaltic oceanic crust, iron cycling, both oxidation and reduction of iron, supports metabolic activity in basalts, however, the microorganisms responsible for Fe oxidation on basalts are not clear (Orcutt et al., 2011). The colonization of basalts collected from subseafloor pillow basalts achieved detection of iron oxidation bacteria (Edwards et al., 2003; Mason et al., 2007; Singer et al., 2011). Edwards et al. (2003) isolated and cultured iron-oxidizing

bacteria from the surfaces of weathered rock and sediments collected in the Juan de Fuca area. Fisk et al (1998) proposed that microbes promote the weathering of basaltic glass by morphologic observation and chemical analysis in the microscopic region of basaltic glass collected from Atlantic, Pacific and Indian Oceans. In addition, Fisk et al., (1998) estimated that bacteria have colonized much of the upper oceanic crust, which has a volume estimated at 10^{18} cubic meters. Lever et al. (2013) first measured carbon isotope of organic carbon of basalts collected from the eastern flank of the Juan de Fuca Ridge and confirmed the coexistence of methane- and sulfur-cycling microbes in the basalts. These studies have shown that microbes probably prevail in the oceanic crust and promote weathering of basaltic crust. However, it is not unclear where deep-seated microbial communities come from, what the nature of the microbial communities harbored in young ridge flanks is, and what their role in the ocean crust weathering is (Modified from Edwards et al., 2012). It is attractive study to examine microbial activity in the hydrologically active, young ridge-flank crust being undergoing progressive oxidative alteration.

On September to November 2011, North Pond on the western flank of the Mid-Atlantic Ridge was explored for revealing the deep biosphere by *JOIDES Resolution* during Integrated Ocean Drilling Program Expedition 336. The characteristics of North Pond are oligotrophic, low-temperature (10-15°C), and fast seawater circulation (2-3 m/hr) (Langseth et al., 1984). North Pond is a good target for comparison to Juan de Fuca, which is high-temperature (~60°C), and slow seawater circulation (1400 ~ 1500 kg/day) (Wheat et al., 2003). In this study, detection of organic carbon and carbon isotopic analyses of basalts and sediments collected from North Pond were conducted for understanding the origin and formation of carbon compounds in relation to possible microbial activity in the basaltic crust.

A.2. Methods

A.2.1. Sampling site

Sediment and basaltic samples were collected from North Pond on the western flank of the Mid-Atlantic Ridge that composed relatively young (~ 8 Ma) basaltic crust and has sediment accumulation (50-300 m) in the valley between step rocky outcrops of oceanic crust (Fig. A.1). North Pond was investigated for several decades (e.g., Hyndman et al., 1984; Detrick et al., 1988; Becker et al., 1998; Gable et al., 1992).

Langseth et al. (1984) reported the sea water circulation from southeast to northwest in the basaltic crust at North Pond (Fig. A.2). We analyzed 29 basaltic samples and 47 sediment samples from several depth at each cores collected by Integrated Ocean Drilling Program (IODP) Expedition 336.

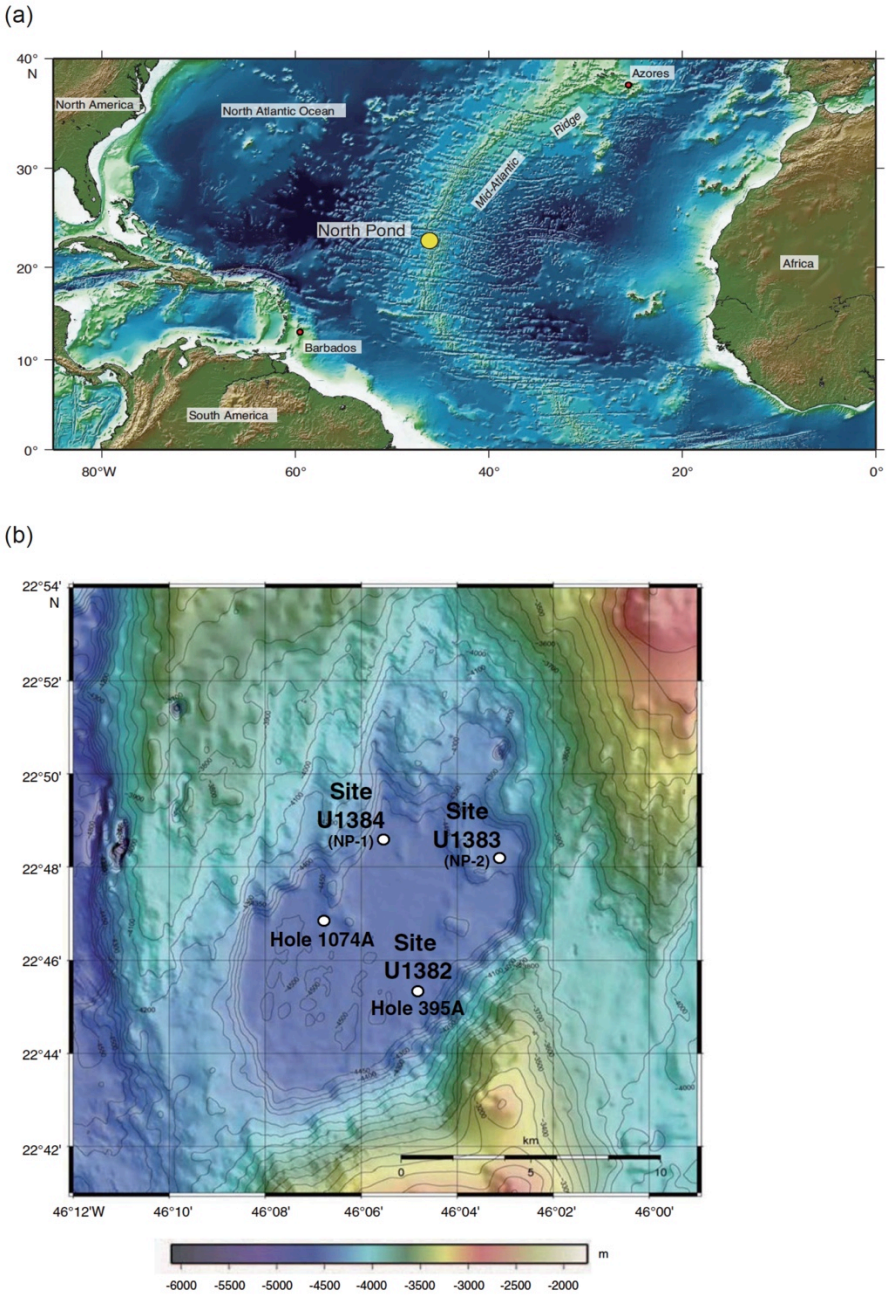

Fig. A.1. (a) Location map of North Pond on the western flank of the Mid-Atlantic Ridge. (b) Bathymetric map of North Pond. DSDP Hole 395A, ODP Hole 1074A, and Sites U1382, U1383, and U1384 are shown (Modified from Edwards et al., 2012).

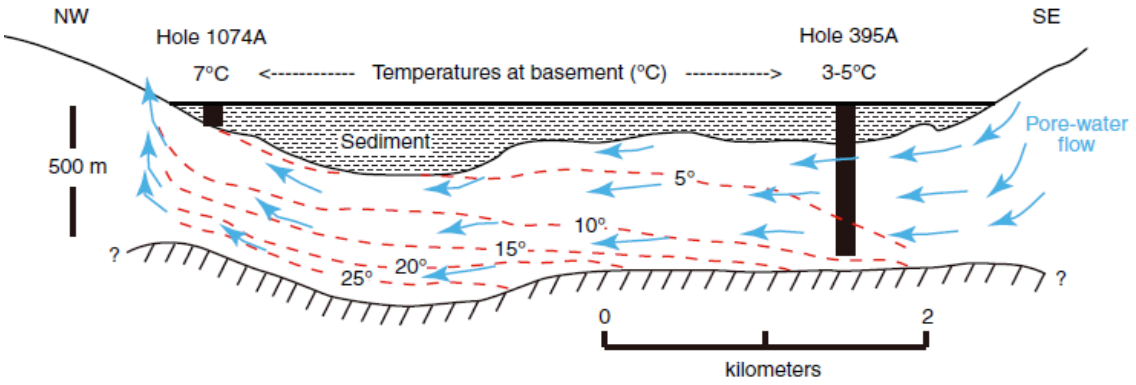

Fig. A.2. Pore-water flow and isotherms below North Pond, assuming laminar flow at a rate of about 1m/hr. (Langseth et al., 1984).

A.2.2. Site summary

Site U1382

Hole U1382A was drilled at 22°45.353´N, 46°04.891´W in 4483 m water depth. The basement was recovered from 110 to 210 mbsf. In total, 32 m of core was recovered and recovery rates were form 15 to 63 %. The cores obtained from U1382A were divided into 8 lithologic units comprising numerous subunits. Major unit boundaries are defined by contacts between massive flows, pillow flows, and interlayered sedimentary units. Basalts are either aphyric or plagioclase-olivine-phyric and have < 3% vesicles. All of the volcanic rocks recovered from Hole U1382A are affected only by low-temperature alteration by seawater, manifesting as replacement of groundmass and phenocrysts, vesicle filling, glassy margin replacement, and vein formation with adjacent brown alteration halos. The extent alteration ranges up to 20%, with clay (smectite and celadonite) being the most abundant secondary phase, followed by Fe oxyhydrroxides and minor zeolites and carbonates. The recovered section has 13-20 veins/m, with vein thickness being usually <0.2 mm. A sedimentary unit in 8R and 9R features a variety of clasts, including plutonic and mantle rocks. The peridotites are weakly serpentinized harzburgites and lherzolites with a protogranular texture.

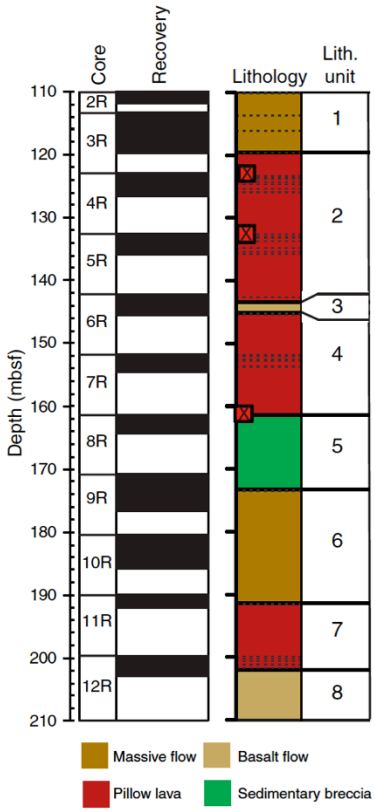

Fig. A.3. Hole U1382A lithologic summary. Broad changes in lithology or primary igneous structure are illustrated with different colors in the sequence column (Modified from Edwards et al., 2012).

Site U1383

Hole U1383C was drilled at 22°48.1241′N, 46°03.1662′W in 4414 m water depth. The basement was recovered from 69.5 to 331.5 mbsf. In total, 50.3 m of core was recovered and recovery rates were 19.2%. Three major lithologic units were distinguished on the basis of primary texture and phenocryst abundance. From 69.5 to 127 mbsf, the core consists of microcrystalline to fine-grained, sparsely plagioclase-phyric basalt with abundant glassy margins and numerous intervals of hard interflow limestone. From 127 to 164 mbsf, massive plagioclase-olivine-phyric basalts occur, occasionally hosting limestone (with and without basalt clasts) as fracture fill. Below 164 mbsf, glassy to variolitic to cryptocrystalline basalts (most likely pillow flows) predominate, and limestone is largely missing. Each of these three main lithologic units is divided into numerous subunits on the basis of hyaloclastite layers

and rare tectonic breccias. The overall abundance of glass is noticeably greater than that in Hole U1382A, and the extent of palagonization ranges from weak to moderate. Basalts are avesicular to sparsely vesicular and show vesicle fills of clay, zeolite (mainly phillipsite), calcium carbonate, and Fe oxyhydroxide. Brownish alteration halos commonly track veins filled with clay or carbonate and zeolite. Within unit 3, a gradational change from glassy to variolitic with abundant hyaloclastite layers, to more massive microcrystalline, and to fine-grained basalt with rare glassy margins can be observed. Althogh the hyaloclatites are noticeably palagonitized throughout the hole, the extent of background alteration appears to decrease downsection. Vein densities average 33 veins/m and increase somewhat downsection to 50 veins/m. Zeolite veins are abundant in the upper section, whereas carbonate veins predominate in the lowermost part. Sparse vesicles are filled with zeolite and clay.

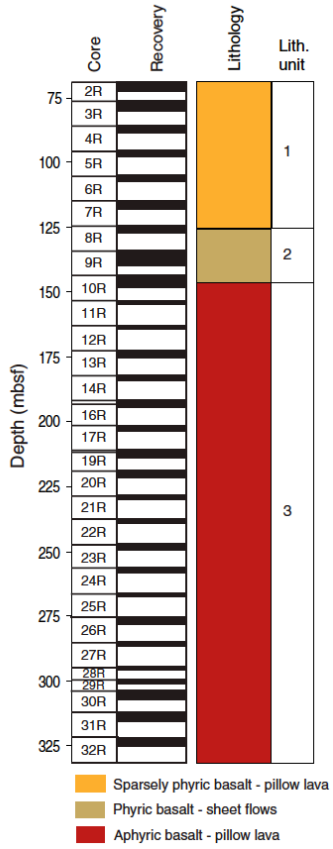

Fig. A.4. Hole U1383C lithologic summary, including major basalt lithologies, lava flows, and abundance of chilled margins, interflow sediments, hyaloclastites, and tectonic breccia, Broad changes in lithology or primary igneous structure are illustrated with different colors in the sequence column (Modified from Edwards et al., 2012).

Sediment and basement contact coring (Holes U1383D, U1383E, U1382B, and U1384A)

In Hole U1383D, 44.3 m of sediments was cored and the lowermost 1 m was cored through basalt and limestone-cemented breccia (0.76 m of basement was recovered). At nearby Hole U1383E, 44.2 m of sediment and 1 m of basaltic basement was cored (0.3 m of basement was recovered). The basalts are aphyric and slightly to moderately altered. They are distinct from the uppermost basaltic flow that was cored in Hole U1383C and hence represent a different lithologic unit.

In Hole U1382B, 90.0 m of sediments was cored and another 8.8 m was cored recovering a piece of basalt and countless millimeter to centimeter-sized pebbles of completely altered plutonic and ultramafic rocks at the basement/sediment interface. The rocks are interpreted to be part of the sedimentary breccia overlying the massive basalt of Unit 1 cored in Hole U1382A.

In Hole U1384A, 93.5 m of sediments was cored and 0.58 m of basalt and limestone-cemented breccia was recovered. The basalt are aphyric and sparsely vesicular with glassy to variolitic to microcrystalline groundmass. They are between 3 and 10 % altered and display brown alteration halos along clay veins and fractures.

The sediments at all sites consistent of foraminifer nanofossil ooze with layers of foraminiferal sand. The bottom several meters of the sediments are brown and appear rich in clay. Sediments from Hole U1382B show moderately rounded rock fragments concentrated in layers or dispersed n the ooze. These fragments range from coarse sand to pebble in grain size and consist of serpentinized mantle peridotite, gabbro, troctolite, and basalt. The basement/sediment interface of U1382B also contains coarse sediment with predominantly serpentinite clasts, including soapstone and talc-tremolite schist. The occurrence of these rock fragments is consistent with the polymict sedimentary breccia recovered during basement drilling Hole U1382A. The deformed and metasomatized lithologies encountered in Hole U1382B corroborate the hypothesis that this material was transported to the Site U1382 area in North Pond by mass wasting events and that its source is an oceanic core complex, probably in the southern rift mountains. Layers of foraminiferal sand are abundant in all holes and many show erosional bases and normal-granded bedding, suggesting that they represent deposits of turbidity currents.

A.2.3. Sample preparation

Site location

At all Expedition 336 sites, GPS coordinates from a precruise site survey (Schmidt-Schierhorn et al., 2012) were used to position the R/V JOIDES Resolution on site. The only seismic system used during the cruise was the Syquest Bathy 2010 CHIRP subbottom profiler, which was monitored on the approach to each site to confirm the seafloor depth. Once the vessel was positioned at a site, the thrusters were lowered and a positioning beacon was dropped to the seafloor. The dynamic positioning control of the vessel uses navigational input from the GPS and triangulation to the seafloor beacon, weighted by the estimated positional accuracy. The final hole position was the mean position calculated from the GPS data collected over the time that the hole was occupied.

Drilling Operation

The advanced position corer (APC), extended core barrel (XCB), and rotary core barrel (RCB) systems were used during Expedition 336. The APC system cuts soft sediment cores with minimal coring disturbance relative to other IODP coring systems. After the APC core barrel is lowered through the drill pipe and lands near the bit, the drill pipe is pressured up until the two shear pins that hold the inner barrel attached to the outer barrel fail. The inner barrel then advances into the formation and cuts the core. The driller can detect a successful cut, or "full stroke," from the pressure gauge on the rig floor. The XCB system is deployed when the formation becomes too stiff for the APC system or when drilling harder substrate, such as chert.

APC refusal is conventionally defined in two ways: (1) the piston fails to achieve a complete stroke (as determined from the pump pressure reading) because the formation is too hard or (2) excessive force (>60,000 lb; ~267 kN) is required to pull the core barrel out of the formation. When full or partial stroke can be achieved but excessive force cannot retrieve the barrel, the core barrel can be "drilled over," that is, after the inner core barrel is successfully shot into the formation, the drill bit is advanced to total depth to free the APC barrel. When an APC core barrel achieves only a partial stroke, the lowermost portion of the core could be material that is "sucked" into the core barrel. Only standard steel core barrels were used during Expedition 336 coring

operations. Most APC/XCB cored intervals were ~9.5 m long, which is the length of a standard core barrel.

The XCB system was used to advance the hole when APC refusal occurred at the sediment/basement contact. The XCB is a rotary system with a small cutting shoe extending below the large rotary APC/XCB bit. The smaller bit can cut a semi-indurated core with less torque and fluid circulation than the main bit and thus optimizes recovery. The XCB cutting shoe (bit) extends up to ~30.5 cm ahead of the main bit in soft sediments but retracts into the main bit if hard formations are encountered.

The RCB system was deployed to core basement rocks. The RCB is a conventional rotary drilling system and requires a dedicated RCB bottom-hole assembly and a dedicated RCB drilling bit (outer diameter of 9 7/8 inch).

IODP depth convention

The methods and nomenclature for calculating sample depth in a hole have changed to be methodspecific, which will ensure that data acquisition, scale mapping, and composite-scale and splice construction are unequivocal. The primary scales are measured by the length of drill string (e.g., drilling depth below rig floor (DRF) and drilling depth below seafloor (DSF)), length of core recovered (e.g., core depth below seafloor (CSF) and core composite depth below seafloor (CCSF), and logging wireline (e.g., wireline log depth below rig floor (WRF) and wireline log depth below seafloor (WSF)). All units are in meters. Relationships between scales are either defined by protocol (such as the rules for computation of CSF from DSF), or they are defined on the basis of user-defined correlations (such as stratigraphic correlation of cores between holes to create a common CCSF scale from the CSF scale of each hole or for core-to-log correlation). The distinction in nomenclature should keep the user aware that a nominal depth value at two different scales usually does not refer to the exact same stratigraphic interval. Unless otherwise noted, all Expedition 336 core depths have been calculated as CSF Method A (CSF-A), and all downhole wireline depths have been calculated as WSF Method A (WSF-A). To more easily communicate shipboard results in this volume, all depths are reported as mbsf, except where otherwise noted.

Core handling

Core handling and flow were adjusted to best meet the microbiological priorities of the expedition. Hard rock cores were immediately split into ~1.5 m long sections and taken to the splitting room, where they were emptied into sterilized split liners. Each split section was labeled every drilling operation and separations to 1.5 m long sections. For examples, cores labeled 2R3 means that this cores were collected at second drilling operation by RCB and the third shallowest 1.5 m long section, cores labeled 4H6 means that this cores were collected at forth drilling operation by APC and the sixth shallowest 1.5 m long sections, and cores labeled 11X1 means that this cores were collected at eleventh drilling operation by XCB and the shallowest 1.5 m long section

Immediate review by microbiologists and petrologists allowed hard rock microbiology samples to be selected and taken. These samples were photographed and then removed to the microbiology laboratory for processing. The normal hard rock core flow was then resumed, with the exception that the outer surfaces of whole-round core pieces of sufficient length were also digitally scanned. Fig. A.5 shows core handling of hard rocks (Expedition 336 Scientists 2012). After the shipboard physical properties measurements and core description, samples for personal studies were cut out and collected.

For sediment cores, the core liner was marked to identify core sections and intensive whole-round samples for microbiology and interstitial water samples. Syringe samples were taken for headspace and microbiological analyses. The core sections remaining after whole-round sampling were taken inside, labeled, and moved to the core refrigerator, where oxygen concentration measurements were made with optodes and interstitial water samples were taken using Rhizon samplers. After collected samples for microbial, oxygen concentration, and interstitial water measurements, shipboard physical properties measurements and core description were conducted. Fig. A.6 shows core handling of sediments (Expedition 336 Scientists 2012). Finally, samples for personal studies were collected by ~ 10 cc syringe.

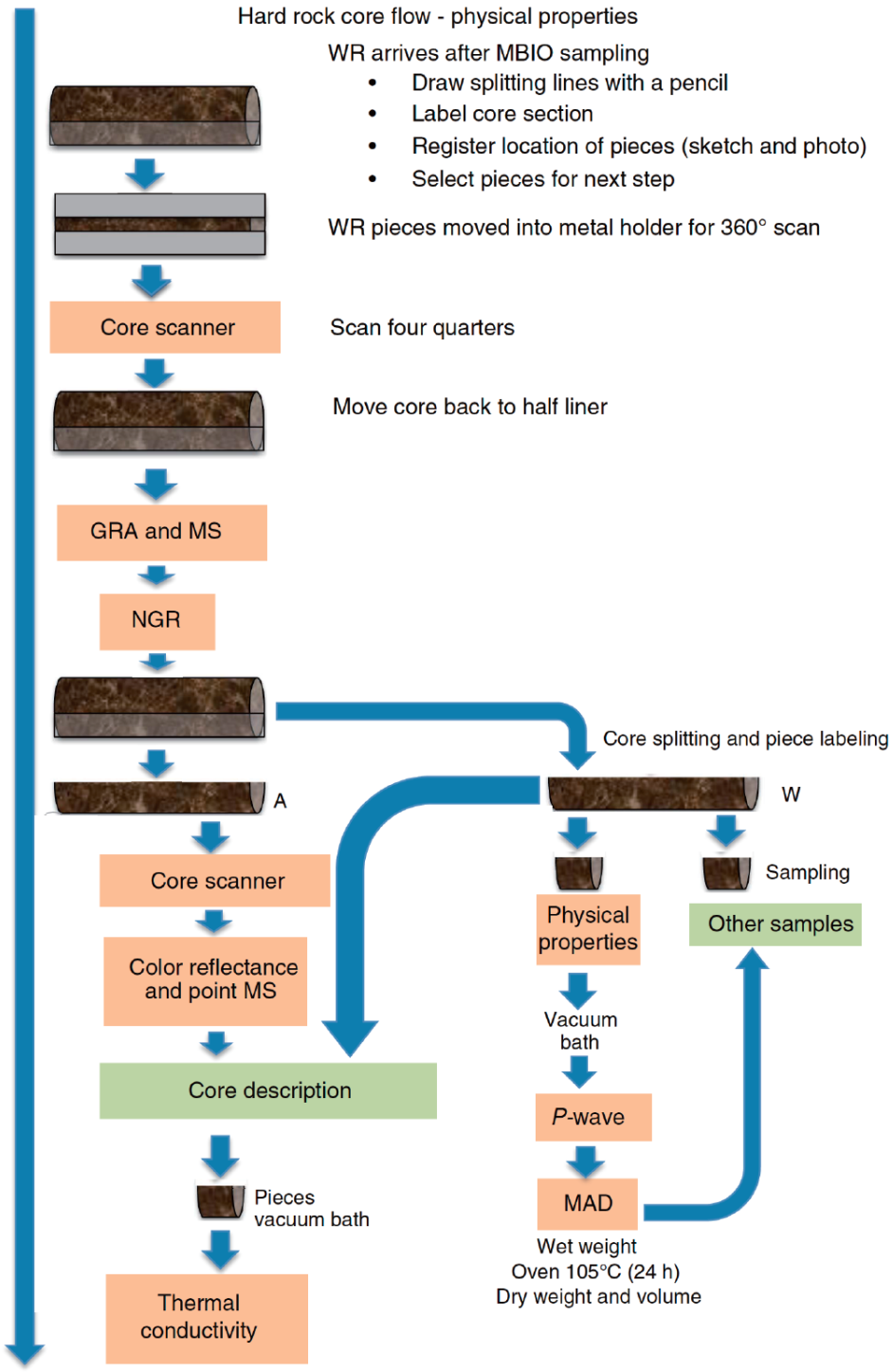

Fig. A.5. Hard rock core flow for physical properties measurements, Expedition 336. Approximate time steps are given per core section. WR = whole round samples, MBIO = means microbiology, GRA = gamma ray attenuation, MS = magnetic susceptibility, NGR = natural gamma radiation, MAD = moisture and density, A = archive half, and W = working half (Modified from Edwards et al., 2012).

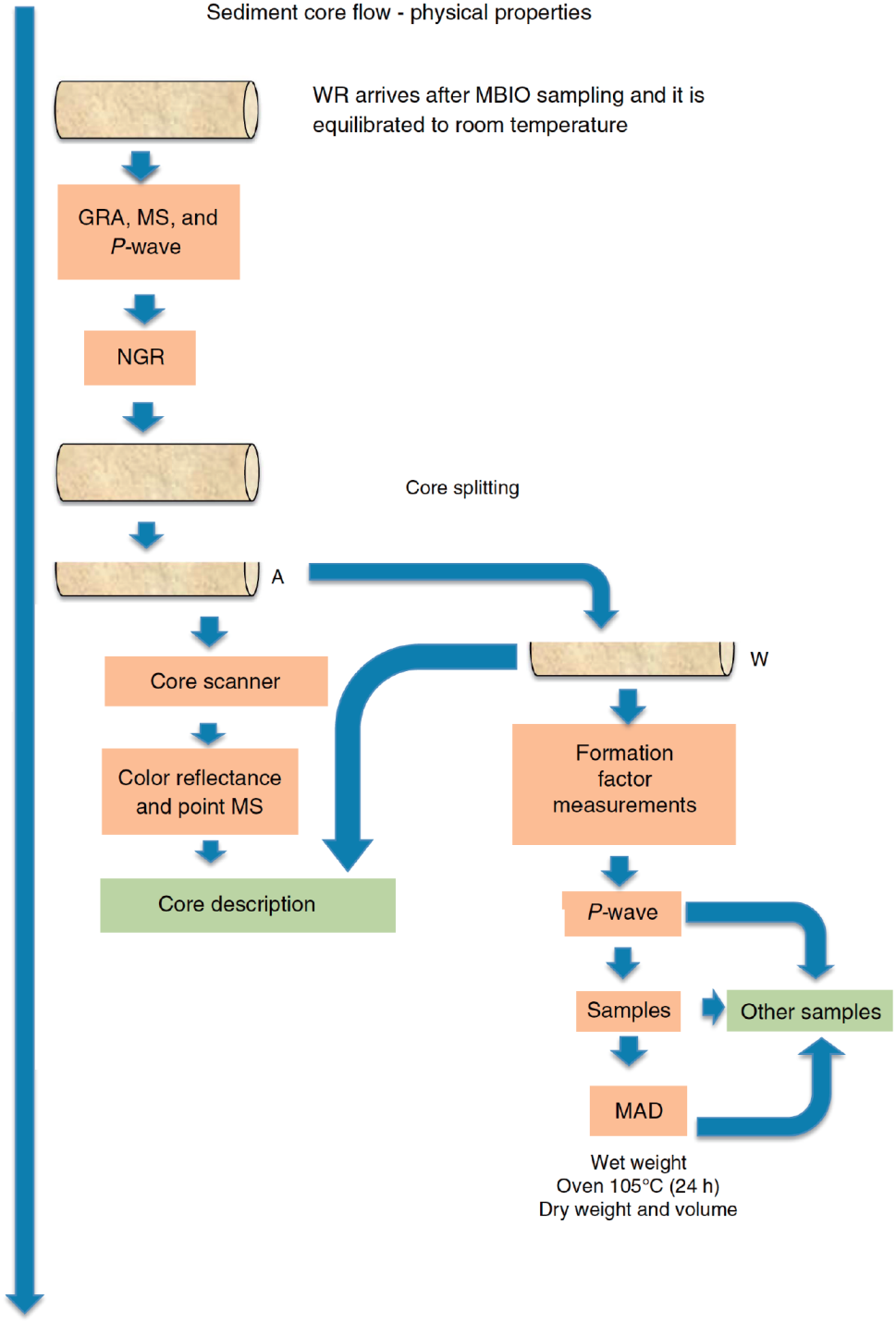

Fig. A.6. Sediment core flow for physical properties measurements, Expedition 336. Approximate time steps are given per core section. WR = whole round samples, MBIO = means microbiology, GRA = gamma ray attenuation, MS = magnetic susceptibility, NGR = natural gamma radiation, MAD = moisture and density, A = archive half, and W = working half (Modified from Edwards et al., 2012).

Sampling sites for organic geochemical analysis of carbon

From U1382A, 11 samples were collected including each lithology, massive flow, basalt flow, sedimentary breccia, and pillow lava (Figs. A.7 and A.8). Each samples was cut in a quarter of cylinder with 3 cm height (Fig. A.8).

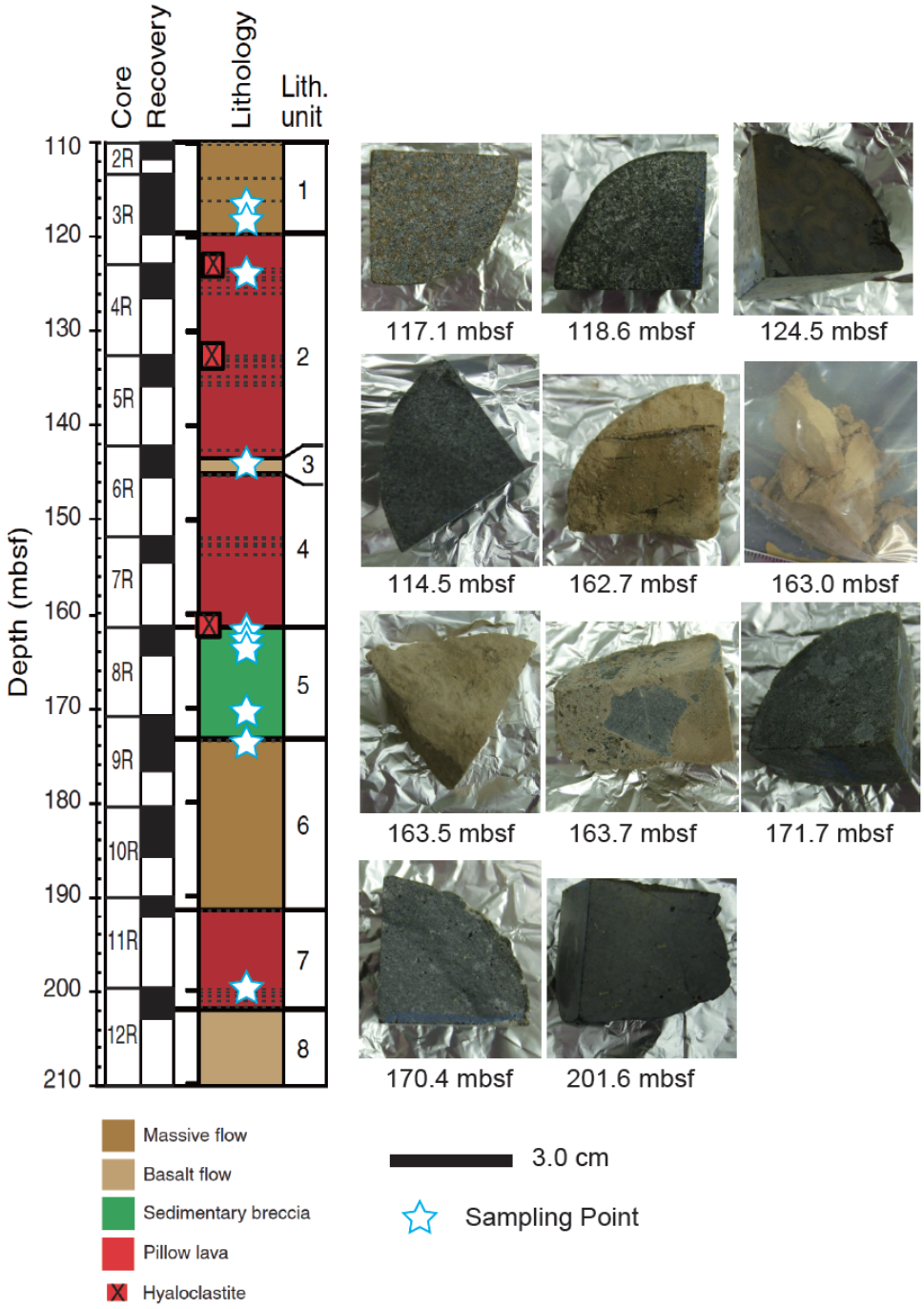

Fig. A.7. Hole U1382A lithologic summary and sampling points for analysis organic geochemical analysis in this study (Modified after Edwards et al., 2012).

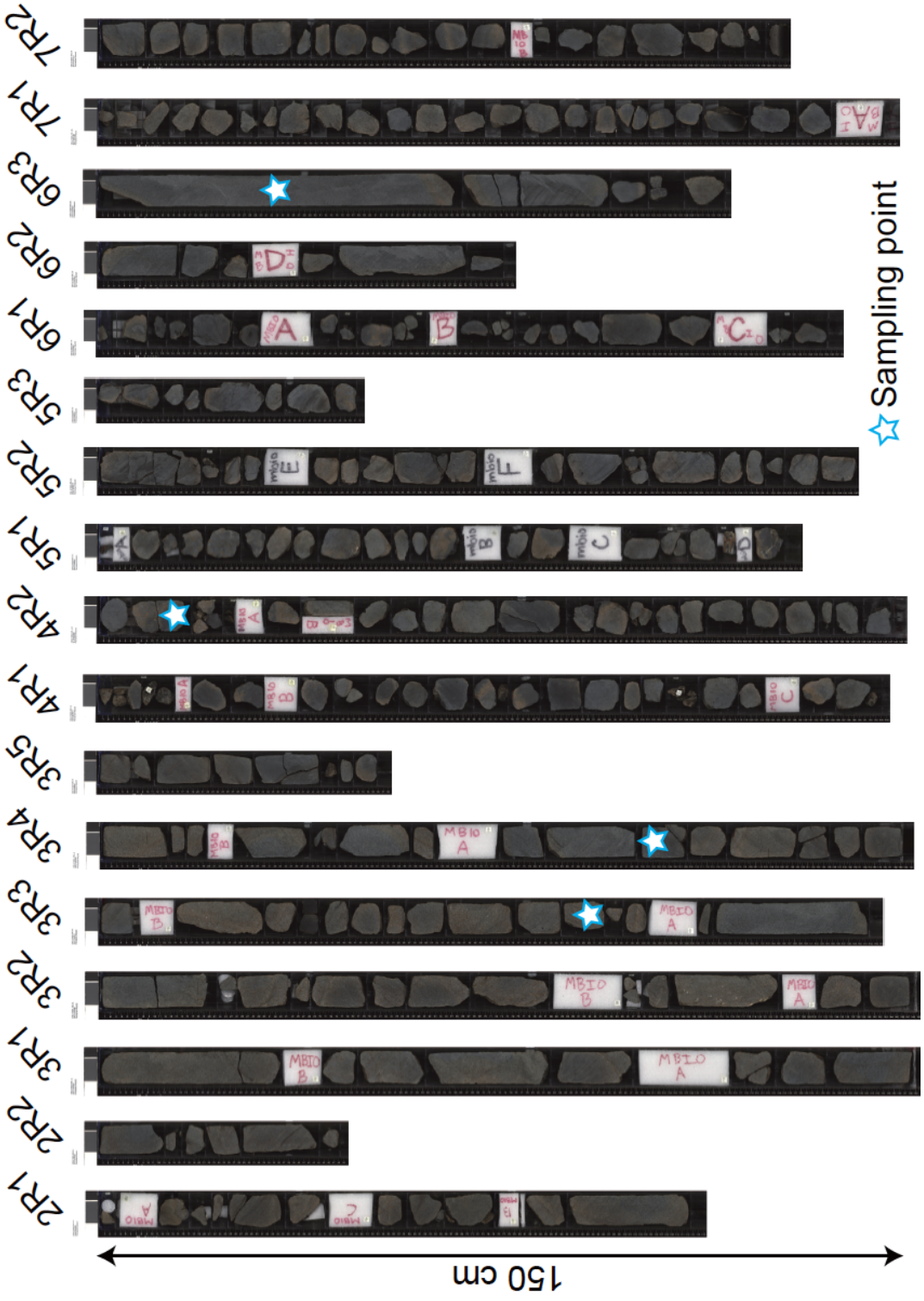

Fig. A.8. Half-cut cores at Hole U1382A and sampling points for organic geochemical analysis in this study. (continued on the next page.)

Fig. A.8. (continued)

From U1383C, 29 samples were collected including each lithology, pillow lava, sheet glow, and pillow lava (Figs. A.9 and A.10). Each samples was also cut in a quarter of cylinder with 3 cm height (Fig. A.10).

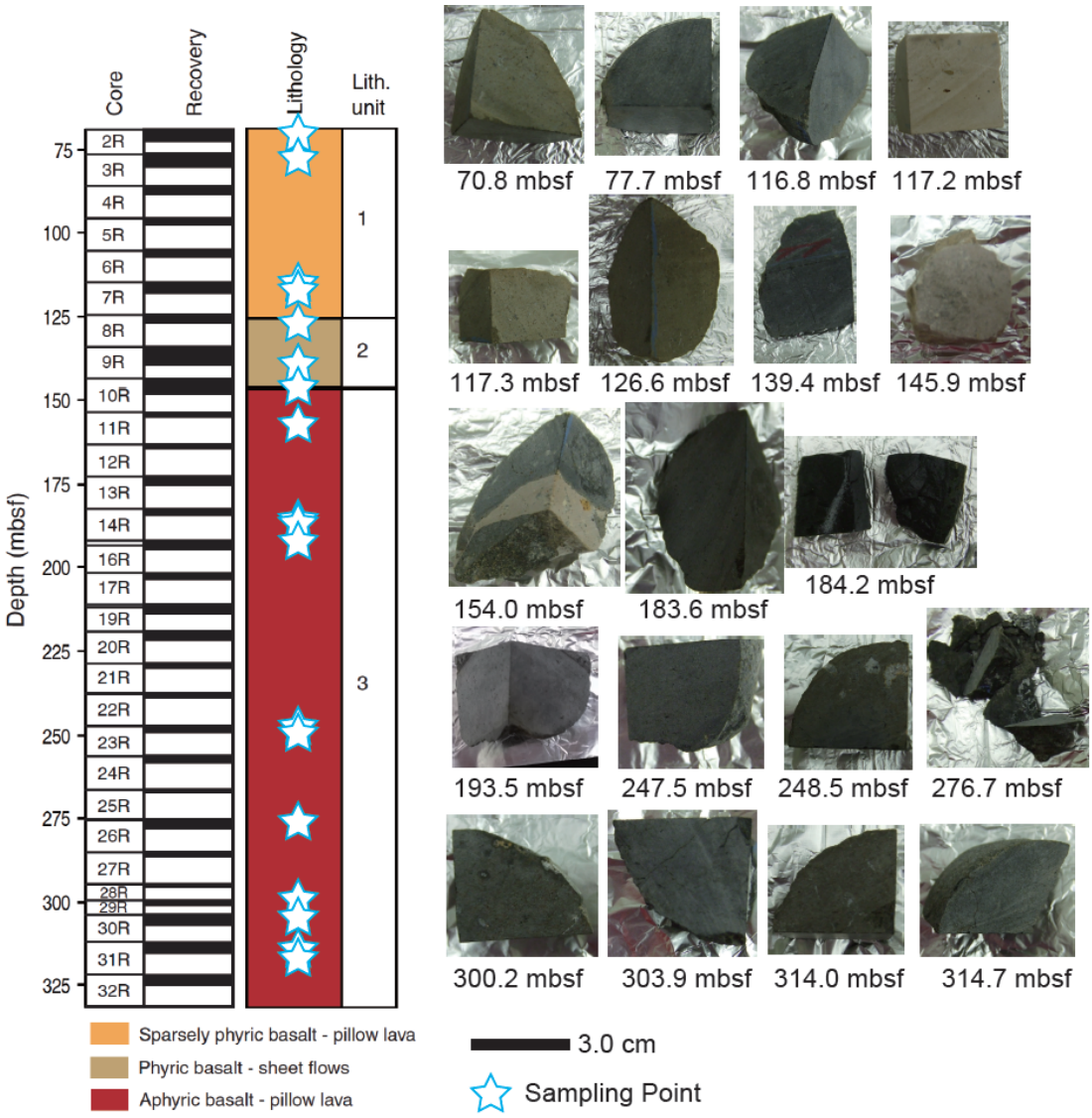

Fig. A.9. Hole U1383C lithologic summary and sampling points for analysis organic geochemical analysis in this study (Modified after Edwards et al., 2012).

Fig. A.10. Half-cut cores at Hole U1383C and sampling points for organic geochemical analysis in this study. (continued on the next page.)

Fig. A.10. (continued).

Fig. A.10. (continued)

From U1382B, U1383D, and U1384A, 16, 13, and 18 sediment samples were collected from several depths (Figs. A.11, A.12 and A.13). Each sample was collected by syringe and sample volume was about 10-20 cc.

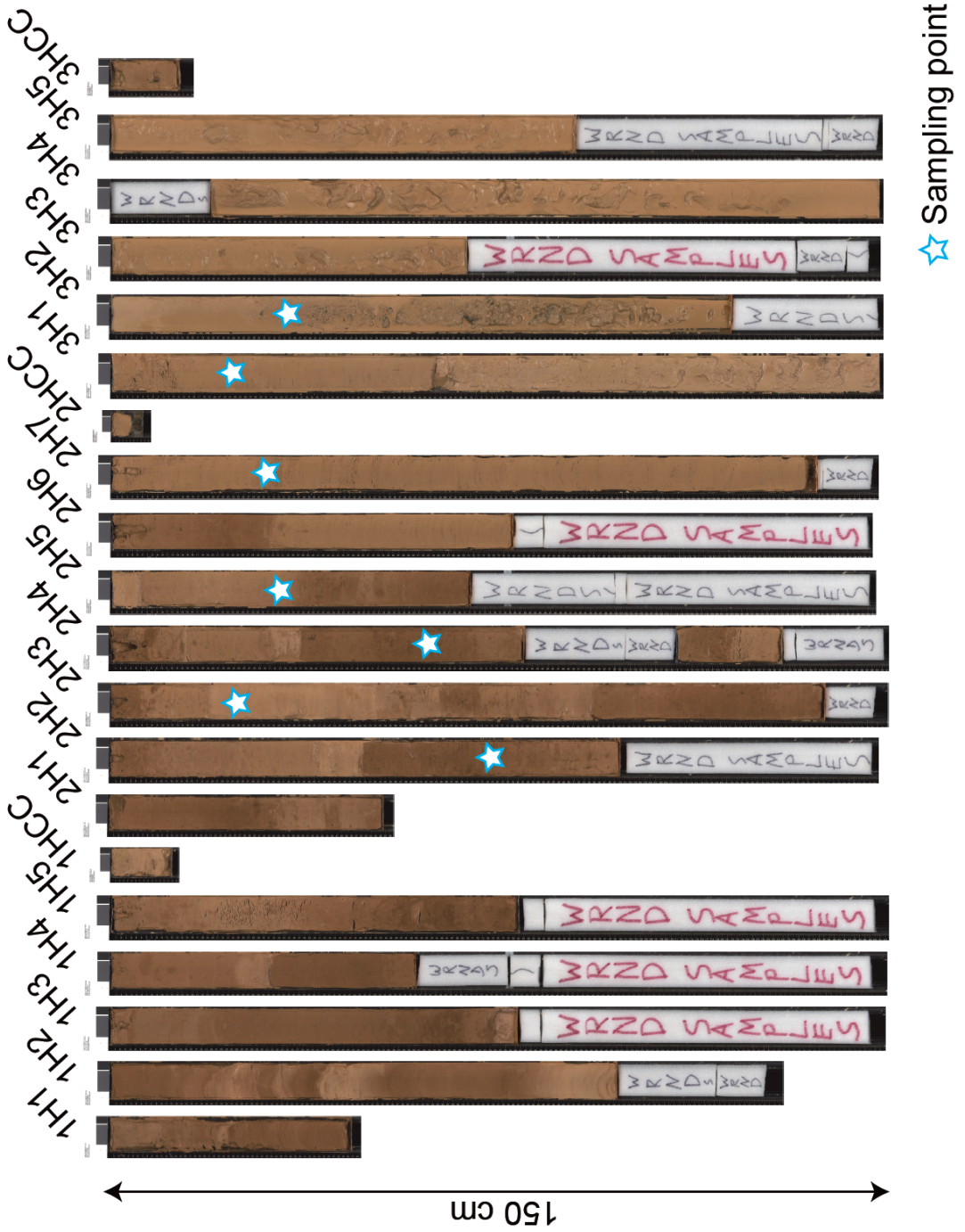

Fig. A.11. Half-cut cores at Hole U1382B and sampling points for organic geochemical analysis in this study. CC and WRND SAMPLES means core catcher and the areas where samples for microbial and interstitial water analysis were collected (continued on the next page.)

Fig. A.11. (continued).

Fig. A.11. (continued)

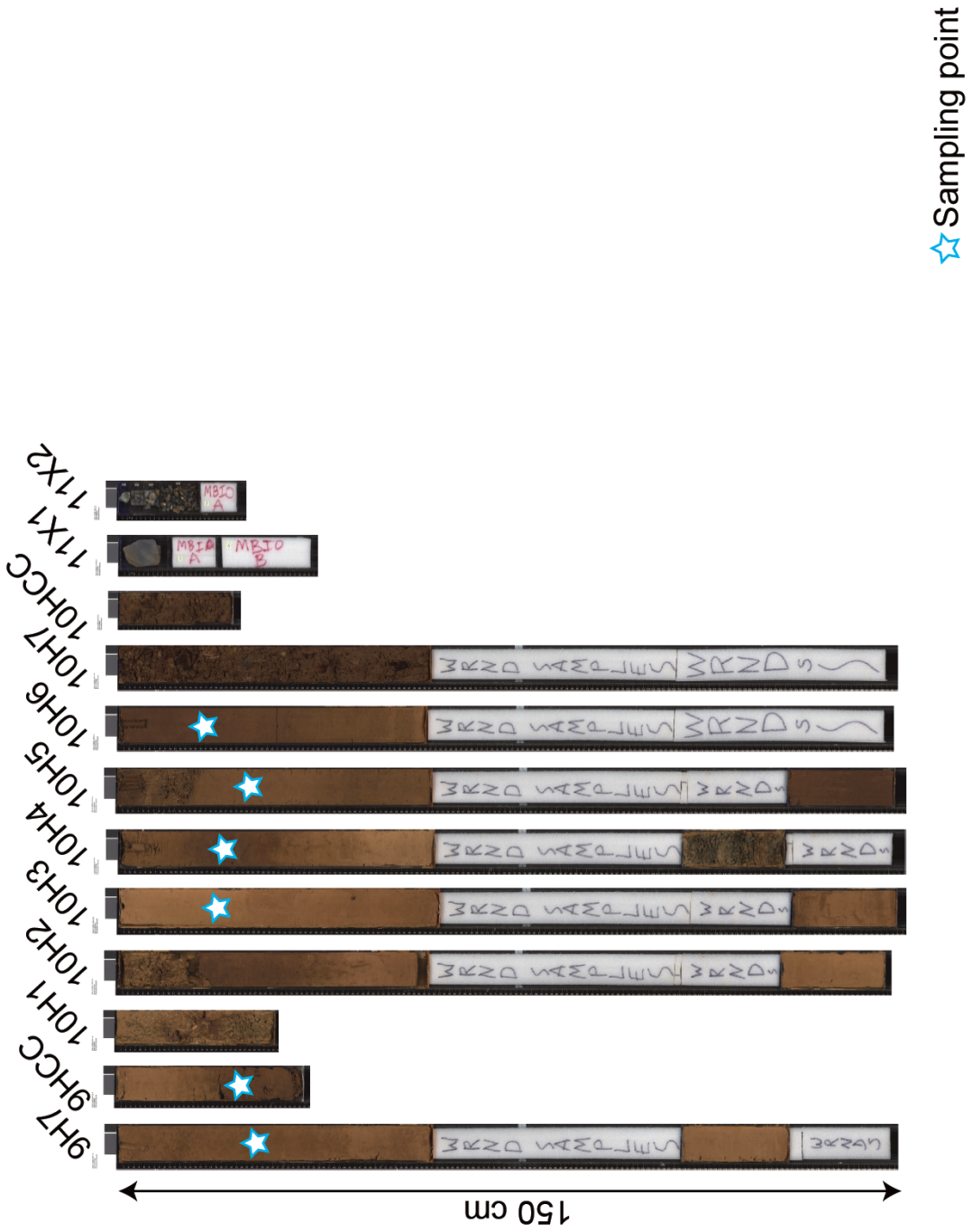

Fig. A.11. (continued).

Fig. A.12. Half-cut cores at Hole U1383D and sampling points for organic geochemical analysis in this study. CC and WRND SAMPLES means core catcher and the areas where samples for microbial and interstitial water analysis were collected (continued on the next page.)

Fig. A.12. (continued)

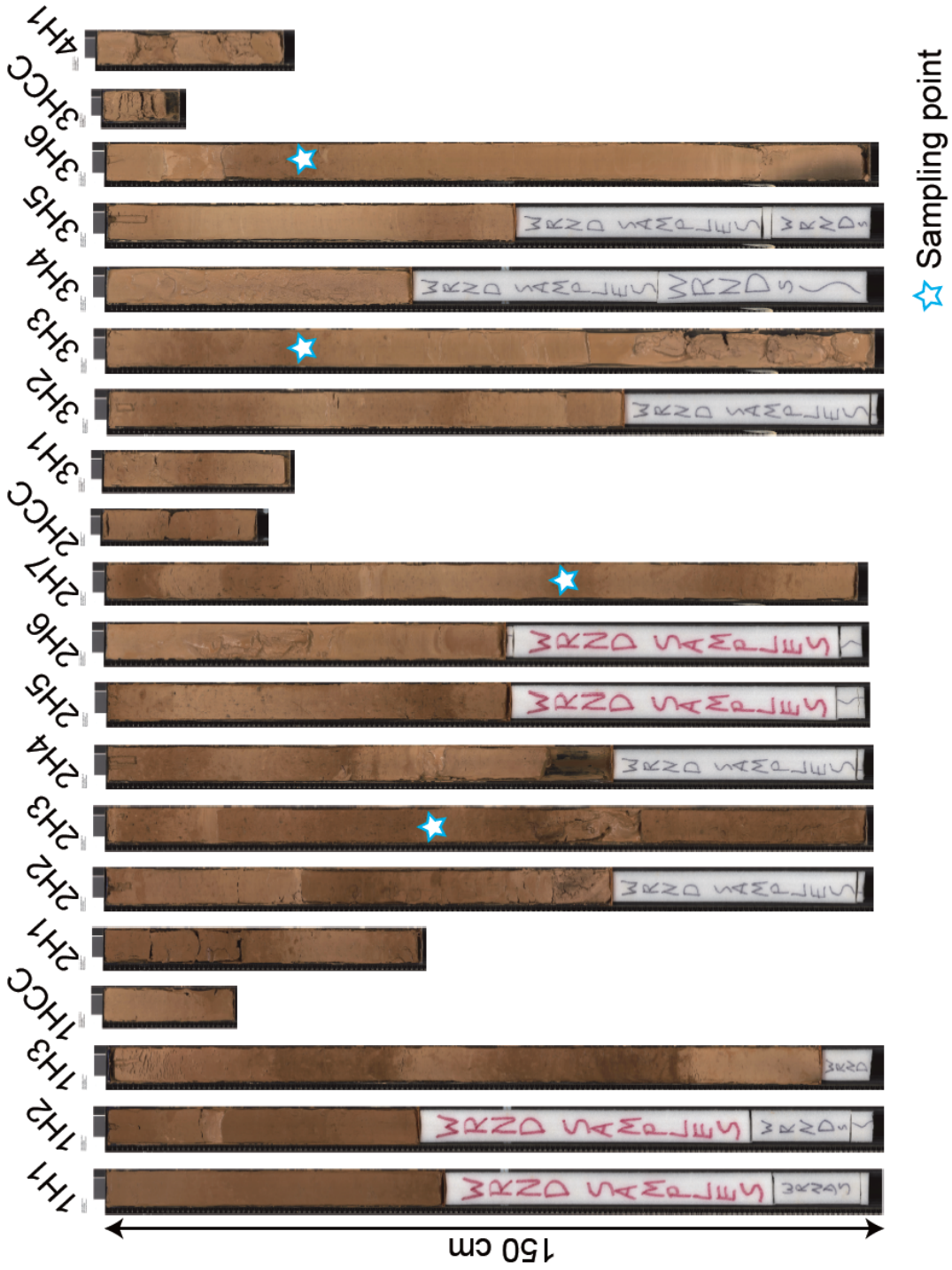

Fig. A.13. Half-cut cores at Hole U1384A and sampling points for organic geochemical analysis in this study. CC and WRND SAMPLES means core catcher and the areas where samples for microbial and interstitial water analysis were collected (continued on the next page.)

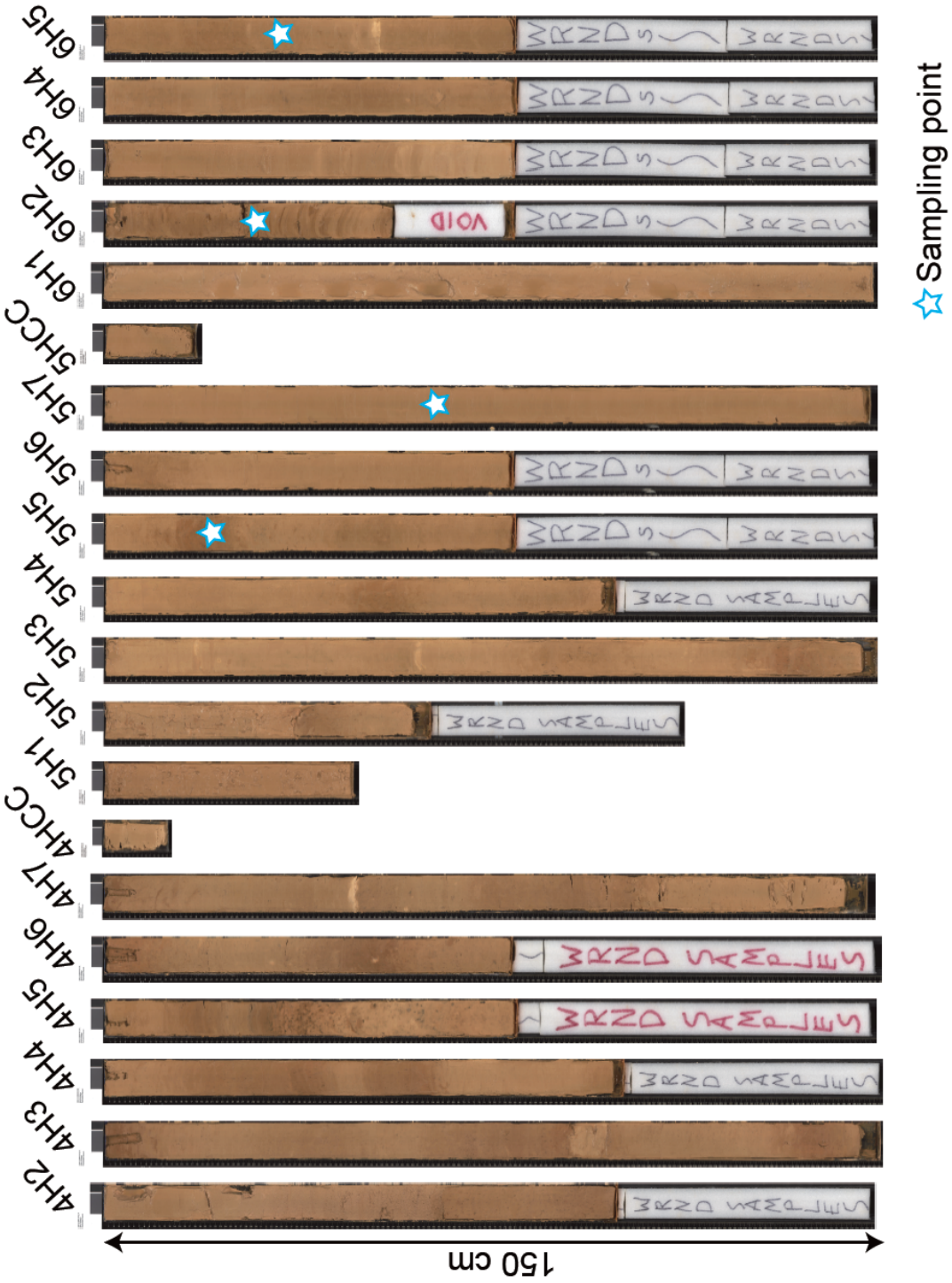

Fig. A.13. (continued)

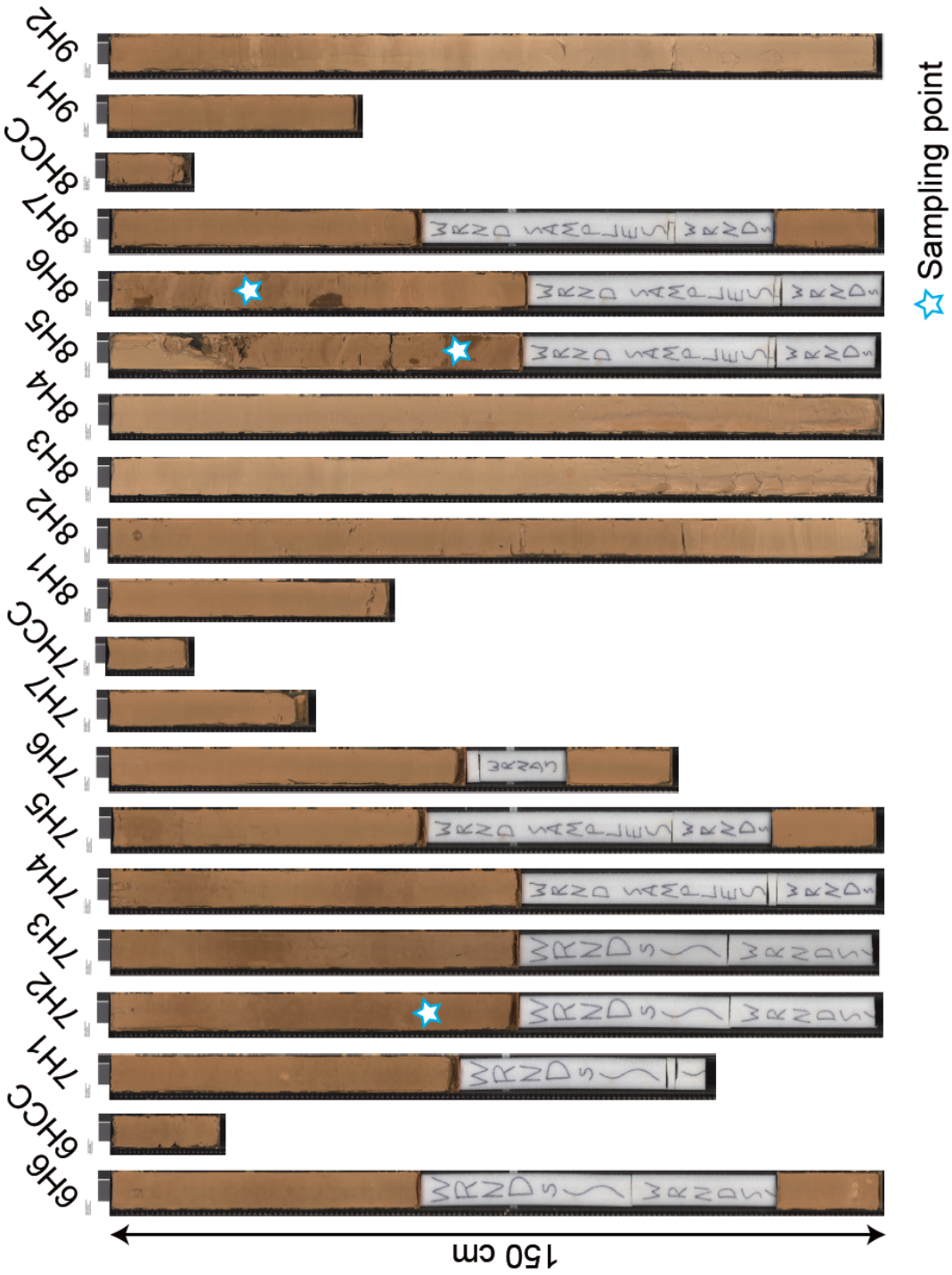

Fig. A.13. (continued)

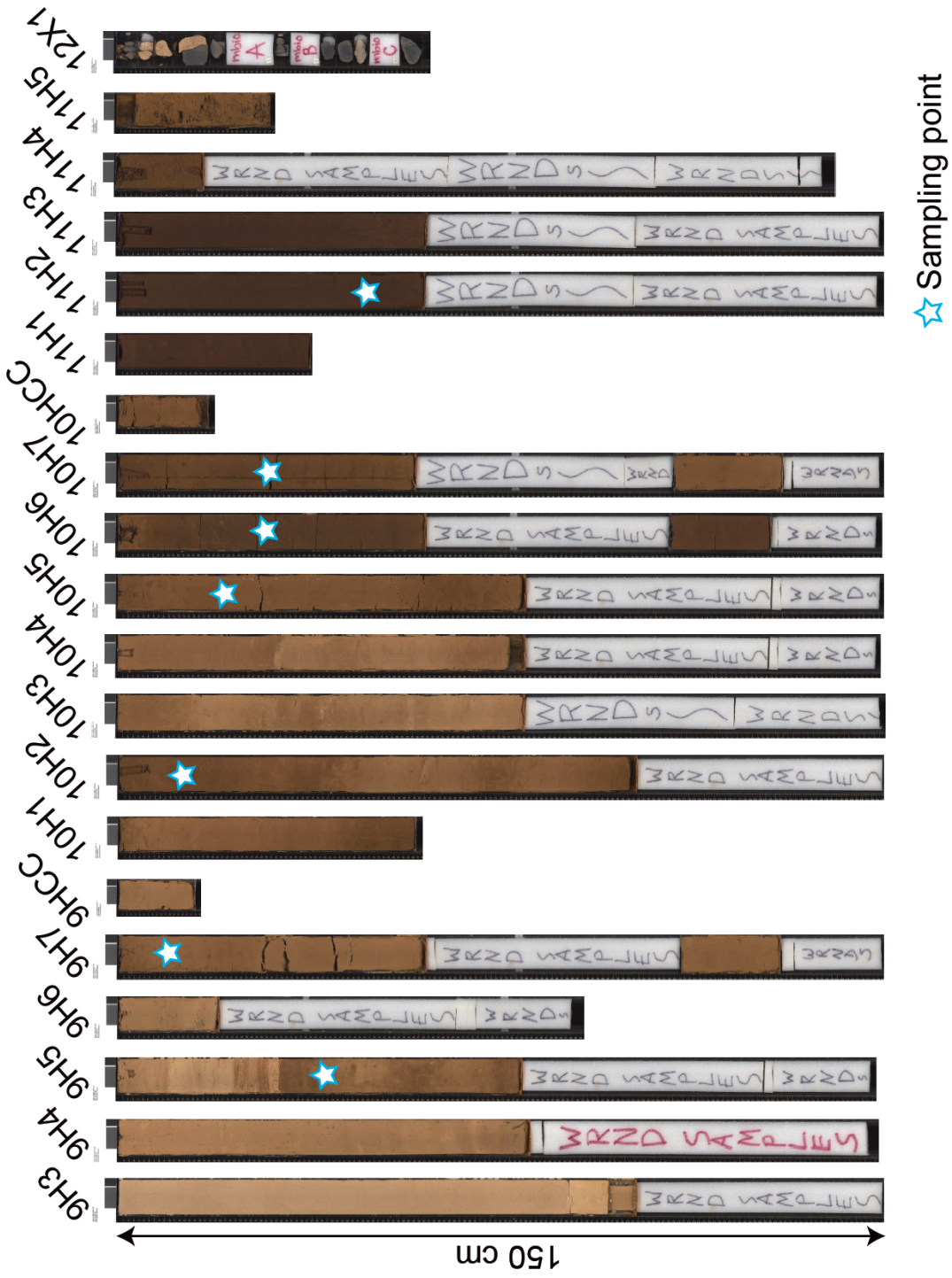

Fig. A.13. (continued).

Preparation of samples for elemental and isotopic analysis

HCl and HF were obtained from Wako Pure Chemical Industries. Procedures for preparing samples are shown in Fig. 4.2. Sediment samples were dried at 45°C and 6 M of HCl were added to remove carbonates. After HCl treatment, the sediment samples were dried at around 70 °C. While, for preparation of basaltic samples, surfaces of the basaltic samples were cut off more than 5.0 mm to prevent contaminations and inner basaltic samples were grounded into powders. Similar to the procedures for sediments, 6 M of HCl were added to these basaltic samples to remove carbonates and these samples were dried at around 70 °C. To extract kerogens, parts of basaltic samples were treated with HCl and HF. 10 g of powdered basaltic samples were washed with 6 N of HCl more than 20 times until supernatant solutions were not yellow issued from iron elution. Samples washed with HCl were added 1N HCl/9N HF. Recovered acid insoluble matters were washed with deionized water (18.2 MΩ) until pH of supernatant solutions were neutral. Finally, insoluble matters were washed with methanol and dried at around 70 °C.

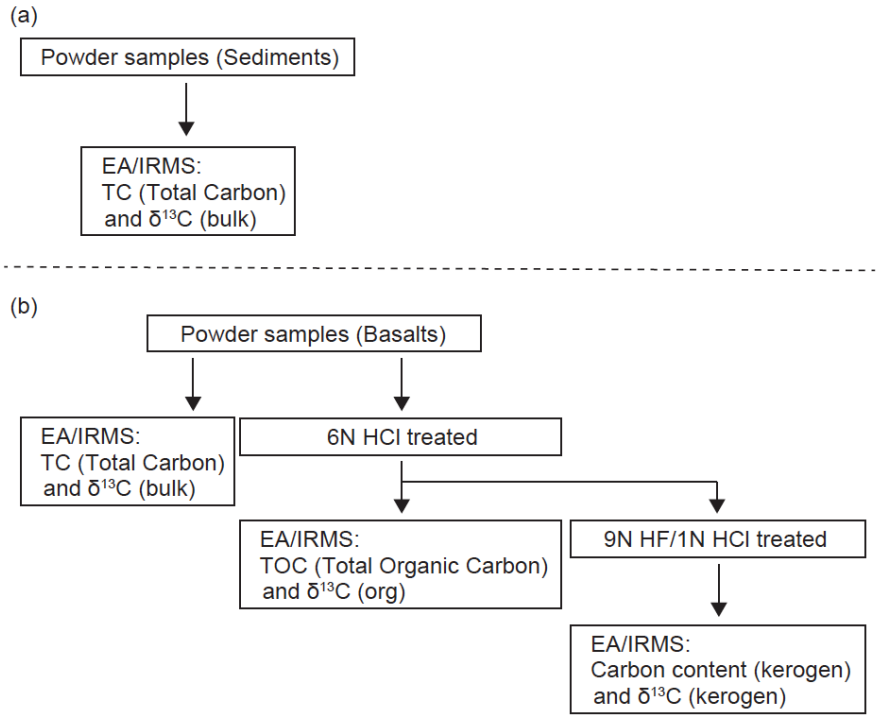

Fig. A.14. Procedure for preparation of samples for elemental and isotopic analysis. (a) Preparation of sediment samples for analysis TC and $\delta^{13}C$ (bulk). (b) Preparation of hard rock samples for analysis of TC, $\delta^{13}C$ (bulk), TOC, $\delta^{13}C$ (org), carbon contents (kerogen), and $\delta^{13}C$ (kerogen).

A.2.4. Elemental and isotopic analysis

All samples were analyzed by elemental analyzer (Flash EA 1112; Thermo Fisher Scientific K.K.)/isotope ratio mass spectrometer (Delta Plus Advantage; Thermo Fisher Scientific K.K.) (EA/IRMS) at Kochi Core Center. We analyzed about 10 and 50 mg of sediment and basaltic samples were analyzed to measure the carbon contents and $\delta^{13}C$ of total carbon, respectively. While, we analyzed about 50 - 100 mg of basaltic samples treated by HCl and kerogen were analyzed to measure the carbon contents and $\delta^{13}C$. Each sample was contained into Sn capsules. Elemental and isotopic compositions were calibrated relative to sulfanilamide and L-alanine, respectively. The values are reported the conventional $\delta^{13}C$ notation relative to the VPDB standard. The analytical error for determination of carbon contents was within 0.005 wt%. The precision of the $\delta^{13}C$ was better than 0.1 ‰.

Seven kerogen samples were analyzed by scanning electron microscopy/energy dispersive spectroscopy (SEM/EDS). These samples were then mounted on Al sample holders under low-vacuumed state. An accelerating voltage of 15.0 kV was used for acquisition of backscatter micrographs and EDS spectra.

A.3. Results and Discussion

A.3.1. Carbon isotopic analysis in the sediments

TC value ranged 6 ~ 11 % for whole sediment samples. Similar depth profiles of TC were observed at the three sites (U1382B, U1383D, and U1384A) (Fig. A.15 (a)). At the depth of 0 ~ 40 mbsf, TC increased with depth and showed maximum value at 20 ~ 40 mbsf. At the depth of 40~ 90 mbsf, TC decreased with depth. $\delta^{13}C$ (bulk) ranged −0.0400 ~ +1.93 ‰ for whole sediment samples (Fig. A.15 (b)). Depth profiles of $\delta^{13}C$ (bulk) were very similar to those of TC. These depth profiles of TC and $\delta^{13}C$ (bulk) appear to have inverse relation with the distributions of O_2 concentration (Fig. A.16; Orcutt et al., 2013). Oxygen is being transported into the sediments from both the water column and from the fluids moving through underlying basement (Orcutt 2013). Oxygen is being consumed within the sediments at a high enough rate to make the middle of the sediments anoxic, but the resupply of oxygen at depth from basement fluids leads to an increase in concentrations towards basement. This may represent that oxidation decomposition of carbonates and organic carbon are inhibited at the middle of the sediments because this depth are anoxic environments. Therefore, $\delta^{13}C$ (bulk) are

high value at the middle of sediments because more carbonate remains in the sediments.

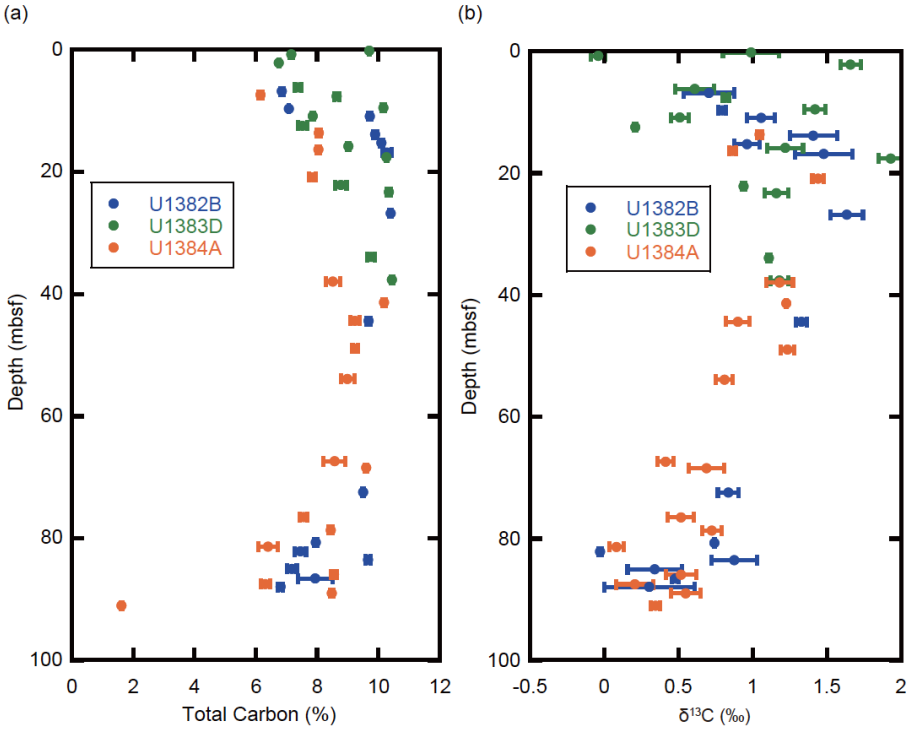

Fig. A.15. Depth related profiles in (a) total carbon (TC) content and (b) $\delta^{13}C$ (bulk) of sediments at Hole U1382B, U1383D, and U1384A.

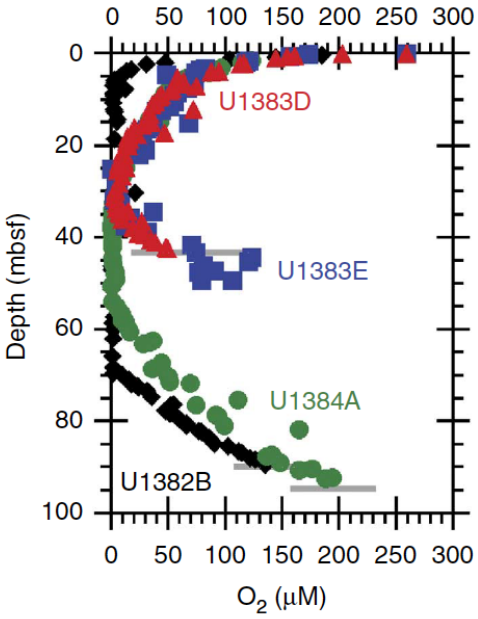

Fig. A.16. Profiles of concentration of oxygen in the sediments at Hole U1382B, U1383D, U1383E, and U1384A (Orcutt et al., 2013).

In addition, the depth profiles of TC and $\delta^{13}C$ (bulk) also appear to have relation ship with the concentration of PO_4, NO_2, NO_3, and NH_4 in the pore water squeezed from sediments (Fig. A.17; Modified from Edwards et al., 2012). Value of NH_4 should be treated with caution about the detection limits. Samples from Hole U1383D had a detection limit of 6 μM due to the dilution. Samples from Hole U1382B and U1384A had a detection limit of 1.5 μM (Edwards et al., 2012). The depth profile of TC is similar to that of nitrate. While, concentrations of NH_4 are below detection limits below 20 mbsf and 0 ~ 60 mbsf at Hole U1382B and U1384A, except for Hole U1383D. This may represent that microbes with nitrification, the process to produce nitrate from ammonium by nitrifier, are active in the sediment.

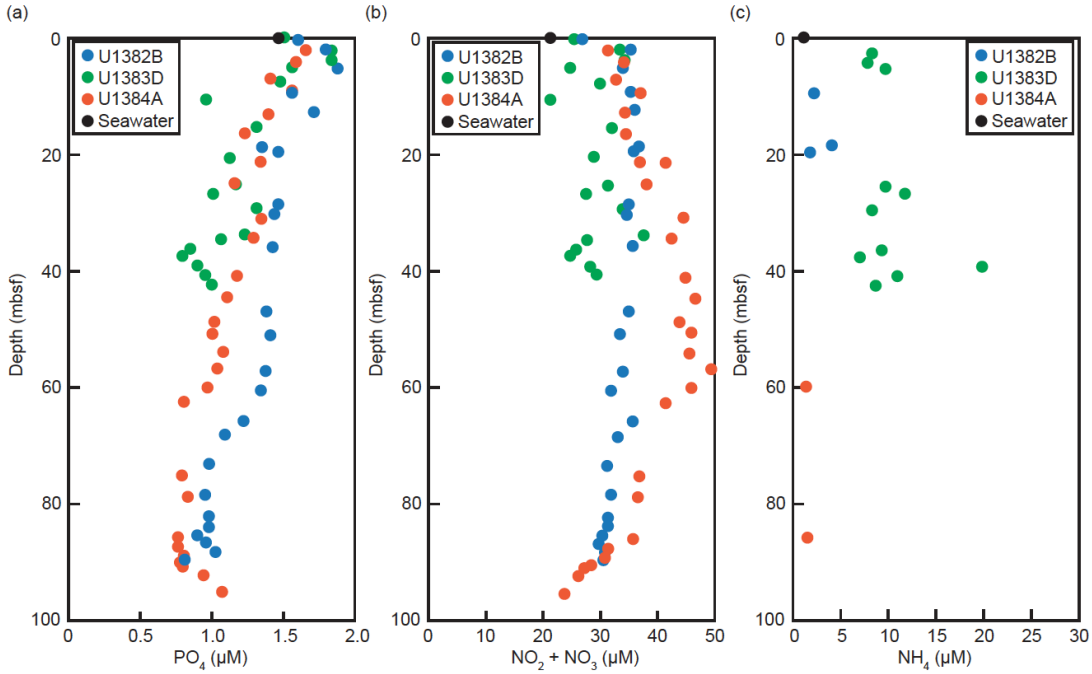

Fig. A.17. Chemical analysis of PO_4, nitrate, and NH_4 in the pore water of sediments at Hole U1382B, U1383D, U1383E, and U1384A. Value of NH_4 should be treated with caution about the detection limits. Samples from Hole U1383D had a detection limit of 6 μM due to the dilution. Samples from Hole U1382B and U1384A had a detection limit of 1.5 μM (Modified after Edwards et al., 2012).

A.3.2. Carbon isotopic analysis and elemental analysis in the basalts

TC (0.01 ~ 0.37 %) and TOC (0.01 ~ 0.03%) values of basalts were almost constant over the depth (Fig. A.18 (b)), while sediment breccias and carbonates

contained more carbon than basalts (3.56 ~ 11.9 %; Fig. A.18 (a)). $\delta^{13}C$ (bulk) of basaltic samples ranged −21.8 ~ +2.69 ‰. Sediment breccias and carbonates had slightly larger $\delta^{13}C$ (bulk), ranging −18.6 ~ +2.82 ‰. $\delta^{13}C$ (org) of basalts, sediment breccias, and carbonates showed similar value (~ −25 ‰) over the depth. $\delta^{13}C$ (kerogen) were slihgtly smaller value (−30.4 ~ −27.6 ‰) than those of $\delta^{13}C$ (org) (Table. A.1). This isotopic range appears to be comparable to the carbon isotopic compositions resulting from carbon fixation pathways with Calvin cycle (Deines, 1980). In addition, it has been reported that some Fe-oxidizing microbes fix CO_2 utilizing Calvin cycle (Davis et al., 2010; Singer et al., 2010). The results may be reflected by the activities of Fe oxidizing bacteria at 70 ~ 315 mbsf. It was also revealed that condensation of sulfur and carbon in the extracted kerogen by SEM/EDS analysis. As a result, sulfur is concentrated in all kerogen samples (Fig. A.19). Sulfate reduction is one of the major metabolisms that can occur in the basalts (Bach and Edwards, 2003). Lever et al. (2013) confirmed the coexistence of methane- and sulfur-cycling microbes in the basalts collected from the eastern flank of the Juan de Fuca Ridge. They measured $\delta^{13}C$ of total organic carbon of basalts and the $\delta^{13}C$ values were corresponding to methane oxidizing archaea ($\delta^{13}C$ = −28 ~ 26 ‰) and sulfate reducer ($\delta^{13}C$ ~ −35 ‰). In this study, $\delta^{13}C$ values are similar to those measured by Lever (2013). In addition, $\delta^{13}C$ values were lower as depth is deeper at both of U1382A and U1383C. Therefore, methane- and sulfur-cycling microbes may be also coexistence in basalts of North Pond. Sulfur-cycling microbes may be more prevail at the deeper depth of oceanic crust because redox environments in the basalt is more reductive environments at the deeper depth than those at shallower depth. This result may suggest that methane- and sulfur-cycling microbes universally prevail in the basaltic aquifer.

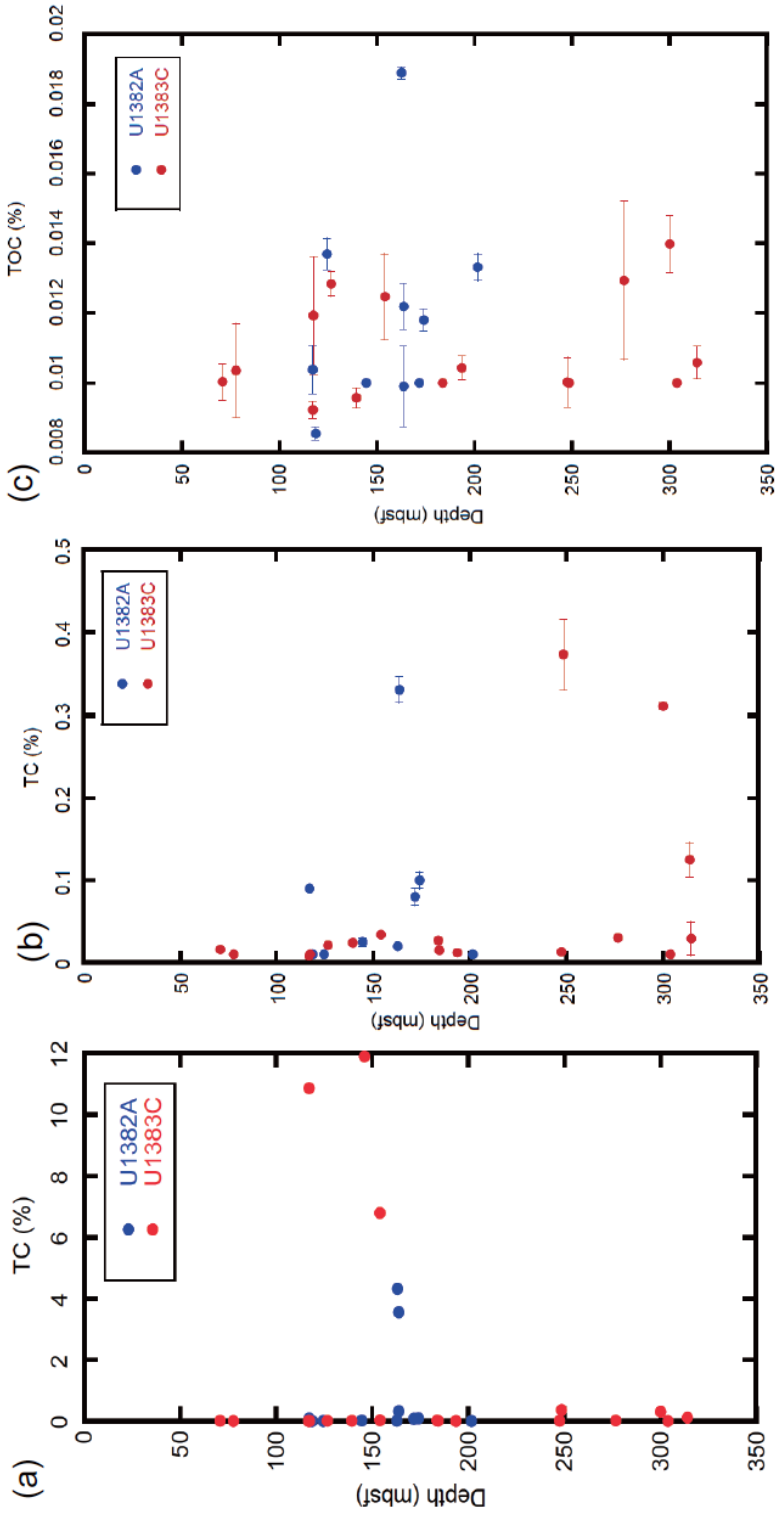

Fig. A.18. Depth-related profiles in (a) total carbon (TC) content, (b) TC (close up of Fig. A.18 (a) below 0.5 %), (c) total organic carbon (TOC) content, (d) $\delta^{13}C$ (bulk), and (e) $\delta^{13}C$ (organic residue) of hard rocks (basalts, carboantes, and sedimentary breccias) at U1382A and U1383C.

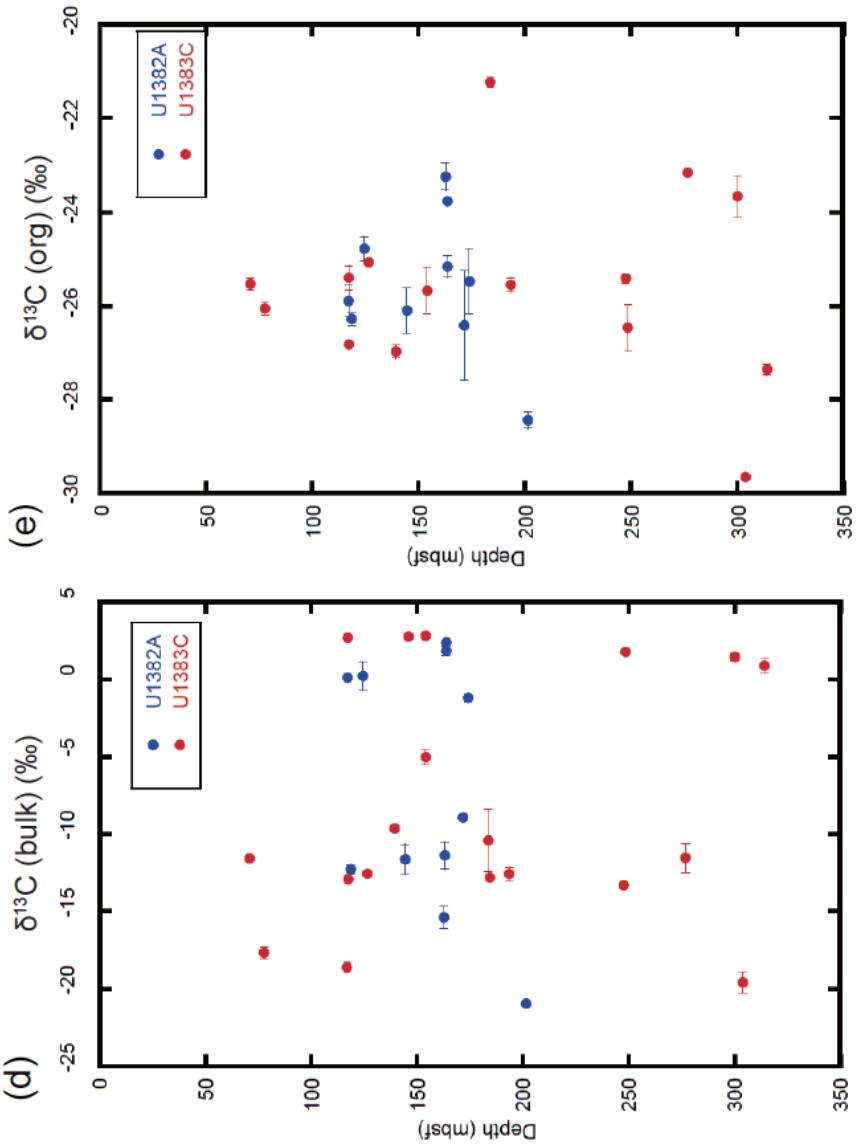

Fig. A.18. (continued).

Table A.1. Carbon contents of kerogen samples extracted from basaltic samples at Hole U1382A and U1383C.

U1382A		
Depth (mbsf)	Carbon contents (%)	$\delta^{13}C$ (kerogen) (‰)
124.50	31.72 (±8.52)	−27.63 (±0.66)
144.54	30.61	−29.87
173.03	8.04 (±2.33)	−29.48 (±0.52)
201.55	8.54 (±0.39)	−30.44 (±0.26)
U1383C		
193.49	2.86 (±0.19)	−29.72 (±0.46)
303.89	21.21 (±0.39)	−29.42 (±0.94)

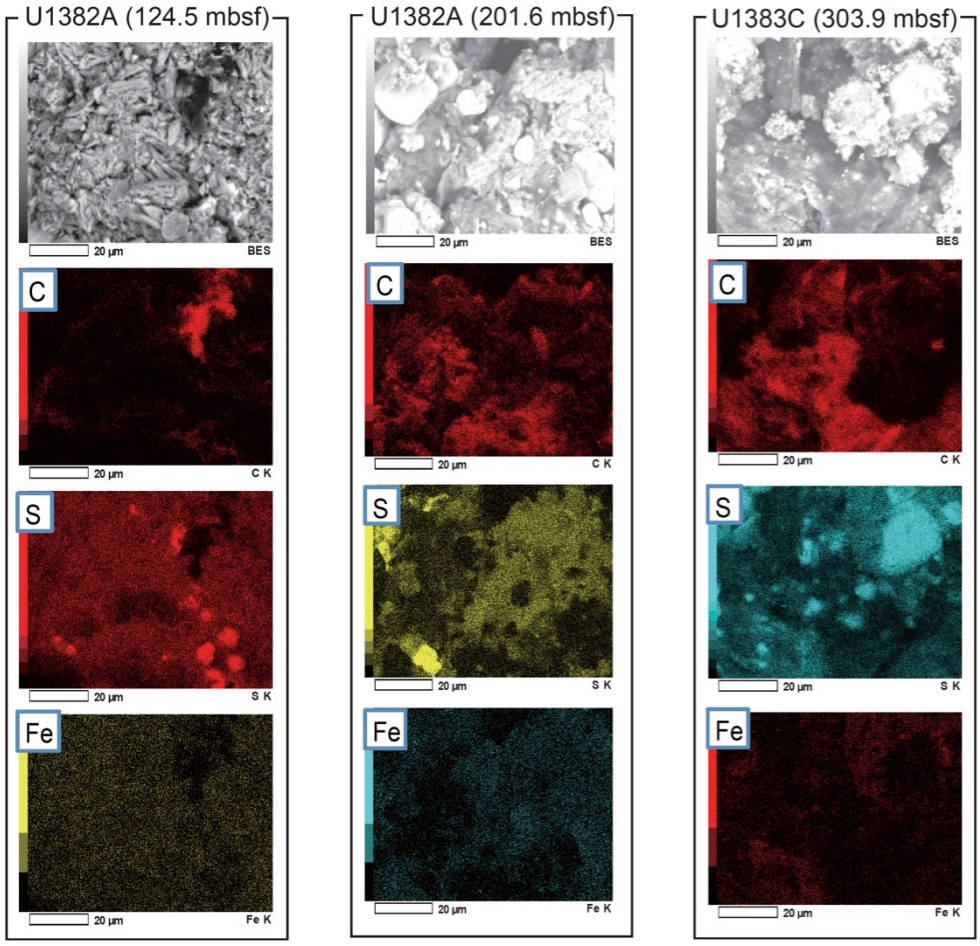

Fig. A.19. Elemental mapping of kerogen extracted from basalts collected from 124.5 and 201.6 mbsf at U1382A and 303.9 mbsf at U1383C, respectively.

A.4. Conclusion

In this study, we detected organic carbon and analyzed carbon isotope of basalts and sediments collected from North Pond for understanding the origin and formation of carbon compounds in relation to possible microbial activity in the basaltic crust. TC value ranged 6 ~ 11 % for whole sediment samples. Depth profiles of $\delta^{13}C$ (bulk) of sediments were very similar to those of TC. These depth profiles of TC and $\delta^{13}C$ (bulk) appear to have inverse relation ship with the distributions of O_2 concentration. This may represent that oxidation decomposition of carbonates and organic carbon are inhibited at the middle of the sediments because this depth are anoxic environments. Therefore, $\delta^{13}C$ (bulk) are high value at the middle of sediments because more carbonate remains in the sediments. In addition, the depth profiles of TC and $\delta^{13}C$ (bulk) of sediments also appear to have a relation with the concentration of PO_4, NO_2, NO_3, and NH_4 in the pore water squeezed from sediments. The depth profile of TC is similar to that of nitrate. While, concentrations of NH_4 are below detection limits below 20 mbsf and 0 ~ 60 mbsf at Hole U1382B and U1384A, except for Hole U1383D. This may represent that microbes with nitrification, the process to produce nitrate from ammonium by nitrifier, are active in the sediment.

TC (0.01 ~ 0.37 %) and TOC (0.01 ~ 0.03%) values of basalts were almost constant over the depth, while sediment breccias and carbonates contained more carbon than basalts (3.56 ~ 11.9 %). $\delta^{13}C$ (bulk) of basalts ranged −21.8 ~ +2.69 ‰. Sediment breccias and carbonates had larger $\delta^{13}C$ (bulk), ranging −18.6 ~ +2.82 ‰. $\delta^{13}C$ (org) of hard rocks showed similar value (~ −25 ‰) over the depth, except for $\delta^{13}C$ values were lower as depth is deeper. It was also revealed that condensation of sulfur and carbon in the extracted kerogen by SEM/EDS analysis. Therefore, methane- and sulfur-cycling microbes may be also coexistence in basalts of North Pond. Sulfur-cycling microbes may be more prevail at the deeper depth of oceanic crust because redox environments in the basalt is more reductive environments at the deeper depth than those at shallower depth. This result may suggest that methane- and sulfur-cycling microbes universally prevail in the basaltic aquifer.

A.5. References

Bach W. and Edwards K. J. (2003) Iron and sulfide oxidation within the basaltic ocean crust: Implications for chemolithoautotrophic microbial biomass production. *Geochim. Cosmochim. Acta* 67, 3871-3887.

Becker, K., Malone, M.J., Arnold E. M., Bartezko A. C. M., Farrell J., Fuller M. D., Goldberg D., Harris R. N., Hirano S., Hurst S. D., Matsumoto T., Moran K. Pezard P. A. and Sun Y. (1998) Proceedings of the ocean drilling program. *Proc. ODP, Init. Repts., 174B: College Station, TX (Ocean Drilling Program).* doi:10.2973/odp.proc.ir.174B.1998

Corliss J. B. (1990) Hot springs and the origin of life. *Nature* 347, 624.

Davis R. E., Klieslich K., Moyer C. L. and Tebo B. M. (2010) Community composition and carbon fixation of neutrophillic iron-oxidising chemoautotrophs at hydrothermal vents. *ASLO*, Portland.

Deines P. (1980) The isotope composition of reduced carbon in the terrestrial environment. *Handbook of environmental isotope geochemistry, 1. The terrestrial environment. Elsevier Amsterdam,* Fritz A. P. and Fontes J. Ch. Eds., 329-407.

Detrick, R., Honnorez, J., Adamson A. C., Brass G. W., Gillis K. M., Humphris S. E., Mevel C. Meyer P. S. Petersen N. Rautenschlein M., Shibata T. Staudigel H. Wooldrodge A. L. and Yamamoto K. (Leg 106) Bryan, W.B., Juteau, T., Adamson A. C. Autio L. K., Becker K., Bina M. M., Eissen J. Fujii T., Grove T. L., Hamano Y., Hebert R., Komor S. C., Kopietz J., Krammer K., Loubet M., Moos D. and Richards H. G. (Leg 109) (1988). Proceedings of the ocean drilling program. *Proc. ODP, Init. Repts., 106/109: College Station, TX (Ocean Drilling Program).* doi:10.2973/odp.proc.ir.106109.1988

Edwards K. J., Rogers D. R., Wirsen C. O. and McCollom T. M. (2003) Proteobacteria from the deep sea chemolithoautotrophic α- and γ- psychrophilic, neutrophilic, Fe-oxidizing. *Appl. Environ. Microbiol.* 69, 2906-2913.

Edwards K. J., Bach W. and McCollom T. M. (2005) Geomicrobiology in oceanography: microbe-mineral interactions at and below the seafloor. *TRENDS in Microbiology* 13, 449-456.

Edwards K. J., Becker K. and Colwell F. (2012) The deep dark energy biosphere: Intraterrestrial life on Earth. *Annu. Rev. Earth Planet. Sci.* 40, 551-568.

Edwards, K. J.; Backert, N.; Bach, W.; Becker, K.; Klaus, A.; Griffin, D. W.; Anderson,

L.; Haddad, A. G.; Harigane, Y.; Campion, P. L.; Hirayama, H.; Mills, H. J.; Hulme, S. M.; Nakamura, K.; Jorgensen, S. L.; Orcutt, B.; Insua, T. L.; Park, Y. -S.; Rennie, V.; Salas, E. C.; Rouxel, O.; Wang, F.; Russel, J. A.; Wheat, C. G.; Sakata, K.; Brown, M.; Magnusson, J. L.; Ettlinger, Z. (2013) Mid-atlantic ridge microbiology: initiation of long-term coupled microbiological, geochemical, and hydrological experimentation within the seafloor at North Pond, western flank of the Mid-Atlantic Ridge *Integrated Ocean Drilling Program: Preliminary Reports* 336. d*oi*:10.2204/iodp.sd.14.05.2012.

Edwards, K. J.; Backert, N.; Bach, W.; Becker, K.; Klaus, A.; Griffin, D. W.; Anderson, L.; Haddad, A. G.; Harigane, Y.; Campion, P. L.; Hirayama, H.; Mills, H. J.; Hulme, S. M.; Nakamura, K.; Jorgensen, S. L.; Orcutt, B.; Insua, T. L.; Park, Y. -S.; Rennie, V.; Salas, E. C.; Rouxel, O.; Wang, F.; Russel, J. A.; Wheat, C. G.; Sakata, K.; Brown, M.; Magnusson, J. L.; Ettlinger, Z. (2012) Initiation of long-term coupled microbiological, geochemical, and hydrological experimentation within the seafloor at North Pond, western flank of the Mid-Atlantic Ridge. *Integrated Ocean Drilling Program: Preliminary Reports* 336. doi:10.2204/iodp.pr.336.2012

Fisher A. T., Davis E. E., Hutnak M., Spiess V., Zuhlsdorff L., Cherkaoul A. Christiansen L., Edwards K. J., Macdonald R., Villinger H. Mottl M. J., Wheat C. G. and Becker K. (2003) Hydrothermal recharge and discharge across 50 km guided by seamounts on a young ridge flank. *Nature* 421, 618-621.

Fisher A. T. (2005) Marine hydrogeology: recent accomplishments and future opportunities. *Hydorogeol. J.* 13, 69-97.

Fisk M. R., Giovannoni S. J. and Thorseth I. H. (1998) Alteration of oceanic volcanic glass: textual evidence of microbial activity. *Science* 281, 978-980.

Graber, K.K., Pollard, E., Jonasson, B., and Schulte, E. (Eds.), (2002). Overview of Ocean Drilling Program engineering tools and hardware. *ODP Tech. Note*, 31. doi:10.2973/odp.tn.31.2002.

Grable R., Morin R. H., Becker K. (1992) Geothermal state of DSDP Holes 333A, 395A and 534A: results from the dianaut program. *Geophys. Res. Let.* 19, 505-508.

Hyndman, R.D., Salisbury, M.H., Ballard A., Becker K., Denis J., Hickman S. H., Jacobson R. S., Langseth M. Mathews M. A., McGowan D., Nechoroshkov V., Ponomarev V., Svitek J. and Wallerstedt R. (1984) Initial Reports of the deep sea

drilling progect. *Init. Repts. DSDP, 78B: Washington, DC (U.S. Govt. Printing Office)*. doi:10.2973/dsdp.proc.78b.1984

Langseth M. G., Becker K., Hickman S, H, and Salisbury M. H. (1984) The hydrogeological regime of isolated sediment ponds in mid-oceanic ridges.

Lever M. A., Rouxel O., Alt J. C., Shimizu N. Ono S., Coggon R. M., Shanks III W. C., Lapham L., Elvert M., Prieto-Mollar X., Hinrichs K., Inagaki F. and Teske A. (2013) Evidence for microbial carbon and sulfur cycling in deeply buried ridge flank basalt. *Science* 339, 1305-1308.

Orcutt B. N., Sylvan J. B., Knab N. J. and Edwards K. J. (2011) Microbial ecology of the dark ocean above, at, and below the seafloor. *Microbiology abd molecular biology reviews* 75, 361-422.

Orcutt B. N., Wheat C. G., Rouxel O., Hulme S., Edwards K. J. and Bach W. (2013) Oxygen consumption rates in subseafloor basaltic crust derived from a reaction transport model. *Nature Communications* doi: 10.1038/ncomms3539.

Parkes R. J., Cragg B. A., Bale S. J., Getliff J. M., Goodman K., Rochelle P. A., Fry J. C., Welghtman A. J. and Harvey S. M. (1994) Deep bacterial biosphere in pacific ocean sediments. *Nature* 371, 410-413.

Schmidt-Schierhorn, F., Kaul, N., Stephan, S., and Villinger, H., 2012. Geophysical site survey results from North Pond (Mid-Atlantic Ridge). In Edwards, K.J., Bach, W., Klaus, A., and the Expedition 336 Scientists, *Proc. IODP, 336*: Tokyo *(Integrated Ocean Drilling Program Management International, Inc.)*. doi:10.2204/ iodp.proc.336.107.2012

Singer E., Emerson D., Webb E. A. and Edwards K. J. (2010) Genomic insights into the first cultured member of the Zetaproteobacteria, the Fe-oxidizing Mariprofundus ferrooxydans PV-1. *ISME*, Seattle.

Wheat C. G., Elderfield H., Mottl M. J. and Monnin C. (2000) Chemical composition of basement fluids within an oceanic ridge flank: Implications for along-strike and across-strike hydrothermal circulation. *Journal of Geophysical Research* 105, 13437-13447.

Wheat C. G., Jannasch H. W., Kastner M., Plant J. N. and DeCarlo E. H. (2003) Seawater transport and reaction in upper oceanic basaltic basement: chemical data from continuous monitoring of sealed boreholes in a ridge flank environment. *Earth. Planet. Sci. Let.* 216, 549-564.

Whitman W. B., Coleman D. C. and Wiebe W. J. (1998) Prokaryotes: The unseen majority. *Proc. Natl. Acad. Sci.* 95, 6578-6583.

Chapter 5

Summary and Implication

In chapter 2, the effects of pH and temperature on the dimerization rate of di-peptides. The dimerization rate significantly changed with pH and reached a maximum at about pH 9.8. Since Gly has three dissociation states (Gly^{+}, $Gly^{\pm}$, and Gly^{-}), the dimerization of Gly can be separated into reactions for each dissociation state. The rates decreased in the order of $Gly^{\pm} + Gly^{-} \rightarrow$ GlyGly (fast), $Gly^{-} + Gly^{-} \rightarrow$ GlyGly (medium), and $Gly^{\pm} + Gly^{\pm} \rightarrow$ GlyGly (slow), and the rate constants differed by as much as a factor of 98. The dimerization rate became greatest at pH 9.8 because the fractions of $Gly^{\pm}$ and Gly^{-} are approximately equal at this pH. The revealed relationship between pH, dissociation state, polymerization rate, and temperature seems to be useful for the evaluation of favorable conditions for chemical evolution of life. Based on these results and previous reports on the stability of amino acids under hydrothermal conditions, we determined that Gly dimerizes most efficiently under alkaline pH (~9.8) at about 150 °C.

In chapter 3, the effects of metal ions on the formation of di- and tri- peptides in the aqueous solutions were evaluated. As a result, high-pH aqueous solutions with Cu^{2+} are the most favorable for prebiotic peptide formation, and triglycine is only produced under these conditions. This observation expands the potential for chemical evolution to new types of deep-sea hydrothermal environments such as the Lost City or South Chamorro sea mount that eruct low-temperature, high-pH fluids because of serpentinization. Metal–amino acid or metal–short peptide complexes have various functions, such as self-organization, self-recombination, and catalysis, which could contribute to origin-of-life reactions. In addition, the complexes have high mobility in the oceans without precipitation of metallic ions and might have facilitated primitive biological functions in the Earth's early oceans.

In chapter 4, the effects of basalt, pressure, and temperature on the reaction of Gly in the aqueous solutions were evaluated. The yields of GlyGly and DKP depended on temperature had maximum at 200 °C. Formation of GlyGly and DKP did not depend on pressure. On the other hand, the yield of GlyGly from solutions containing basalt was 2.6 times higher than those from solutions without basalt. The dimerization rate with basalt was 13 times higher than that without basalt. These catalytic effects of basalt result from the removal of intramolecular interaction between $–COO^{-}$ and $–NH_3^{+}$ groups within amino acid molecules and increasing of the electrophilicity of carbonyl carbon in the amino acids. It is difficult to promote the polymerization of amino acids in the

aqueous solution and interaction of amino acids and basaltic surfaces are one of the prospective catalysts at hydrothermal systems. The flow paths beneath the hydrothermal vents are probably one of the most suitable environments for polymerization of amino acids.

In Appendix, we detected of organic carbon and analyzed carbon isotope of basalts and sediments collected from North Pond for understanding the origin and formation of carbon compounds in relation to possible microbial activity in the basaltic crust. As a result, methane- and sulfur-cycling microbes may be coexistence in basalts of North Pond and sulfur-cycling microbes may be more prevail at the deeper depth of oceanic crust. These results suggest that methane- and sulfur-cycling microbes universally prevail in the basaltic aquifer above 300 mbsf.

As a result, the most suitable environments for polymerization of amino acids are the flow paths beneath the hydrothermal vents flowing hydrothermal fluids that is basic (~ pH 9.8), relatively cold (150 ~ 200 °C) and rich in Cu^{2+} (Fig. 5.1). In the present hydrothermal systems, deep underground of south Chammoro sea mount is the most suitable environments for chemical evolution of organics.

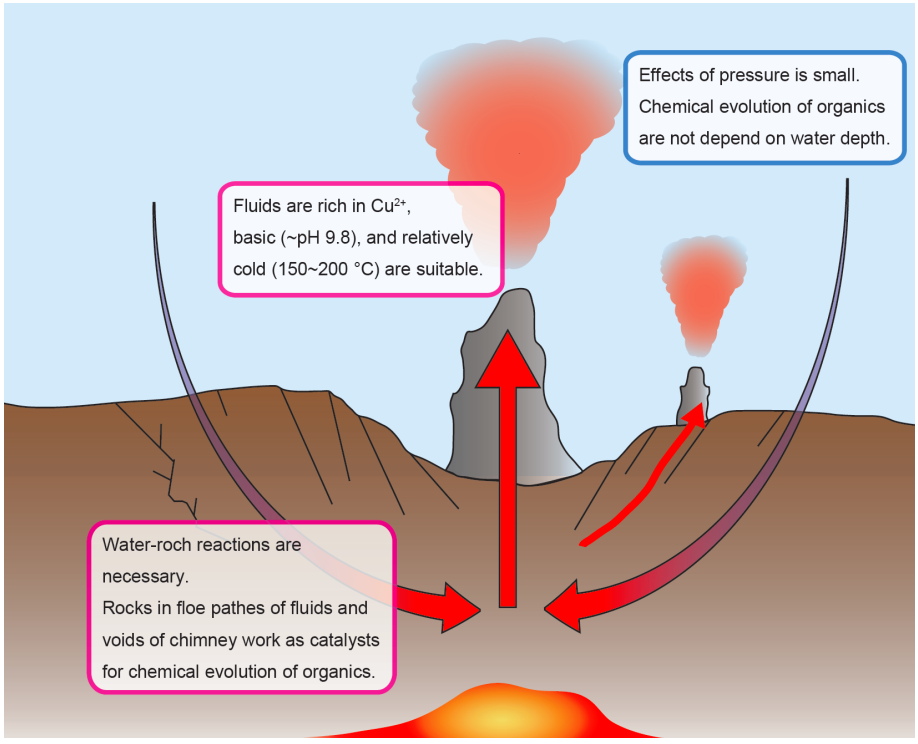

Fig. 5.1. Schemes of the most suitable hydrothermal environment for chemical evolutions of organics.

Water–rock interaction produces a broad range of pH and redox conditions in hydrothermal fluids. These dynamic changes of physical and chemical properties of water are attractive environments for synthesis of organics and deep subseafloor biospheres. These dynamic changes probably had major roles to synthesis organics having metabolic function, one of the most important biological functions because metabolic functions work out by transport of electron. In this Ph. D. thesis, we studied about closed systems. Polymerization of amino acids may be promoted under non-equilibrium conditions. Redox reactions of organics in the non-equilibrium conditions may be a key to resolve how organics having biofunction were formed.

At present earth, the water-rock reactions release energy for supporting metabolisms of chemosynthetic microbes. In addition, transition metals are erich in the hydrothermal systems and metal–amino acid or metal–short peptide complexes have various functions. The complexes have high mobility in the oceans without precipitation of metallic ions as minerals and might have facilitated primitive biological functions in the Earth's early oceans. Abundant ecosystems might have prevailed under the hydrothermal systems in the primitive earth after chemical evolution of organic materials leading to life.

Various lives prevail all over the present earth and detections of abiotic synthesis of organic materials in the earth may be more difficult than those in extraterrestrial planets. The aouthor prospect that the process of abiotic organic synthesis leading to origin of life and abundant ecosystems will be detected at extraterrestrial planets having interior oceans or hydrothermal systems, such as Europa or Enceladus, in the future.

Lists of publications and presentations

Peer reviewed papers

1. Sakata K., Kitadai N. and Yokoyama T. (2010) Effects of pH and temperature on dimerization rate of glycine: Evaluation of favorable environmental conditions for chemical evolution of life. *Geochimica et Cosmochimica Acta*. **74**, 6841-6851.
2. Sakata K., Yabuta H. and Kondo T. Effect of metal ions and pH on the formation and decomposition rates of di- and tripeptides in aqueous solution. *Geochemical Journal*, in press.
3. Edwards, K. J.; Backert, N.; Bach, W.; Becker, K.; Klaus, A.; Griffin, D. W.; Anderson, L.; Haddad, A. G.; Harigane, Y.; Campion, P. L.; Hirayama, H.; Mills, H. J.; Hulme, S. M.; Nakamura, K.; Jorgensen, S. L.; Orcutt, B.; Insua, T. L.; Park, Y. -S.; Rennie, V.; Salas, E. C.; Rouxel, O.; Wang, F.; Russel, J. A.; Wheat, C. G.; Sakata, K.; Brown, M.; Magnusson, J. L.; Ettlinger, Z. (2013) Mid-atlantic ridge microbiology: initiation of long-term coupled microbiological, geochemical, and hydrological experimentation within the seafloor at North Pond, western flank of the Mid-Atlantic Ridge. *Integrated Ocean Drilling Program: Preliminary Reports* **336**. d*oi*:10.2204/iodp.sd.14.05.2012.
4. Edwards K. J.; Backert, N.; Bach, W.; Becker, K.; Klaus, A.; Griffin, D. W.; Anderson, L.; Haddad, A. G.; Harigane, Y.; Campion, P. L.; Hirayama, H.; Mills, H. J.; Hulme, S. M.; Nakamura, K.; Jorgensen, S. L.; Orcutt, B.; Insua, T. L.; Park, Y. -S.; Rennie, V.; Salas, E. C.; Rouxel, O.; Wang, F.; Russel, J. A.; Wheat, C. G.; Sakata, K.; Brown, M.; Magnusson, J. L.; Ettlinger, Z. (2012) Initiation of long-term coupled microbiological, geochemical, and hydrological experimentation within the seafloor at North Pond, western flank of the Mid-Atlantic Ridge. *Integrated Ocean Drilling Program: Preliminary Reports* **336**. doi:10.2204/iodp.pr.336.2012

Proceedings

Sakata K., Kitadai N. and Nakashima S. (2009) Effects of pH and silica on the polymerization rate of an amino acid. *Geochim. Cosmochim. Acta* 73, A1148-A1148.

Presentations in international conferences

1. Sakata K., Kitadai N. and Nakashima S., Effects of pH and silica on the polymerization rate of an amino acid. 19th Goldschmid Conference, AA1148, Davos, Switzerland, June, 2009 (Poster presentation).
2. Sakata K. and Yabuta H., Metal ion effects on the kinetics of abiotic formation of glycylglycine and diketopiperazine under the simulated conditions of the Lost City hydrothermal field. 2010 American Geophysical Union (AGU) Fall Meeting, San Francisco, California, USA, December, 2010 (Poster presentation)..
3. Sakata K., Kitadai N. and Yokoyama T. Effects of pH and temperature on dimerization rate of glycine: Evaluation of favorable environmental conditions for chemical evolution of life. ISSOL and bioastronomy joint international conference, Montpellier, France, July, 2011 (Poster presentation).
4. Sakata K., Yabuta H., Ikehara M. and Kondo T. Carbon isotopic analyses of basalts (U1382A and U1383C) and sediments (U1382B, U1383D and U1384A) in North Pond. CDEX Science Post- Cruise Meeting (Expedition 336), Los Angeles, USA, November 30-December 1. 2012 (Poster presentation).

Presentations in domestic conference

Oral presentations

1. 坂田霞，北台紀夫，中嶋悟：アミノ酸重合反応における pH 効果の定量的評価．生命の起源および進化学会，Viva Origino, 37, 5, p.5, 2009, 京都，3 月，2009 年.
2. 坂田霞，北台紀夫，中嶋悟：アミノ酸重合反応における pH 効果の速度論的評価．地球惑星科学連合 2009 年大会，千葉幕張，5 月 2009 年.
3. 坂田霞，北台紀夫，横山正：グリシンの重合速度に対する pH 及び解離状態の影響．地球惑星科学連合 2010 年大会，千葉幕張，5 月 2010 年.
4. 坂田霞，北台紀夫，横山正：塩化カルシウムが及ぼす水溶液中のグリシン二量化反応速度への影響．地球惑星科学連合 2011 年大会，千葉幕張，5 月 2011 年.
5. 中村謙太郎・平山仙子・針金由美子・坂田霞：IODP 第 336 次航海概要．地球惑星科学連合 2012 年大会，千葉幕張，5 月 2012 年.
6. 坂田霞，薮田ひかる，近藤忠：海底熱水の多様性と SIPF 反応速度．生命の起源および進化学会，Viva Origino, 37, 5, p.5, 2013, 福岡，3 月，2013 年.

Poster presentations

1. 坂田霞，北台紀夫，田中良典，中嶋悟：アミノ酸重合反応における pH の効果．日本地球化学会第 55 回年会，東京，9 月，2008 年.
2. 坂田霞，北台紀夫，横山正：アミノ酸重合反応における解離状態の効果．日本地球化学会第 56 回年会，広島，9 月，2009 年.
3. 坂田霞，薮田ひかる：Kinetic study of glycylglycine formation under conditions simulating the ion composition of Lost City alkaline hydrothermal system．地球惑星科学連合 2010 年大会，千葉幕張，5 月 2010 年.
4. 坂田霞，薮田ひかる：アルカリ熱水中でのグリシン二量化速度における金属イオンの効果．日本地球化学会第 57 回年会，埼玉，9 月，2010 年.
5. 坂田霞，薮田ひかる：塩化カルシウムが及ぼす水溶液中のグリシン二量化反応速度への影響．地球惑星科学連合 2011 年大会，千葉幕張，5 月，2011 年.
6. 坂田霞，薮田ひかる：Effects of metal ions (Ca^{2+}, Mg^{2+}, Zn^{2+}, Cu^{2+}) and pH on the formation and decomposition rates of di- and tripeptides in aqueous solution．地球惑星科学連合 2012 年大会，千葉幕張，5 月 2012 年.
7. 坂田霞, 薮田ひかる, 近藤忠:IODP 第 336 次研究航海で掘削した北大西洋中央海嶺 North Pond 玄武岩コア試料中のケロジェンの検出とその炭素同位体比．日本有機地球化学 2013 倉敷シンポジウム，岡山，8 月 2013 年.
8. 坂田霞，薮田ひかる，近藤忠：北大西洋中央海嶺 North Pond 玄武岩地下生命圏を有機地球化学的に探る試み．日本地球化学会第 60 回年会，茨城，9 月 2013 年.

Commendation

日本地球惑星科学連合 2012 年大会　地球生命科学セッション学生優秀発表賞

坂田霞，薮田ひかる：Effects of metal ions (Ca^{2+}, Mg^{2+}, Zn^{2+}, Cu^{2+}) and pH on the formation and decomposition rates of di- and tripeptides in aqueous solution．地球惑星科学連合 2012 年大会，千葉幕張，5 月 2012 年.